Role of Sas-4/CPAP in building functional centrosomes and cilia

Inaugural dissertation

for the attainment of the degree of **Doctor of Natural Sciences (Dr. rer. nat.)** in the Faculty of Mathematics and Natural Sciences at Heinrich-Heine-University, Dusseldorf

Presented by

Anand Ramani

From Mumbai, India

Dusseldorf, July 2019

From the Laboratory for Centrosome and Cytoskeleton Biology, Institute of human Genetics, Heinrich-Heine-University, Dusseldorf.

Supervisor: Prof. Dr. Jay Gopalakrishnan
Mentor: Prof. Dr. Thomas Klein

Published by permission of the Faculty of Mathematics and Natural Sciences at Heinrich-Heine-University, Duesseldorf

Supervisor : Prof. Dr. Jay Gopalakrishnan
Co-supervisor : Prof. Dr. Thomas Klein

Date of oral examination: 03/07/2019

Table of contents

Introduction

Eukaryotic cells encompass numerous membrane-bound and non-membrane- bound organelles that have a myriad of functions (Heald and Cohen-Fix, 2014; Nigg and Raff, 2009). These functions need to be executed precisely at different stages of the cell cycle. The spatio-temporal function and co-ordination among the different organelles preclude efficient cellular processes and ultimately cell division (van Bergeijk et al., 2016). One such organelle residing within this complex environment is the centrosome **(Figure 1)**. The centrosome was first identified in 1883 by Edouard Van Beneden; however, it was subsequently named in 1888 by Theodor Boveri, when he was analyzing the mitotic spindles in the cleaving eggs of sea Urchins (Scheer, 2014). Boveri regarded the centrosome as a "Dynamic Center" of the cell and his key findings related to centrosomes brought him international recognition (Scheer, 2014).

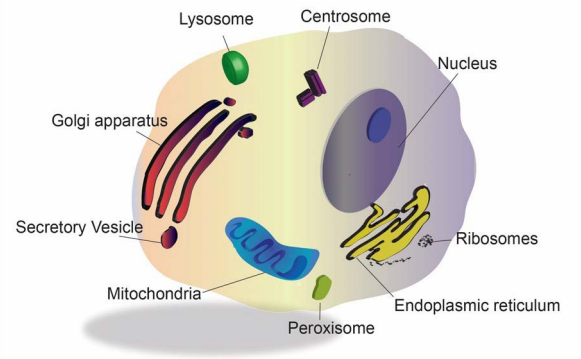

Fig. 1 Components of animal cells

Animal cell showing different organelles. The centrosome consists of two barrel shaped centrioles present in the cytoplasm (marked in purple).

Centrosomes are non-membrane bound organelles serving as the major microtubule organizing centers in animal cells (Bettencourt-Dias and Glover, 2007; Megraw et al., 2002). They are required for several fundamental cellular processes such as microtubule nucleation, cell polarity maintenance, cell shape, segregation of DNA at mitosis and cilium formation (Azimzadeh and Marshall, 2010; Bettencourt-Dias et al., 2011; Nigg and Raff, 2009).

Deregulation of centrosome functions during an organism's development leads to several developmental disorders including Seckel syndrome, Dwarfism, Microcephaly, Joubert syndrome, Bardet-Biedl syndrome and Cancer (Chavali et al., 2014; Gabriel et al., 2016; Nigg and Raff, 2009). Centrosome numbers in normally functioning cells are strictly regulated to duplicate only once per cell cycle. On the other hand, centrosomes are amplified in cancer cells and centrosome amplification is considered to be a hallmark of human cancers. Therefore, the numbers of centrosomes need to be strictly controlled to prevent any cellular abnormalities.

Typically, a centrosome consists of a pair or orthogonally arranged centrioles surrounded by a proteinaceous material called the pericentriolar material (PCM) (Chavali et al., 2014; Gopalakrishnan et al., 2011; Varadarajan and Rusan, 2018) **(Figure 2)**. The centrioles & associated structures are highly conserved among different organisms; however, they are indeed found to vary in size and shape (Winey and O'Toole, 2014). The centrioles form the basic architecture of the centrosomes and facilitate the formation of cilium when the cells exit the cell cycle in G_0 and serve as the major microtubule organizing centers (MTOCs) at mitosis. Therefore, these cylindrical structures have multiple roles during the different phases of the cell cycle.

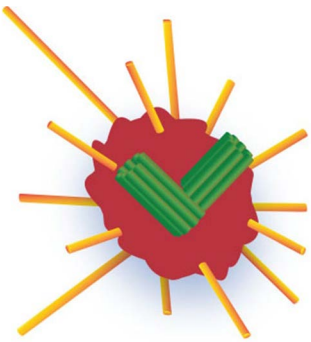

Fig. 2 Functional centrosome The two centrioles (in green) surrounded by the pericentriolar material (in red) form the functional centrosome. The centrosomes nucleate microtubules which is seen here as yellow tubules.

The centriole structure

Mammalian centrioles are normally 250 nm in diameter, with a length of approximately 500 nm (Dammermann et al., 2008). Each centriole is composed of a conserved cartwheel attached to nine microtubule triplets. Each cartwheel contains a central hub and radiating spokes which binds to microtubule triplets (Wang et al., 2017). These triplets consist of A, B and C tubules; wherein the A-tubule is composed of 13 protofilaments, while the B and C have 10 protofilaments each (Winey and O'Toole, 2014). The A-tubule is believed to exist at the beginning to which the B and C tubules are added. The C-tubule of each triplet is connected to the A tubule of the preceding triplet via a linker to form a connected structure **(Figure 3)**. Similar to the cytoplasmic microtubules, the centriolar microtubules contain the α and β tubulin dimers (Wang et al., 2017).

These tubulin dimers need to be recruited from the pool of cytoplasmic tubulin to the growing centriolar structures in a spatio-temporal manner. The centriolar microtubules are very similar to cytoplasmic microtubules; however, they undergo acetylation and polyglutamylation, which gives them high stability (Wloga and Gaertig, 2010). In contrast, cytoplasmic microtubules are highly dynamic and undergo rapid polymerization and depolymerization, a process termed as dynamic instability (Horio and Murata, 2014). This

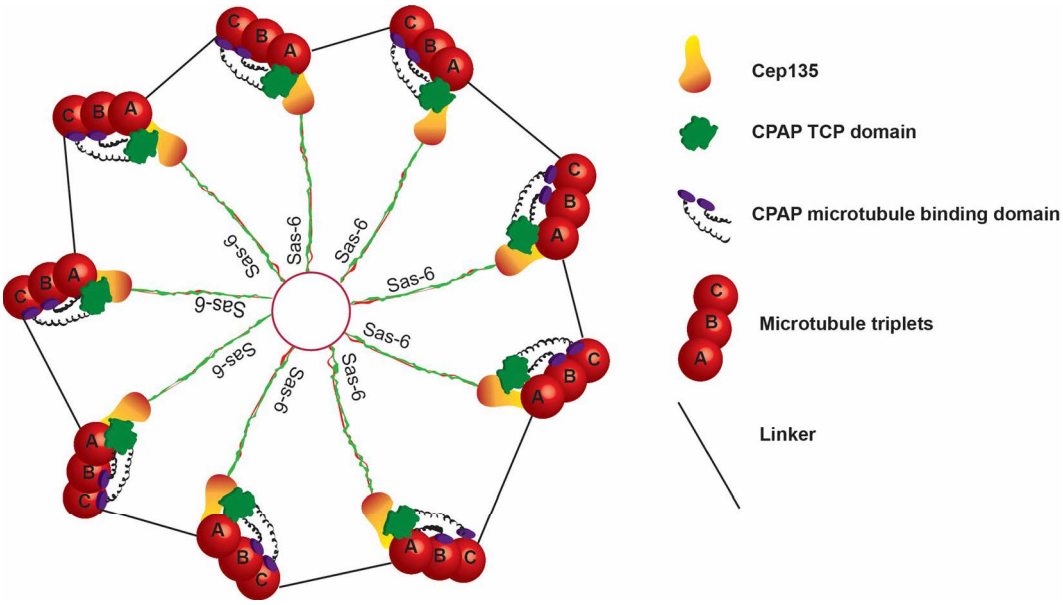

Fig. 3 Centriole Cartwheel structure

Sas-6 forms the core of the centriolar cartwheel structure. The Sas-6 spokes comprise the C-terminal domain of Sas-6, which connects to the pinhead harboring Cep135. Cep135 protein interacts with the TCP domain of CPAP in close proximity of the A- microtubules. In addition, CPAP binds to the B and C-microtubules via its microtubule binding domain (MBD). Each C-microtubule is linked to the preceding A-microtubule via a protein linker.

stability of centriolar microtubules helps in their slow and controlled growth during the elongation phase; however, any error in the delivery of tubulin to the centrioles can result in shorter or non-functional centrioles. How these tubulin dimers are recruited in a timely manner to the centrioles and the resulting cilium has not been well studied in the past. Many proteins have been implicated in centriole length control. Overexpression of Sas-4 (in flies)/ centrosomal-P4.1-associated protein (CPAP, in humans) and its interacting partner CEP120 leads to elongation of centrioles; whereas, the overexpression of CP110 or CEP97 that cap the distal ends of the centrioles lead to shorter centrioles (Schmidt et al., 2009; Sharma et al., 2016; Zheng et al., 2016). Therefore, a need to understand the exact mechanism regulating tubulin delivery to the growing centriolar and ciliary microtubule structures was one of the focus of this thesis.

Among the two centrioles in the pair, one is larger than the other and is the mother centriole. The mother centriole is also known as the mature centriole. The smaller one is the daughter centriole (Azimzadeh, 2014). In addition, there exists an asymmetry along the proximal-distal axis, especially along the mother centriole. The proximal half of the mother centriole is similar to the daughter centriole; however, at the distal part, it consists of specialized structures called the subdistal and distal appendages. The subdistal appendages are required for anchoring microtubules during interphase; whereas, the distal appendages play an important role by docking at the plasma membrane to function as the basal body. This is required for the formation of the primary cilium (Chavali et al., 2014; Dammermann et al., 2008). The basal body is similar to the canonical centriole but has a transition zone for the transport of ciliary proteins. Moreover, in certain cells such as the tracheal cells or sperm cells, the centrioles template the formation of a specialized form of cilium known as the motile cilium (Carvalho-Santos et al., 2011). Although centrosomes are absolutely important for accurate cell divisions in mammals, they are absent in higher plants and fungi, which use certain acentrosomal mechanisms for cell division (Marshall, 2009). In summary, indeed centrosomes are dispensable for cell division in some organisms; however, they are absolutely important for cilium formation (Kobayashi and Dynlacht, 2011; Nigg and Raff, 2009; Werner et al., 2017).

The duplication of centrosomes in cells is tightly controlled as the cell divides, which is also known as the centrosome cycle (Nigg and Stearns, 2011). The centrosome cycle is closely associated with the cell cycle and is strictly regulated to ensure that the centrosomes duplicate only once per cell cycle (Nigg and Raff, 2009). Any aberration in the centrosome cycle could lead to aneuploidy or result in a cancer situation.

The centrosome cycle

The centrosome cycle consists of several phases, which depend on the activation of specific proteins and kinases that interact to form functional centrosomes **(Figure 4)**. The important phases are 1. Centrosomal disengagement 2. Centriole duplication 3. Pro-centriole elongation 4. Centrosome maturation and 5. Centrosome separation (Leske et al., 1989). Centrosomal disengagement is a process that occurs at the end of mitosis prior to the start of the next centrosome cycle. During this phase, the orthogonal position of the two centrioles is lost, which is a pre-requisite for templating new centrioles in the subsequent S-phase (Wang et al., 2014). This process is mediated via the coordinated functions of Polo/

Polo-like kinase (Plk1)/ and separase (Tsou et al., 2009). A recent report has shown that in flies, Asterless (Asl) licenses newly formed centrioles to duplicate for the first time and provides a second license to the mother centrioles to re-duplicate (Novak et al., 2014). However, the same mechanism is yet to be shown in vertebrate models.

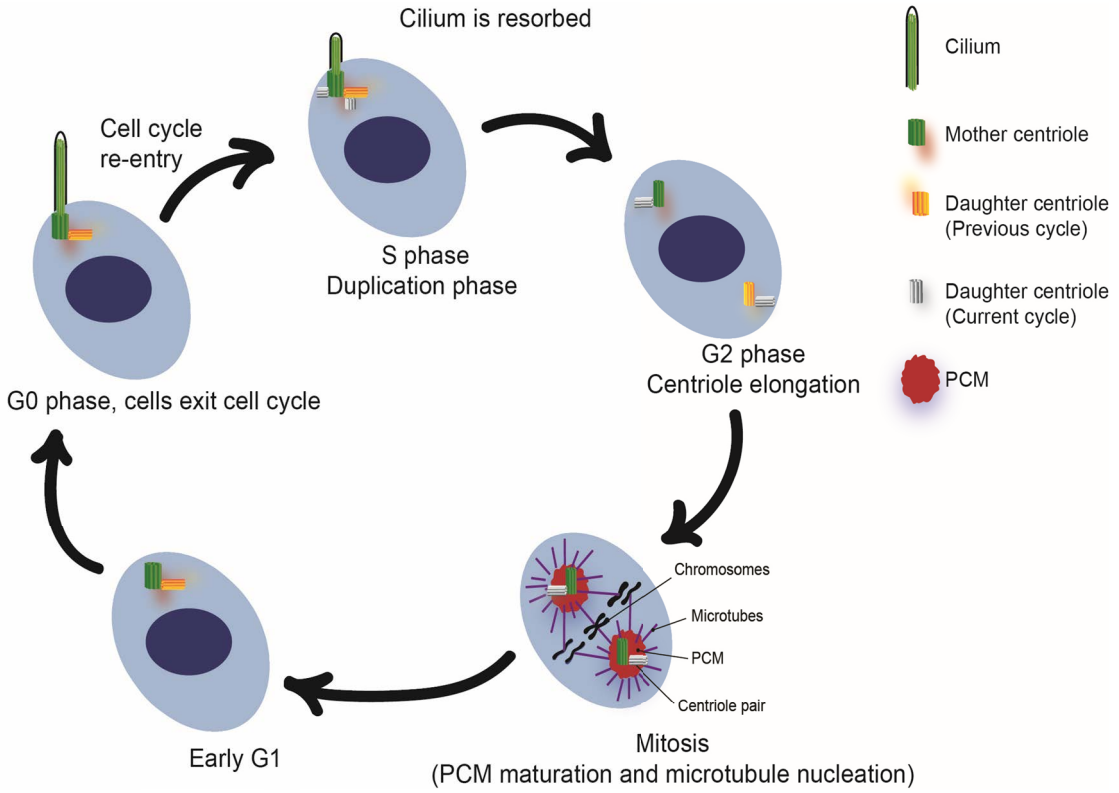

Fig. 4 Centrosome cycle

The mature mother centriole in each centriolar pair templates the formation of cilium when cells exit cell cycle in G0 phase. In the S phase, the centrosomes begin to duplicate after the primary cilium is resorbed. In the G2 phase, the centrosomes elongate, making preparation for mitosis. As cells enter mitosis, the amount of PCM dramatically increases, which serve as microtubule organizing centers (MTOCs).

Centriole duplication and maintenance of centriole numbers

Centriole duplication begins at the end of the G1 phase of cell cycle. This is regulated by SAK (*Drosophila*)/ Plk4 (humans), which is considered to be the master regulator for centriole duplication (Habedanck et al., 2005; Martin et al., 2014). Firstly, Plk4 is recruited to the centrioles by the coordinated activity of Asl/Cep152 and Spd-2/ Cep192 (Sonnen et al., 2013). The recruited Plk4 needs to interact with STIL protein to get activated. Subsequently, the activated form of Plk4 phosphorylates STIL, which is required for recruiting Sas-6 to form the cartwheel structure at the proximal part of the growing

procentrioles (Arquint and Nigg, 2016) **(Figure 5)**. In addition, the interaction between Plk4 and STIL helps to incorporate STIL into the procentrioles. These events help to establish the basic cartwheel, into which the second wave of proteins such as Sas-4/ CPAP and CEP120 are incorporated for building the microtubule structures.

The centriole duplication step is a spatio-temporally controlled mechanism to limit the duplication to only once per cell cycle (Nigg and Holland, 2018). The procentriole normally develops at the proximal part of the parent centrioles. The attachment of the procentriole to the wall of the parent centriole inhibits re-duplication of the parent centriole during the same cell cycle (Nigg and Holland, 2018). This has been very well described in a previous study in which, separation of newly formed daughter centrioles from the mother centrioles in S-phase arrested cells gives rise to multiple daughter centrioles from the same mother centriole (Loncarek et al., 2008). In other words, when the two centrioles are engaged, the parent centrioles are unable to re-duplicate. Therefore, disengagement of the mother and daughter/procentriole, which normally occurs at the end of mitosis, is required for licensing the mother centriole to re-duplicate during the next cell cycle (Shukla et al., 2015). In human cells, Pericentrin (PCNT) has been shown to be a key player in centriole disengagement and depends on the activity of Plk1, which phosphorylates PCNT thereby activating separase driven cleavage. In flies, Plk1 helps in recruiting the conserved protein Asl via a CDK1 mediated process, which is required for disengagement. (Kim et al., 2015; Novak et al., 2014).

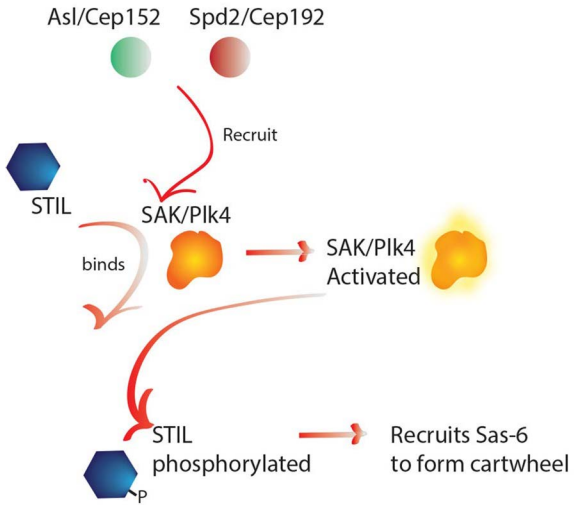

Fig. 5 Centriole cartwheel initiation

Model depicting the activation of SAK/Plk4, which phosphorylates centriolar components to assemble the initial cartwheel structure. Sas-6 forms the initial structure of the cartwheel, which is bound by other centriolar components to nucleate the procentriole.

In addition, since Plk4 is a key regulator in controlling centriole duplication, the levels of Plk4 in a cell need to be strictly maintained to avoid aberration in centriole numbers (Lopes et al., 2015). Plk4 has been well studied to maintain its own levels by auto-phosphorylation, triggering ubiquitin-mediated proteolysis (Cunha-Ferreira et al., 2013). Moreover, studies have shown that Plk4 degradation is indeed reduced at the site of procentrioles by the interaction between Plk4 and STIL, which stabilizes the protein and

ensures proper centriole numbers (Ohta et al., 2014). Although centriole numbers are strictly maintained in cycling cells, some of the post-mitotic epithelial cells that have multiple motile cilia have modified centrosomes called Deuterosomes (Klos Dehring et al., 2013; Zhang and Mitchell, 2015). These structures template several daughter centrioles that dock at the plasma membrane and form the basal body to further template the axoneme. It is noteworthy that once a cell enters into mitosis, the centrioles cannot duplicate, owing to the fact that CDK1 inhibits the interaction between Plk4 and STIL (Zitouni et al., 2016).

Centriole elongation

Centriole elongation is a process in which the newly formed procentrioles elongate to reach 80% of the parent centriole lengths. Each newly formed centriole requires approximately 1.5 cell cycles to mature into matured parent centrioles (Mattison and Winey, 2006). Sas-6 is one of the proteins that is recruited at the early stages to build the centriolar cartwheel. Subsequently, Bld10/Cep135, Sas-4/CPAP, and Ana-2/STIL interact with each other to build the procentrioles (Zheng et al., 2014). A recent study showed that Ana1/ CEP295 is recruited to the distal centrioles and is required for interaction of CPAP and CEP192 with microtubules, and depletion of CEP295 not only blocks the recruitment of POC5, but also inhibits acetylation and polyglutamylation of centriolar microtubules, which results in unstable and shorter centrioles (Chang et al., 2016).

The length of the centrioles is strictly regulated. Sas-4/CPAP interacts with Cep120 to elongate the centrioles by directly interacting with tubulin dimers and microtubules; whereas, CP110 antagonizes this process **(Figure 6)**. This opposing actions help in regulating normal lengths of the centrioles (Cormier et al., 2009; Hung et al., 2004; Schmidt et al., 2009; Zheng et al., 2016).

Although CPAP regulates centriole length, none of the previous studies address the mechanism of tubulin incorporation into growing centriolar structures. After the centrioles elongate during G2 phase, they enter the maturation phase, where the PCM expands, preparing centrosomes to function as MTOCs during mitosis.

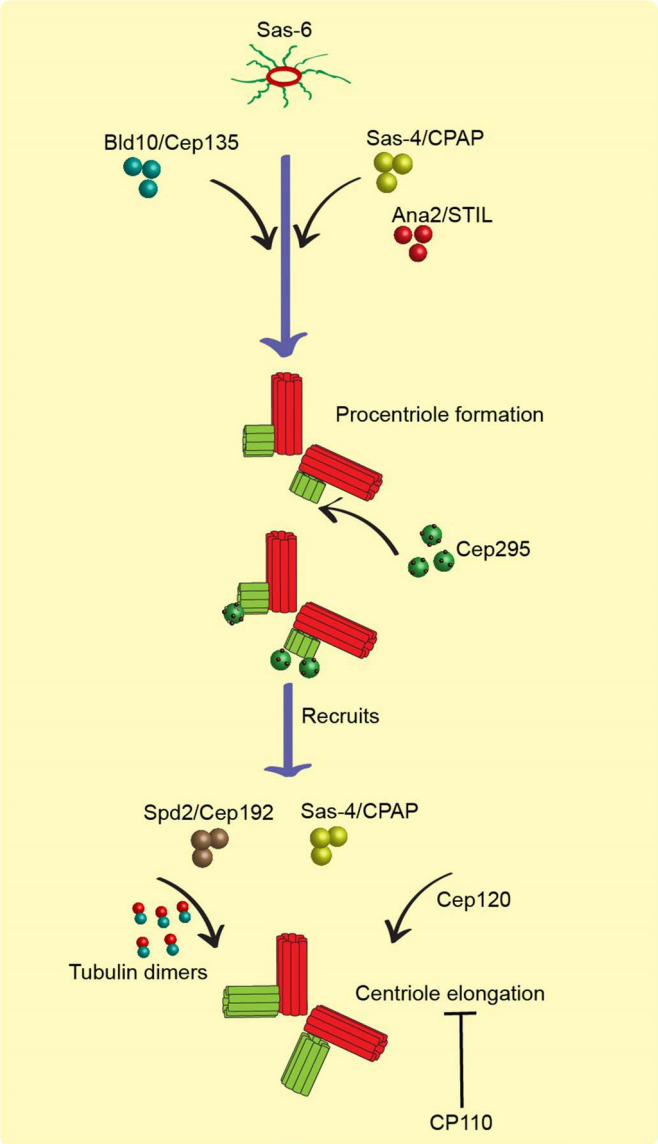

Fig. 6 Process of centriole elongation

Sas-6 lays down the foundation of the centriole cartwheel. Subsequently, Bld10/Cep135, Sas-4/CPAP and Ana2/STIL initiate the procentriole formation. Localization of Ana1/Cep295 to the distal ends of the centrioles recruit Spd-2/Cep192 and Sas-4/CPAP to the growing microtubules. Sas-4/CPAP coordinates with Cep120 to directly interact with tubulin dimers and add them to the growing microtubule structures.
The centriole elongation step is inhibited by CP110 which localizes to the distal ends of growing centrioles.

Centrosome maturation

Centrosome maturation is a complex process wherein, the PCM around the centrioles expand and initiate microtubule nucleation (Bettencourt-Dias and Glover, 2007). At interphase, the amount of PCM is minimal; however, as cells enter mitosis, the amount of PCM dramatically increases (Chou et al., 2016; Conduit et al., 2014). A number of mechanisms triggering this expansion have been proposed by different groups, which is also a key finding of this thesis. Proteomic analysis identified several key proteins required for expanding the PCM of mitotic centrosomes (Alves-Cruzeiro et al., 2014; Muller et al., 2010). Many of these proteins have coiled-coil structures required for mediating protein-protein interactions (Bettencourt-Dias and Glover, 2007; Salisbury, 2003). Some of the identified key proteins required for this expansion are Cnn/CDK5RAP2, Spd-2/Cep192, D-PLP/ Pericentrin, Asl/ Cep152, γ-Tubulin and kinases such as Polo/ Plk1, Aurora A and Cdk1. Cnn in *Drosophila melanogaster* has been widely studied by the Raff Laboratory and found to be a bona-fide PCM protein required for PCM expansion at mitosis.

Cnn is a dynamic protein which localizes near the centrioles and then extends outwards across the PCM at mitosis (Conduit et al., 2010). Polo/Plk1 phosphorylates Cnn, which in turn scaffolds other PCM proteins such as Spd-2 in fly embryos. Mutations in Cnn dramatically reduces its binding ability to other PCM proteins and subsequently microtubule nucleation (Conduit et al., 2014). CDK5RAP2, the human ortholog of Cnn has a similar scaffolding function at mitosis (Fong et al., 2008; Prosser and Pelletier, 2015). Therefore, the MTOC activity of matured centrosomes depends on the PCM load at mitosis. This could be supported by the fact that interphase centrosomes have minimal PCM and therefore do not nucleate robust microtubule asters (Rusan and Rogers, 2009). Cnn interacts with Spd-2 and D-PLP to form a lattice structure which helps to dock γ-Tubulin and its associated proteins (Varadarajan and Rusan, 2018; Zhang and Megraw, 2007) **(Figure 7)**. Similar findings have been obtained in *C. elegans*, where SPD-5 (ortholog of Spd-2) is required for PCM expansion (Prosser and Pelletier, 2015).

In addition, in humans, CDK5RAP2 and Pericentrin (PCNT) directly interact and recruit γ-Tubulin and its ring proteins. On the other hand, CEP192 interacts with NEDD1 protein to recruit γ-Tubulin (Gomez-Ferreria et al., 2012). Therefore, the PCM expansion is mediated via multiple mechanisms.

PCNT and CDK5RAP2 are well-studied proteins known to extend like a lattice from the centriolar wall into the PCM as cells enter mitosis. At interphase, they exist within toroidal layers that are highly organized; however, in mitosis, they are more unorganized and have an expanded conformation. This is required for docking other PCM proteins throughout interphase, priming the centrosomes to mature at mitosis. (Fu and Glover, 2012; Mennella et al., 2014; Varadarajan and Rusan, 2018). In contrast to human pericentrin, fly D-PLP does not expand at mitosis and localizes close to the centriole wall. This is also contrasting to the other bona-fide PCM proteins such as Cnn, Spd-2 and γ-Tubulin, which expand during mitosis in both flies and human cells. In the past, centrosome was described as a mere amorphous substance using electron microscopy; however, at present using advanced light microscopic techniques, the composition and localization of different proteins have been clearly described (Fu and Glover, 2012). Some centrosomal proteins do not seem to perform similar function across species. For example, SPD-2 is required for centriole assembly in *C. elegans*; however, in flies, it only plays a role in PCM expansion on entry into mitosis (Dix and Raff, 2007). The coordinated function of Cnn and Spd-2 in flies is required for the recruitment of γ-Tubulin and its ring complexes, which nucleate robust microtubule asters.

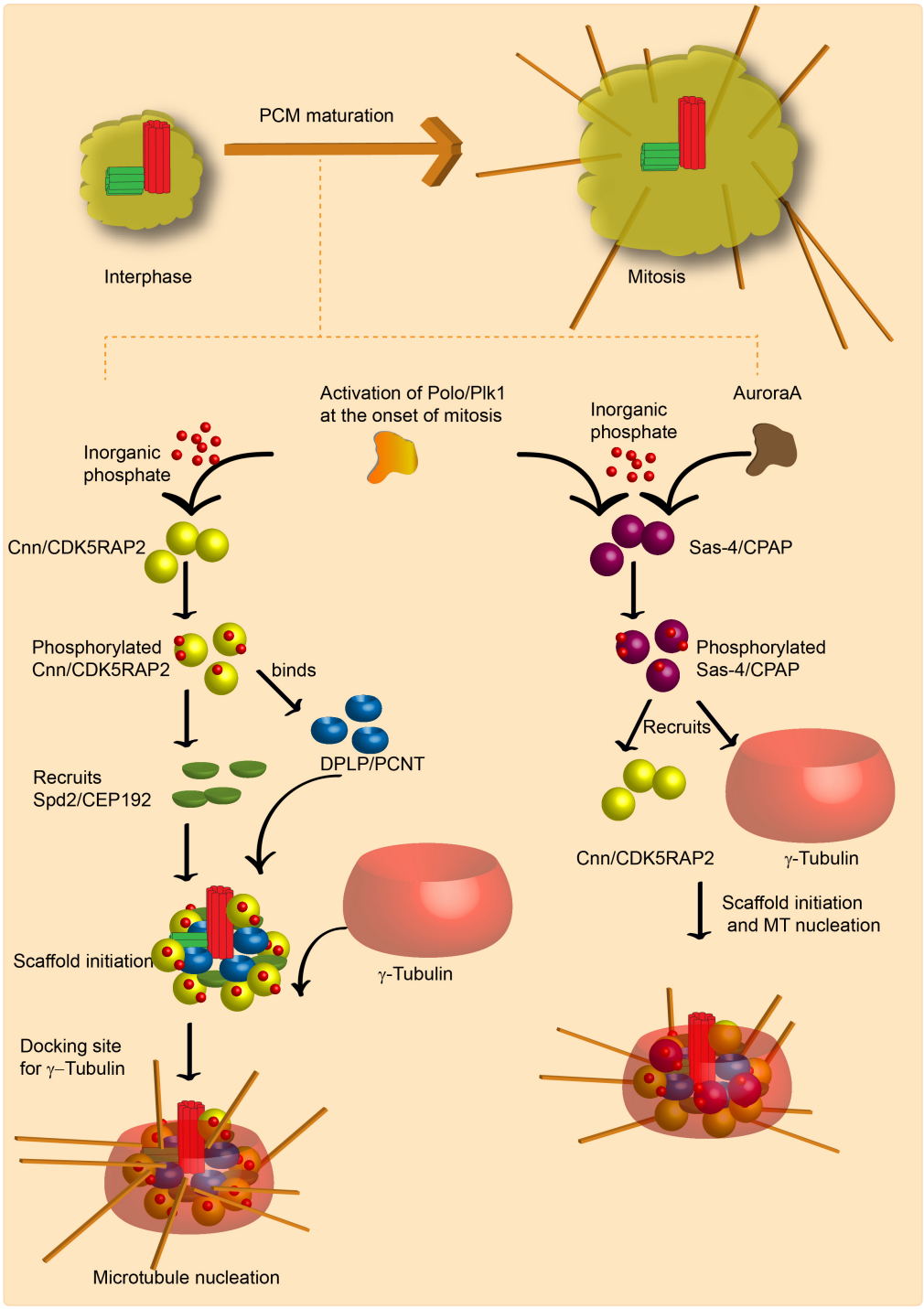

Fig. 7 Mechanisms of PCM maturation at the onset of mitosis

The canonical mitotic kinases Plk1 and Aurora A get activated at the onset of mitosis. Plk1/Polo and Aurora A phosphorylate centrosomal proteins that initiate the scaffold assembly. Subsequently, this leads to centrosome maturation and microtubule nucleation

In humans, Plk1 initiates the recruitment of CDK5RAP2 and Cep192, which in turn anchor γ-Tubulin (Haren et al., 2009) **(Figure 7)**. It is noteworthy that, although elevated levels of Spd-2 in flies recruit more Cnn and expand PCM, the overexpression of Cep192 does not have a similar effect in human cells (Lawo et al., 2012). Therefore,

although the centrosomal proteins are highly conserved among the different species, they might play slightly different roles. Recent super-resolution microscopic studies have shed light on the precise location of the different centrosomal proteins and defined the spatial arrangement of individual components in both flies and human cells (Fu and Glover, 2012; Lawo et al., 2012; Mennella et al., 2012). The outermost region of the PCM comprises of γ-Tubulin and its ring complexes. γ-Tubulin is one of the key proteins required for microtubule nucleation and is located in the PCM cloud which surrounds the centrioles (Varadarajan and Rusan, 2018). Basically, it functions by capping the minus end of centriolar microtubules, with the plus ends moving towards the chromosomes for faithful segregation of DNA at mitosis (Wiese and Zheng, 2000). In the absence of γ-Tubulin or its ring complexes, centrosome-mediated microtubule nucleation is nearly abolished (Wiese and Zheng, 2006). γ-Tubulin exists as γ-Tubulin- ring complexes (γ-TuRCs), consisting γ-Tubulin small complexes (γ-TuSCs) and additional proteins to form the γ-TuRCs. Recent studies have shown that the γ-TuSCs, which consists of the dGRIP84 and dGRIP91 (in *Drosophila*) or GCP2/GCP3 in humans is required for forming higher order structures and initiating microtubule nucleation (Farache et al., 2018; Kollman et al., 2008). γ-Tubulin is also involved in microtubule nucleation in cells following the non-canonical centrosome- independent pathway which is seen in Drosophila oocytes and also in higher plants (Brown and Lemmon, 2011; Rome and Ohkura, 2018).

Asl/CEP152 and Sas-4/CPAP have long been implicated in centriole duplication (Dammermann et al., 2008; Fujita et al., 2016). They have never been considered as bona-fide PCM proteins required for centrosome maturation. However, a recent study indeed shows that both Sas-4 and Asl are required for maturation of centrosomes at mitosis (Novak et al., 2016). This process requires the phosphorylation of Sas-4 by CDK1, which in turn allows the binding of Polo to the daughter centrioles. The bound Polo in turn, recruits Asl to the centrioles, which brings about “centriole to centrosome conversion” or “mitotic centriole conversion” and enhanced PCM recruitment (Fu et al., 2016). Although Novak et al. show that Asl does play a role in PCM recruitment, there is evidence from previous studies that centrioles free of Asl are still able to assemble PCM complexes (Galletta et al., 2016). Therefore, the exact role of Asl/CEP152 in the process of centrosome maturation needs to be re-examined.

Sas-4, on the other hand, although required for centriole formation and duplication, also plays a role in scaffolding other PCM proteins (Gopalakrishnan et al., 2011). Studies in the past claimed that Sas-4/CPAP was merely a centriole duplication factor that

resided close to the centriole wall (Gogendeau et al., 2011; Leidel and Gonczy, 2003); however, this has been challenged at present with the help of super-resolution microscopic studies (Lawo et al., 2012). In these studies, Sas-4/CPAP is found to exhibit a ring confirmation around the centrioles, proposing its role not only as a centriole associated protein but also being involved as a PCM scaffold. This scaffolding ability of Sas-4/CPAP has been critically analyzed in the past, where mutations in the Sas-4 PN2-3 domain dramatically reduced its binding to other PCM proteins (Gopalakrishnan et al., 2011). This has been validated in both flies and *C. elegans*, where Sas-4 plays a crucial role in expanding PCM of mitotic centrosomes (Kirkham et al., 2003; Novak et al., 2016). In summary, Sas-4/CPAP has multiple functions in building a functional centrosome, owing to the fact that it not only helps in centriole duplication and elongation but also is required for PCM expansion (Cormier et al., 2009; Novak et al., 2016; Sharma et al., 2016; Zheng et al., 2016). The importance of Sas-4 in the PCM maturation step is a key finding in this thesis, which is a significant contribution in the field of centrosome biology.

Domains of CPAP/Sas-4 and their importance in centriole and centrosome maturation

CPAP/Sas-4 have several functional domains that have been characterized *in vitro* and *in vivo* using fly models. The identification of the conserved PN2-3 domain of CPAP by the Tang Lab highlighted the role of CPAP in sequestering tubulin dimers (Hung et al., 2004) **(Figure 8 & Figure 9)**. Subsequently, Jay Gopalakrishnan and colleagues characterized the PN2-3 domain of Sas-4, where Sas-4 was found to sequester several PCM proteins and tubulin dimers via its PN2-3 domain (Gopalakrishnan et al., 2011). In addition, tubulin dimers not only bind Sas-4 but also negatively regulate the ability of Sas-4 to bind other PCM proteins depending on the bound nucleotide status of tubulin dimers (Gopalakrishnan et al., 2012). The C-terminal region of CPAP (TCP domain) was later crystallized and was shown to play a role in tethering CPAP/Sas-4 and its bound PCM components to the centrioles (Zheng et al., 2014). This shows the complexity of CPAP/Sas-4 mediated PCM and tubulin sequestration mechanisms.

Identification of the CPAP microtubule-destabilizing domain (MDD) and the microtubule-binding domain (MBD or A5N domain) has been the first step to understand the role of CPAP-tubulin interaction in microtubule growth (Zheng et al., 2014) **(Figure 7)**. This is further reaffirmed by the study showing that CPAP does play a role in centriole microtubule elongation; however, the understanding of the exact mechanism

involved in delivering tubulin dimers to growing microtubule structures was lacking (Lin et al., 2013; Tang et al., 2009). Recent studies by the Steinmetz Lab and Jay Gopalakrishnan Lab showed the crystal structure of PN2-3 tubulin, which significantly brought clarity in tubulin sequestration mechanisms of CPAP and its role in centriolar and cytoplasmic microtubule elongation (Sharma et al., 2016; Zheng et al., 2016). In summary, CPAP/Sas-4 is indeed an important molecule regulating the activities of both centriolar microtubules and PCM proteins, which is required for centriole and centrosome maturation. Now the question is what would happen if cells lacked CPAP/Sas-4?

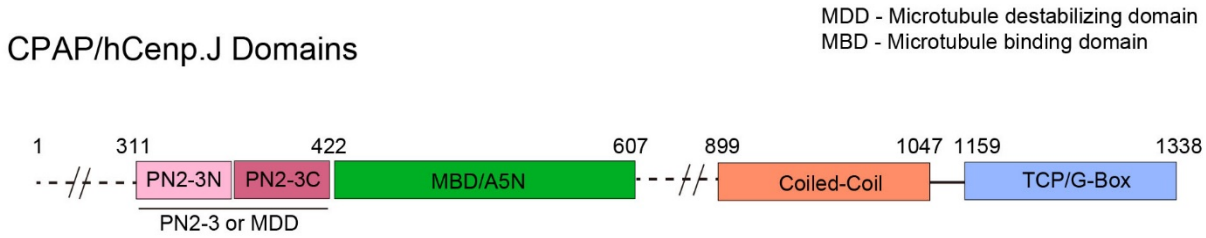

Fig. 8 Domains of human CPAP

Figure represents the different domains of human CPAP. The PN2-3/MDD and the MBD are conserved among species and were studied as a part of this thesis

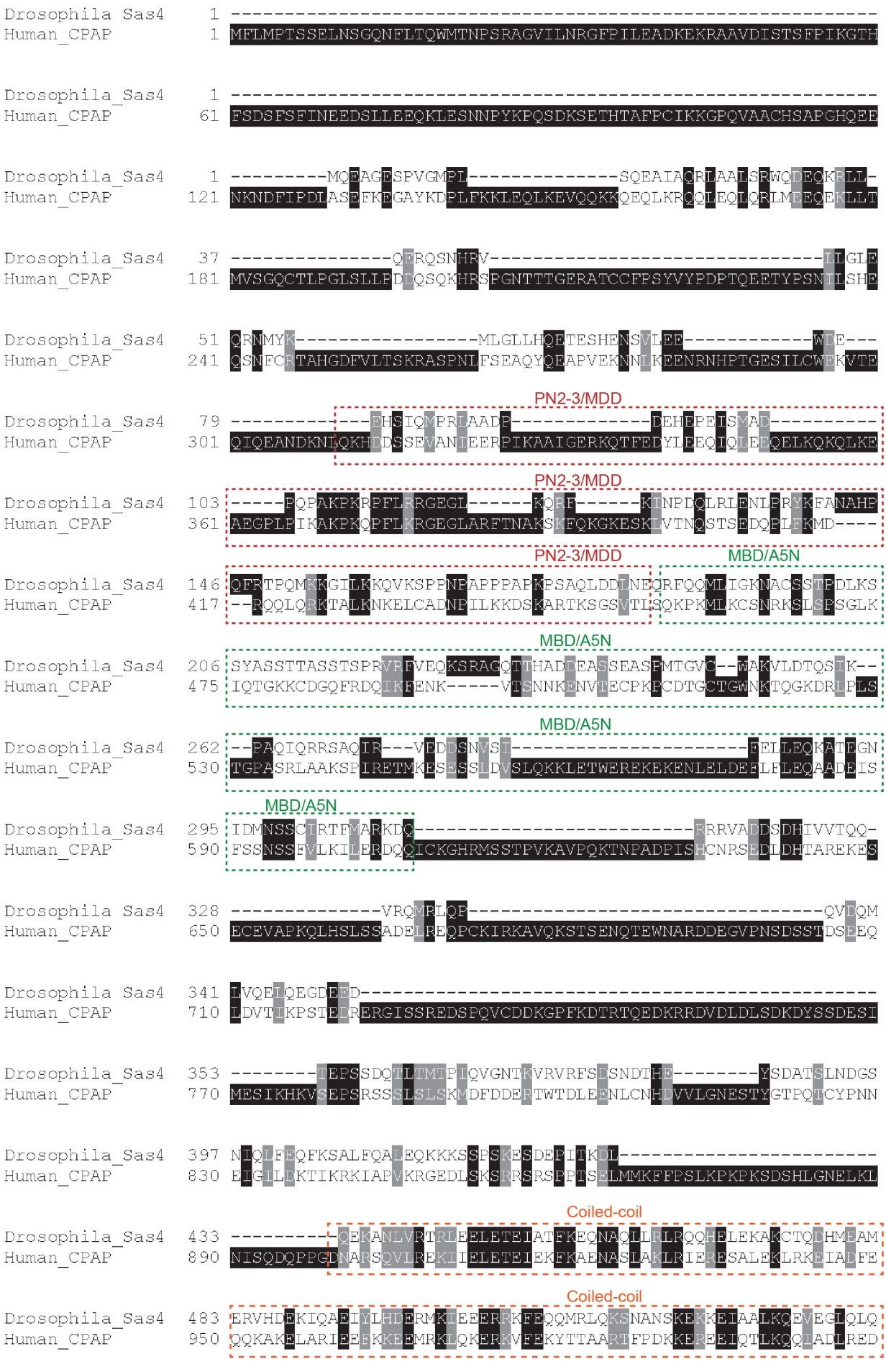
Drosophila_Sas4
Human_CPAP
PN2-3/MDD
MBD/A5N
Coiled-coil

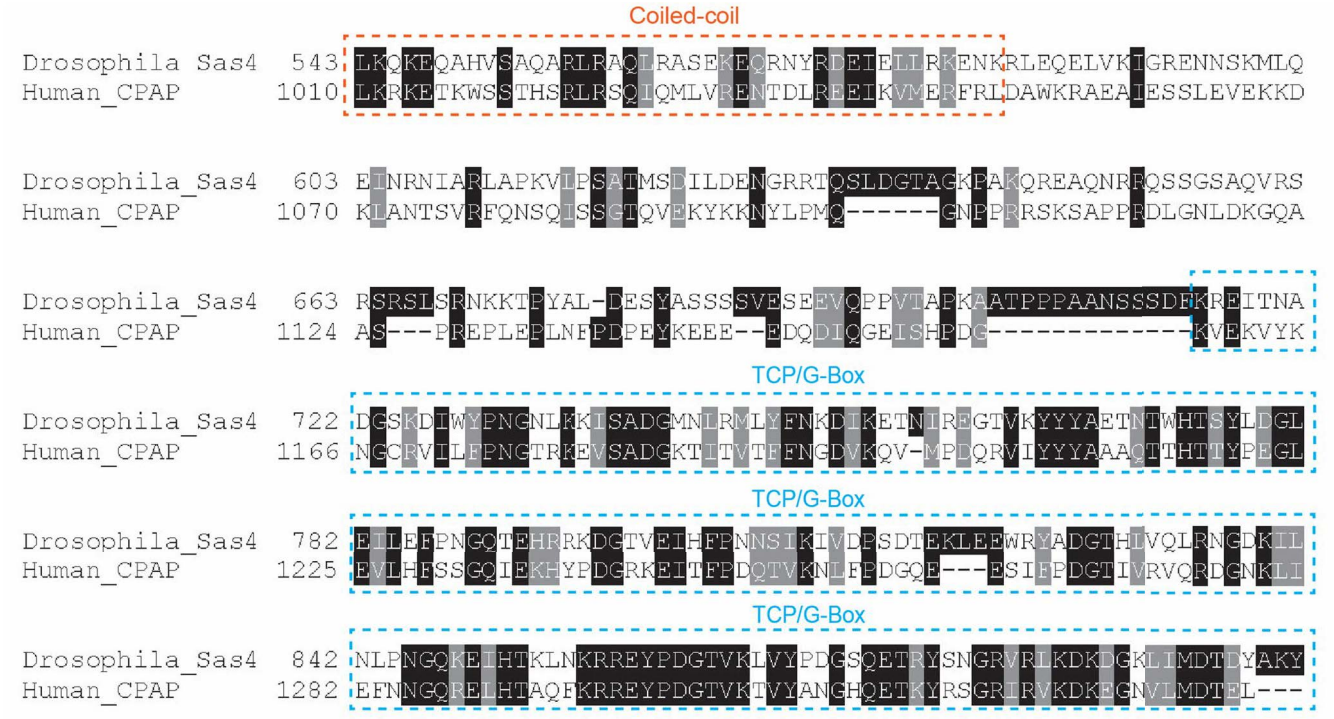

Fig. 9 Multiple alignment file of Sas-4/CPAP protein

The multiple alignment file highlighting the different domains of Sas-4/CPAP is depicted. The conserved residues are highlighted with shades of black color.

Importance of CPAP/Sas-4 in life

Since CPAP/Sas-4 is required for centriole duplication, perturbing the protein function results in abnormal centrosomal numbers (Arquint and Nigg, 2016; Basto et al., 2006; Chang et al., 2010; Vulprecht et al., 2012). In humans, reduced levels of CPAP or mutations in CPAP that alter its functions have far more drastic phenotypes compared to its fly counterpart. Primary microcephaly in humans is indeed one such disorder arising due to a defect in CPAP function (Gabriel et al., 2016; Garcez et al., 2015). This is attributed to the decline in neural progenitor pool, premature differentiation into immature neurons, which in turn reduces the brain size. The mitotic surveillance pathway is believed to get activated in these cells with centrosome defects (Zitouni et al., 2016). Mammalian cells without centrioles normally arrest in the next G1 phase due to the activation of spindle assembly checkpoint (Raaijmakers et al., 2018; Uetake et al., 2007). On the other hand, *Drosophila* cells lacking Sas-4 have no centrioles; however, successfully complete cell division even without canonical bi-polar spindles (Lecland et al., 2013).

In *Drosophila*, although centriole or centrosomes play an important role in cell division, they are not absolutely essential for adult fly development. *Drosophila* Sas-4 homozygous mutants that arise by crossing heterozygous parents (which have Sas-4) do develop like normal flies at near normal times; however, die shortly after eclosion (Basto et al., 2006). This is due to the maternal contribution of Sas-4 to the embryos, which form functional centrioles. The same is not true in *C. elegans,* wherein the absence of centrioles lead to arrest of the embryos right after the first division (Bazzi and Anderson, 2014). Therefore, in flies, the maternally contributed Sas-4 forms the initial centrioles and subsequent centrosomes which help embryos to successfully complete the initial embryonic stages. However, the number of centrioles reduce as the embryos develop into the first instar larvae due to a reduction in Sas-4 levels. Most of the centrioles are lost by the time the embryos enter the third instar larval stage; however, the larvae are still able to progress into the pupae stage. The larval cells are able to divide in the absence of centrioles via acentriolar mechanisms that involve the RanGTP pathway; wherein, instead of centrosomes, the chromosomes nucleate microtubules which attach to the spindle poles (Cavazza and Vernos, 2015). Although the pupae further develop into the adult flies, the development is slightly slower compared to normal flies. This shows that centrioles and centrosomes are only required at the initial stages of embryonic development and are non-essential for the development of adult flies (Basto et al., 2006). Although these mutant embryos develop into adult flies, they soon die after eclosion due to the lack of cilia in type I mechanosensory neurons. The flies are severely un-coordinated, cannot mate and eventually die due to starvation and dehydration (Basto et al., 2006; Dubruille et al., 2002). This indeed proves that although centrosomes are not absolutely essential for post-embryonic fly development, they are indispensable for cilium formation.

Role of centrioles and centrosomes in cilium formation

The centrioles or the centrosomes are believed to play a dual role during the cell cycle. They act as MTOCs to nucleate microtubules during mitosis and template the formation of primary cilium during cell cycle exit at G0 (Avidor-Reiss and Gopalakrishnan, 2013; Lattao et al., 2017; Mahjoub, 2013) **(Figure 4)**. These two important responsibilities of centrosomes need to be well coordinated to avoid cell cycle associated defects (Nigg and Raff, 2009).

During cell cycle exit, the mother centrioles travel to the plasma membrane and dock with the help of distal appendages. The Golgi derived vesicles bind to the distal end of the mature centrioles and initiate the first steps in cilium formation (Tanos et al., 2013). The mother centriole that templates the cilium is known as the basal body and contains triplet microtubules, consisting of A, B and C tubules **(Figure 3)**. During cilium formation, only the A and B tubules extend upwards to form the axoneme (Mizuno et al., 2012). The ciliary membrane, which is a part of the plasma membrane surrounds the axoneme, as it extends outwards from the cell surface. The basal body also has a barrier at the base of the cilium, known as the transition zone, which controls and traffics different proteins into the ciliary axoneme. Normally cells have only one primary cilium since each cell has only one mature mother centriole that templates one cilium **(Figure 4)**. However, certain specialized cells have multiple cilia that arise from specialized centriolar structures called Deuterosomes (Bettencourt-Dias and Glover, 2007). Also, since the ciliary axoneme is an extension of the centriolar microtubules, any defect in the centriolar microtubule architecture can cause defects in the formation and function of the primary cilium. Therefore, centrioles play a crucial role to initiate the formation of primary cilium, which is further involved in a number of cell signaling processes.

Since several proteins are required for efficient formation of centriolar structures, proper recruitment of these proteins in a timely manner precludes a fully functional centriole and the subsequent cilium. As described above, Sas-4/CPAP along with other proteins regulate the centriole length. Since CPAP has been shown to interact with tubulin dimers and the microtubules itself, it is one of the key molecules that could also regulate the ciliary length, which is also a microtubule-based structure (Wu and Tang, 2012; Zheng et al., 2016). The role of CPAP in ciliary length control is one of the key aspects of this thesis.

Scientific doctoral publications related to the thesis

1. Ramani A, Mariappan A, Gottardo M, Mandad S, Urlaub H, Avidor-Reiss T, Riparbelli M, Callaini G, Debec A, Feederle R, Gopalakrishnan J*. Plk1/Polo Phosphorylates Sas-4 at the Onset of Mitosis for an Efficient Recruitment of Pericentriolar Material to Centrosomes. ***Cell Reports***. 25(13): 3618-3630 (2018)

2. Zheng X*, **Ramani A***, Soni K, Gottardo M, Zheng S, Ming Gooi L, Li W, Feng S, Mariappan A, Wason A, Widlund P, Pozniakovsky A, Poser I, Deng H, Ou G, Riparbelli M, Giuliano C, Hyman AA, Sattler M, Gopalakrishnan J*, Li H*. Molecular basis for CPAP-tubulin interaction in controlling centriolar and ciliary length. ***Nature Communications.*** 7: 11874 (2016)

* Shared first author

Additional publications

1. Mariappan A, Soni K, Schorpp K, Zhao F, Minakar A, Zheng X, Mandad S, Macheleidt I, **Ramani A**, Kubelka T, Dawidowski M, Golfmann K, Wason A, Yang C, Simons J, Schmalz HG, Hyman AA, Aneja R, Ullrich R, Urlaub H, Odenthal M, Büttner R, Li H, Sattler M, Hadian K, Gopalakrishnan J*. Inhibition of CPAP-tubulin interaction prevents proliferation of centrosome-amplified cancer cells. ***EMBO Journal***. 25(13):3618-3630 (2018)
   My Role: Performed Immunoprecipitation and pulldown experiments.

2. Gabriel E, **Ramani A**, Karow U, Gottardo M, Natarajan K, Gooi LM, Goranci-Buzhala G, Krut O, Peters F, Nikolic M, Kuivanen S, Korhonen E, Smura T, Vapalahti O, Papantonis A, Schmidt-Chanasit J, Riparbelli M, Callaini G, Krönke M, Utermöhlen O, Gopalakrishnan J*. Recent Zika virus isolates induce premature differentiation of neural progenitors in human brain organoids. ***Cell Stem Cell***. 20:1-10 (2017).
   My Role: Performed immunostaining, analysis and statistics of ZIKV infected organoids and neural progenitor cells (NPCs).

3. Gabriel E, Wason A, **Ramani A**, Gooi LM, Keller P, Pozniakovsky A, Poser I, Noack F, Telugu NS, Calegari F, Šarić T, Hescheler J, Hyman AA, Gottardo M, Callaini G, Alkuraya FS, Gopalakrishnan J*. CPAP promotes timely cilium disassembly to maintain neural progenitor pool. ***EMBO Journal***. 35(8):803-19 (2016).
   My Role: Performed molecular biology for the relevant genes.

4. **Ramani A**, Gooi LM and Gopalakrishnan J*. Building the meat of pericentriolar material surrounding the skeleton of centriole. ***Cell News***. 02:24-27 (2015).
   My Role: Participated in conceptualization and writing of the review article.

Key findings of this thesis

- The C-terminal PN2-3 domain of centrosomal-P4.1-associated protein (CPAP) is a loop-helix structure and binds to β-Tubulin at an acidic microtubule outer region with an affinity of 25.6nM.
- The N-terminal PN2-3 domain of CPAP is a helical motif and forms a necklace by binding the α-β surface of β-Tubulin.
- CPAP^{F375A}/Sas-4^{F112A} mutation dramatically reduces the affinity for tubulin dimers and results in shorter centrioles and cilium in human cells and *Drosophila* spermatocytes.
- CPAP^{EE343RR}/Sas-4^{EE78RR} mutation slightly reduces the affinity for tubulin dimers and results in elongated centrioles and cilium.
- CPAP regulates centriole and cilium length by controlling the release of bound tubulin via the F375 and EE343 residues by a clutch-like mechanism.
- *Drosophila* Sas-4 is phosphorylated at the onset of mitosis.
- Plk1/Polo phosphorylates Sas-4 at the onset of mitosis at two threonine residues TT211.
- Phosphorylation of Sas-4 at two threonine residues TT211 sites is required for efficient recruitment of bona-fide PCM proteins such as Cnn and γ-Tubulin.
- Phosphorylation of Sas-4 is required for PCM expansion.

References

Alves-Cruzeiro, J.M., Nogales-Cadenas, R., and Pascual-Montano, A.D. (2014). CentrosomeDB: a new generation of the centrosomal proteins database for Human and Drosophila melanogaster. Nucleic Acids Res *42*, D430-436.

Arquint, C., and Nigg, E.A. (2016). The PLK4-STIL-SAS-6 module at the core of centriole duplication. Biochem Soc Trans *44*, 1253-1263.

Avidor-Reiss, T., and Gopalakrishnan, J. (2013). Cell Cycle Regulation of the Centrosome and Cilium. Drug Discov Today Dis Mech *10*, e119-e124.

Azimzadeh, J. (2014). Exploring the evolutionary history of centrosomes. Philosophical transactions of the Royal Society of London Series B, Biological sciences *369*.

Azimzadeh, J., and Marshall, W.F. (2010). Building the centriole. Current biology : CB *20*, R816-825.

Basto, R., Lau, J., Vinogradova, T., Gardiol, A., Woods, C.G., Khodjakov, A., and Raff, J.W. (2006). Flies without Centrioles. Cell *125*, 1375-1386.

Bazzi, H., and Anderson, K.V. (2014). Acentriolar mitosis activates a p53-dependent apoptosis pathway in the mouse embryo. Proceedings of the National Academy of Sciences of the United States of America *111*, E1491-1500.

Bettencourt-Dias, M., and Glover, D.M. (2007). Centrosome biogenesis and function: centrosomics brings new understanding. Nature reviews Molecular cell biology *8*, 451-463.

Bettencourt-Dias, M., Hildebrandt, F., Pellman, D., Woods, G., and Godinho, S.A. (2011). Centrosomes and cilia in human disease. Trends Genet *27*, 307-315.

Brown, R.C., and Lemmon, B.E. (2011). Dividing without centrioles: innovative plant microtubule organizing centres organize mitotic spindles in bryophytes, the earliest extant lineages of land plants. AoB Plants *2011*, plr028.

Carvalho-Santos, Z., Azimzadeh, J., Pereira-Leal, J.B., and Bettencourt-Dias, M. (2011). Evolution: Tracing the origins of centrioles, cilia, and flagella. The Journal of cell biology *194*, 165-175.

Cavazza, T., and Vernos, I. (2015). The RanGTP Pathway: From Nucleo-Cytoplasmic Transport to Spindle Assembly and Beyond. Front Cell Dev Biol *3*, 82.

Chang, C.W., Hsu, W.B., Tsai, J.J., Tang, C.J., and Tang, T.K. (2016). CEP295 interacts with microtubules and is required for centriole elongation. J Cell Sci *129*, 2501-2513.

Chang, J., Cizmecioglu, O., Hoffmann, I., and Rhee, K. (2010). PLK2 phosphorylation is critical for CPAP function in procentriole formation during the centrosome cycle. The EMBO journal *29*, 2395-2406.

Chavali, P.L., Putz, M., and Gergely, F. (2014). Small organelle, big responsibility: the role of centrosomes in development and disease. Philosophical transactions of the Royal Society of London Series B, Biological sciences *369*.

Chou, E.J., Hung, L.Y., Tang, C.J., Hsu, W.B., Wu, H.Y., Liao, P.C., and Tang, T.K. (2016). Phosphorylation of CPAP by Aurora-A Maintains Spindle Pole Integrity during Mitosis. Cell Rep *14*, 2975-2987.

Conduit, P.T., Brunk, K., Dobbelaere, J., Dix, C.I., Lucas, E.P., and Raff, J.W. (2010). Centrioles regulate centrosome size by controlling the rate of Cnn incorporation into the PCM. Current biology : CB *20*, 2178-2186.

Conduit, P.T., Feng, Z., Richens, J.H., Baumbach, J., Wainman, A., Bakshi, S.D., Dobbelaere, J., Johnson, S., Lea, S.M., and Raff, J.W. (2014). The centrosome-specific phosphorylation of Cnn by Polo/Plk1 drives Cnn scaffold assembly and centrosome maturation. Developmental cell *28*, 659-669.

Cormier, A., Clement, M.J., Knossow, M., Lachkar, S., Savarin, P., Toma, F., Sobel, A., Gigant, B., and Curmi, P.A. (2009). The PN2-3 domain of centrosomal P4.1-associated protein implements a novel mechanism for tubulin sequestration. The Journal of biological chemistry *284*, 6909-6917.

Cunha-Ferreira, I., Bento, I., Pimenta-Marques, A., Jana, S.C., Lince-Faria, M., Duarte, P., Borrego-Pinto, J., Gilberto, S., Amado, T., Brito, D.*, et al.* (2013). Regulation of autophosphorylation controls PLK4 self-destruction and centriole number. Current biology : CB *23*, 2245-2254.

Dammermann, A., Maddox, P.S., Desai, A., and Oegema, K. (2008). SAS-4 is recruited to a dynamic structure in newly forming centrioles that is stabilized by the gamma-tubulin-mediated addition of centriolar microtubules. The Journal of cell biology *180*, 771-785.

Dix, C.I., and Raff, J.W. (2007). Drosophila Spd-2 recruits PCM to the sperm centriole, but is dispensable for centriole duplication. Current biology : CB *17*, 1759-1764.

Dubruille, R., Laurencon, A., Vandaele, C., Shishido, E., Coulon-Bublex, M., Swoboda, P., Couble, P., Kernan, M., and Durand, B. (2002). Drosophila regulatory factor X is necessary for ciliated sensory neuron differentiation. Development *129*, 5487-5498.

Farache, D., Emorine, L., Haren, L., and Merdes, A. (2018). Assembly and regulation of gamma-tubulin complexes. Open Biol *8*.

Fong, K.W., Choi, Y.K., Rattner, J.B., and Qi, R.Z. (2008). CDK5RAP2 is a pericentriolar protein that functions in centrosomal attachment of the gamma-tubulin ring complex. Molecular biology of the cell *19*, 115-125.

Fu, J., and Glover, D.M. (2012). Structured illumination of the interface between centriole and peri-centriolar material. Open Biol *2*, 120104.

Fu, J., Lipinszki, Z., Rangone, H., Min, M., Mykura, C., Chao-Chu, J., Schneider, S., Dzhindzhev, N.S., Gottardo, M., Riparbelli, M.G.*, et al.* (2016). Conserved molecular interactions in centriole-to-centrosome conversion. Nature cell biology *18*, 87-99.

Fujita, H., Yoshino, Y., and Chiba, N. (2016). Regulation of the centrosome cycle. Mol Cell Oncol *3*, e1075643.

Gabriel, E., Wason, A., Ramani, A., Gooi, L.M., Keller, P., Pozniakovsky, A., Poser, I., Noack, F., Telugu, N.S., Calegari, F.*, et al.* (2016). CPAP promotes timely cilium disassembly to maintain neural progenitor pool. The EMBO journal *35*, 803-819.

Galletta, B.J., Jacobs, K.C., Fagerstrom, C.J., and Rusan, N.M. (2016). Asterless is required for centriole length control and sperm development. The Journal of cell biology *213*, 435-450.

Garcez, P.P., Diaz-Alonso, J., Crespo-Enriquez, I., Castro, D., Bell, D., and Guillemot, F. (2015). Cenpj/CPAP regulates progenitor divisions and neuronal migration in the cerebral cortex downstream of Ascl1. Nature communications *6*, 6474.

Gogendeau, D., Hurbain, I., Raposo, G., Cohen, J., Koll, F., and Basto, R. (2011). Sas-4 proteins are required during basal body duplication in Paramecium. Molecular biology of the cell *22*, 1035-1044.

Gomez-Ferreria, M.A., Bashkurov, M., Mullin, M., Gingras, A.C., and Pelletier, L. (2012). CEP192 interacts physically and functionally with the K63-deubiquitinase CYLD to promote mitotic spindle assembly. Cell cycle *11*, 3555-3558.

Gopalakrishnan, J., Chim, Y.C., Ha, A., Basiri, M.L., Lerit, D.A., Rusan, N.M., and Avidor-Reiss, T. (2012). Tubulin nucleotide status controls Sas-4-dependent pericentriolar material recruitment. Nature cell biology *14*, 865-873.

Gopalakrishnan, J., Mennella, V., Blachon, S., Zhai, B., Smith, A.H., Megraw, T.L., Nicastro, D., Gygi, S.P., Agard, D.A., and Avidor-Reiss, T. (2011). Sas-4 provides a scaffold for cytoplasmic complexes and tethers them in a centrosome. Nature communications *2*, 359.

Habedanck, R., Stierhof, Y.D., Wilkinson, C.J., and Nigg, E.A. (2005). The Polo kinase Plk4 functions in centriole duplication. Nature cell biology *7*, 1140-1146.

Haren, L., Stearns, T., and Luders, J. (2009). Plk1-dependent recruitment of gamma-tubulin complexes to mitotic centrosomes involves multiple PCM components. PLoS One *4*, e5976.

Heald, R., and Cohen-Fix, O. (2014). Morphology and function of membrane-bound organelles. Curr Opin Cell Biol *26*, 79-86.

Horio, T., and Murata, T. (2014). The role of dynamic instability in microtubule organization. Front Plant Sci *5*, 511.

Hung, L.Y., Chen, H.L., Chang, C.W., Li, B.R., and Tang, T.K. (2004). Identification of a novel microtubule-destabilizing motif in CPAP that binds to tubulin heterodimers and inhibits microtubule assembly. Molecular biology of the cell *15*, 2697-2706.

Kim, J., Lee, K., and Rhee, K. (2015). PLK1 regulation of PCNT cleavage ensures fidelity of centriole separation during mitotic exit. Nature communications *6*, 10076.

Kirkham, M., Muller-Reichert, T., Oegema, K., Grill, S., and Hyman, A.A. (2003). SAS-4 is a C. elegans centriolar protein that controls centrosome size. Cell *112*, 575-587.

Klos Dehring, D.A., Vladar, E.K., Werner, M.E., Mitchell, J.W., Hwang, P., and Mitchell, B.J. (2013). Deuterosome-mediated centriole biogenesis. Developmental cell *27*, 103-112.

Kobayashi, T., and Dynlacht, B.D. (2011). Regulating the transition from centriole to basal body. The Journal of cell biology *193*, 435-444.

Kollman, J.M., Zelter, A., Muller, E.G., Fox, B., Rice, L.M., Davis, T.N., and Agard, D.A. (2008). The structure of the gamma-tubulin small complex: implications of its architecture and flexibility for microtubule nucleation. Molecular biology of the cell *19*, 207-215.

Lattao, R., Kovacs, L., and Glover, D.M. (2017). The Centrioles, Centrosomes, Basal Bodies, and Cilia of Drosophila melanogaster. Genetics *206*, 33-53.

Lawo, S., Hasegan, M., Gupta, G.D., and Pelletier, L. (2012). Subdiffraction imaging of centrosomes reveals higher-order organizational features of pericentriolar material. Nature cell biology *14*, 1148-1158.

Lecland, N., Debec, A., Delmas, A., Moutinho-Pereira, S., Malmanche, N., Bouissou, A., Dupre, C., Jourdan, A., Raynaud-Messina, B., Maiato, H.*, et al.* (2013). Establishment and mitotic characterization of new Drosophila acentriolar cell lines from DSas-4 mutant. Biol Open *2*, 314-323.

Leidel, S., and Gonczy, P. (2003). SAS-4 is essential for centrosome duplication in C elegans and is recruited to daughter centrioles once per cell cycle. Developmental cell *4*, 431-439.

Leske, M.C., Connell, A.M., and Kehoe, R. (1989). A pilot project of glaucoma in Barbados. Br J Ophthalmol *73*, 365-369.

Lin, Y.N., Wu, C.T., Lin, Y.C., Hsu, W.B., Tang, C.J., Chang, C.W., and Tang, T.K. (2013). CEP120 interacts with CPAP and positively regulates centriole elongation. The Journal of cell biology *202*, 211-219.

Loncarek, J., Hergert, P., Magidson, V., and Khodjakov, A. (2008). Control of daughter centriole formation by the pericentriolar material. Nature cell biology *10*, 322-328.

Lopes, C.A., Jana, S.C., Cunha-Ferreira, I., Zitouni, S., Bento, I., Duarte, P., Gilberto, S., Freixo, F., Guerrero, A., Francia, M.*, et al.* (2015). PLK4 trans-Autoactivation Controls Centriole Biogenesis in Space. Developmental cell *35*, 222-235.

Mahjoub, M.R. (2013). The importance of a single primary cilium. Organogenesis *9*, 61-69.

Marshall, W.F. (2009). Centriole evolution. Curr Opin Cell Biol *21*, 14-19.

Martin, C.A., Ahmad, I., Klingseisen, A., Hussain, M.S., Bicknell, L.S., Leitch, A., Nurnberg, G., Toliat, M.R., Murray, J.E., Hunt, D.*, et al.* (2014). Mutations in PLK4, encoding a master regulator of centriole biogenesis, cause microcephaly, growth failure and retinopathy. Nat Genet *46*, 1283-1292.

Mattison, C.P., and Winey, M. (2006). The centrosome cycle. Results Probl Cell Differ *42*, 111-146.

Megraw, T.L., Kilaru, S., Turner, F.R., and Kaufman, T.C. (2002). The centrosome is a dynamic structure that ejects PCM flares. J Cell Sci *115*, 4707-4718.

Mennella, V., Agard, D.A., Huang, B., and Pelletier, L. (2014). Amorphous no more: subdiffraction view of the pericentriolar material architecture. Trends Cell Biol *24*, 188-197.

Mennella, V., Keszthelyi, B., McDonald, K.L., Chhun, B., Kan, F., Rogers, G.C., Huang, B., and Agard, D.A. (2012). Subdiffraction-resolution fluorescence microscopy reveals a domain of the centrosome critical for pericentriolar material organization. Nature cell biology *14*, 1159-1168.

Mizuno, N., Taschner, M., Engel, B.D., and Lorentzen, E. (2012). Structural studies of ciliary components. J Mol Biol *422*, 163-180.

Muller, H., Schmidt, D., Steinbrink, S., Mirgorodskaya, E., Lehmann, V., Habermann, K., Dreher, F., Gustavsson, N., Kessler, T., Lehrach, H.*, et al.* (2010). Proteomic and functional analysis of the mitotic Drosophila centrosome. The EMBO journal *29*, 3344-3357.

Nigg, E.A., and Holland, A.J. (2018). Once and only once: mechanisms of centriole duplication and their deregulation in disease. Nature reviews Molecular cell biology *19*, 297-312.

Nigg, E.A., and Raff, J.W. (2009). Centrioles, centrosomes, and cilia in health and disease. Cell *139*, 663-678.

Nigg, E.A., and Stearns, T. (2011). The centrosome cycle: Centriole biogenesis, duplication and inherent asymmetries. Nature cell biology *13*, 1154-1160.

Novak, Z.A., Conduit, P.T., Wainman, A., and Raff, J.W. (2014). Asterless licenses daughter centrioles to duplicate for the first time in Drosophila embryos. Current biology : CB *24*, 1276-1282.

Novak, Z.A., Wainman, A., Gartenmann, L., and Raff, J.W. (2016). Cdk1 Phosphorylates Drosophila Sas-4 to Recruit Polo to Daughter Centrioles and Convert Them to Centrosomes. Developmental cell *37*, 545-557.

Ohta, M., Ashikawa, T., Nozaki, Y., Kozuka-Hata, H., Goto, H., Inagaki, M., Oyama, M., and Kitagawa, D. (2014). Direct interaction of Plk4 with STIL ensures formation of a single procentriole per parental centriole. Nature communications *5*, 5267.

Prosser, S.L., and Pelletier, L. (2015). Centrosome biology: the ins and outs of centrosome assembly. Current biology : CB *25*, R656-659.

Raaijmakers, J.A., van Heesbeen, R., Blomen, V.A., Janssen, L.M.E., van Diemen, F., Brummelkamp, T.R., and Medema, R.H. (2018). BUB1 Is Essential for the Viability of Human Cells in which the Spindle Assembly Checkpoint Is Compromised. Cell Rep *22*, 1424-1438.

Rome, P., and Ohkura, H. (2018). A novel microtubule nucleation pathway for meiotic spindle assembly in oocytes. The Journal of cell biology *217*, 3431-3445.

Rusan, N.M., and Rogers, G.C. (2009). Centrosome function: sometimes less is more. Traffic *10*, 472-481.

Salisbury, J.L. (2003). Centrosomes: coiled-coils organize the cell center. Current biology : CB *13*, R88-90.

Scheer, U. (2014). Historical roots of centrosome research: discovery of Boveri's microscope slides in Wurzburg. Philosophical transactions of the Royal Society of London Series B, Biological sciences *369*.

Schmidt, T.I., Kleylein-Sohn, J., Westendorf, J., Le Clech, M., Lavoie, S.B., Stierhof, Y.D., and Nigg, E.A. (2009). Control of centriole length by CPAP and CP110. Current biology : CB *19*, 1005-1011.

Sharma, A., Aher, A., Dynes, N.J., Frey, D., Katrukha, E.A., Jaussi, R., Grigoriev, I., Croisier, M., Kammerer, R.A., Akhmanova, A*., et al.* (2016). Centriolar CPAP/SAS-4 Imparts Slow Processive Microtubule Growth. Developmental cell *37*, 362-376.

Shukla, A., Kong, D., Sharma, M., Magidson, V., and Loncarek, J. (2015). Plk1 relieves centriole block to reduplication by promoting daughter centriole maturation. Nature communications *6*, 8077.

Sonnen, K.F., Gabryjonczyk, A.M., Anselm, E., Stierhof, Y.D., and Nigg, E.A. (2013). Human Cep192 and Cep152 cooperate in Plk4 recruitment and centriole duplication. J Cell Sci *126*, 3223-3233.

Tang, C.J., Fu, R.H., Wu, K.S., Hsu, W.B., and Tang, T.K. (2009). CPAP is a cell-cycle regulated protein that controls centriole length. Nature cell biology *11*, 825-831.

Tanos, B.E., Yang, H.J., Soni, R., Wang, W.J., Macaluso, F.P., Asara, J.M., and Tsou, M.F. (2013). Centriole distal appendages promote membrane docking, leading to cilia initiation. Genes Dev *27*, 163-168.

Tsou, M.F., Wang, W.J., George, K.A., Uryu, K., Stearns, T., and Jallepalli, P.V. (2009). Polo kinase and separase regulate the mitotic licensing of centriole duplication in human cells. Developmental cell *17*, 344-354.

Uetake, Y., Loncarek, J., Nordberg, J.J., English, C.N., La Terra, S., Khodjakov, A., and Sluder, G. (2007). Cell cycle progression and de novo centriole assembly after centrosomal removal in untransformed human cells. The Journal of cell biology *176*, 173-182.

van Bergeijk, P., Hoogenraad, C.C., and Kapitein, L.C. (2016). Right Time, Right Place: Probing the Functions of Organelle Positioning. Trends Cell Biol *26*, 121-134.

Varadarajan, R., and Rusan, N.M. (2018). Bridging centrioles and PCM in proper space and time. Essays Biochem *62*, 793-801.

Vulprecht, J., David, A., Tibelius, A., Castiel, A., Konotop, G., Liu, F., Bestvater, F., Raab, M.S., Zentgraf, H., Izraeli, S.*, et al.* (2012). STIL is required for centriole duplication in human cells. J Cell Sci *125*, 1353-1362.

Wang, G., Jiang, Q., and Zhang, C. (2014). The role of mitotic kinases in coupling the centrosome cycle with the assembly of the mitotic spindle. J Cell Sci *127*, 4111-4122.

Wang, J.T., Kong, D., Hoerner, C.R., Loncarek, J., and Stearns, T. (2017). Centriole triplet microtubules are required for stable centriole formation and inheritance in human cells. eLife *6*.

Werner, S., Pimenta-Marques, A., and Bettencourt-Dias, M. (2017). Maintaining centrosomes and cilia. J Cell Sci *130*, 3789-3800.

Wiese, C., and Zheng, Y. (2000). A new function for the gamma-tubulin ring complex as a microtubule minus-end cap. Nature cell biology *2*, 358-364.

Wiese, C., and Zheng, Y. (2006). Microtubule nucleation: gamma-tubulin and beyond. J Cell Sci *119*, 4143-4153.

Winey, M., and O'Toole, E. (2014). Centriole structure. Philosophical transactions of the Royal Society of London Series B, Biological sciences *369*.

Wloga, D., and Gaertig, J. (2010). Post-translational modifications of microtubules. J Cell Sci *123*, 3447-3455.

Wu, K.S., and Tang, T.K. (2012). CPAP is required for cilia formation in neuronal cells. Biol Open *1*, 559-565.

Zhang, J., and Megraw, T.L. (2007). Proper recruitment of gamma-tubulin and D-TACC/Msps to embryonic Drosophila centrosomes requires Centrosomin Motif 1. Molecular biology of the cell *18*, 4037-4049.
Zhang, S., and Mitchell, B.J. (2015). Centriole biogenesis and function in multiciliated cells. Methods Cell Biol *129*, 103-127.
Zheng, X., Gooi, L.M., Wason, A., Gabriel, E., Mehrjardi, N.Z., Yang, Q., Zhang, X., Debec, A., Basiri, M.L., Avidor-Reiss, T.*, et al.* (2014). Conserved TCP domain of Sas-4/CPAP is essential for pericentriolar material tethering during centrosome biogenesis. Proceedings of the National Academy of Sciences of the United States of America *111*, E354-363.
Zheng, X., Ramani, A., Soni, K., Gottardo, M., Zheng, S., Ming Gooi, L., Li, W., Feng, S., Mariappan, A., Wason, A.*, et al.* (2016). Molecular basis for CPAP-tubulin interaction in controlling centriolar and ciliary length. Nature communications *7*, 11874.
Zitouni, S., Francia, M.E., Leal, F., Montenegro Gouveia, S., Nabais, C., Duarte, P., Gilberto, S., Brito, D., Moyer, T., Kandels-Lewis, S.*, et al.* (2016). CDK1 Prevents Unscheduled PLK4-STIL Complex Assembly in Centriole Biogenesis. Current biology : CB *26*, 1127-1137.

Chapter I

Molecular basis for CPAP-tubulin interaction in controlling centriolar and ciliary length.

Journal : Nature Communications
Year: 2016

Relevant publication:
Zheng X*, **Ramani A***, Soni K, Gottardo M, Zheng S, Ming Gooi L, Li W, Feng S, Mariappan A, Wason A, Widlund P, Pozniakovsky A, Poser I, Deng H, Ou G, Riparbelli M, Giuliano C, Hyman AA, Sattler M, Gopalakrishnan J*, Li H*. Molecular basis for CPAP-tubulin interaction in controlling centriolar and ciliary length. ***Nature Communications.*** 7: 11874 (2016).

Link to publication: https://doi.org/10.1038/ncomms11874

My contribution to this work

- Cell biology of CPAP and Sas-4 genes in regulating centriole and cilium length.
- Functional analysis of Sas-4/ CPAP-tubulin interaction in *Drosophila* and in human cells

nature COMMUNICATIONS

ARTICLE

Received 9 Jan 2016 | Accepted 9 May 2016 | Published 16 Jun 2016

DOI: 10.1038/ncomms11874 OPEN

Molecular basis for CPAP-tubulin interaction in controlling centriolar and ciliary length

Xiangdong Zheng[1,2,3,*], Anand Ramani[4,*], Komal Soni[5,6], Marco Gottardo[7], Shuangping Zheng[1,2], Li Ming Gooi[4], Wenjing Li[2,3], Shan Feng[2,3], Aruljothi Mariappan[4], Arpit Wason[4], Per Widlund[8], Andrei Pozniakovsky[8], Ina Poser[8], Haiteng Deng[2], Guangshuo Ou[2,3], Maria Riparbelli[7], Callaini Giuliano[7], Anthony A. Hyman[8], Michael Sattler[5,6], Jay Gopalakrishnan[4,*] & Haitao Li[1,2,9,*]

Centrioles and cilia are microtubule-based structures, whose precise formation requires controlled cytoplasmic tubulin incorporation. How cytoplasmic tubulin is recognized for centriolar/ciliary-microtubule construction remains poorly understood. Centrosomal-P4.1-associated-protein (CPAP) binds tubulin via its PN2-3 domain. Here, we show that a C-terminal loop-helix in PN2-3 targets β-tubulin at the microtubule outer surface, while an N-terminal helical motif caps microtubule's α-β surface of β-tubulin. Through this, PN2-3 forms a high-affinity complex with GTP-tubulin, crucial for defining numbers and lengths of centriolar/ciliary-microtubules. Surprisingly, two distinct mutations in PN2-3 exhibit opposite effects on centriolar/ciliary-microtubule lengths. CPAP^{F375A}, with strongly reduced tubulin interaction, causes shorter centrioles and cilia exhibiting doublet- instead of triplet-microtubules. CPAP^{EE343RR} that unmasks the β-tubulin polymerization surface displays slightly reduced tubulin-binding affinity inducing over-elongation of newly forming centriolar/ciliary-microtubules by enhanced dynamic release of its bound tubulin. Thus CPAP regulates delivery of its bound-tubulin to define the size of microtubule-based cellular structures using a 'clutch-like' mechanism.

[1] Beijing Advanced Innovation Center for Structural Biology, Department of Basic Medical Sciences, School of Medicine, Tsinghua University, Beijing 100084, China. [2] MOE Key Laboratory of Protein Sciences, School of Life Sciences, Tsinghua University, Beijing 100084, China. [3] Tsinghua-Peking Center for Life Sciences, Tsinghua University, Beijing 100084, China. [4] Institute for Biochemistry I and Center for Molecular Medicine of the University of Cologne, Robert-Koch-Str. 21, Cologne 50931, Germany. [5] Institute of Structural Biology, Helmholtz Zentrum München, Ingolstädter Landstr. 1, Neuherberg 85764, Germany. [6] Biomolecular NMR at Center for Integrated Protein Science Munich and Department Chemie, Technische Universität München, Lichtenbergstr. 4, Garching 85747, Germany. [7] Department of Life Sciences, University of Siena, Siena 53100, Italy. [8] Max Planck Institute of Molecular Cell Biology and Genetics, Pfotenhauer Str. 108, Dresden 01307, Germany. [9] Collaborative Innovation Center for Biotherapy, West China Hospital, Sichuan University, Chengdu 610041, China. * These authors contributed equally to this work. Correspondence and requests for materials should be addressed to J.G. (email: jay.gopalakrishnan@uni-koeln.de) or to H.L. (email: lht@tsinghua.edu.cn).

Centrioles are microtubule-based eukaryotic structures that build centrosomes and cilia, which are required for accurate cell division and cellular signaling[1–5]. Centrioles have highly conserved architecture displaying defined numbers and lengths of microtubules. Tubulin heterodimers (hereafter tubulin) are the building blocks of centriolar- and ciliary-microtubules. During cilium construction, intraflagellar transport (IFT) machineries mediate the transport of ciliary building blocks of tubulin from the cytoplasmic ciliary base to the tip[6–8]. However, it remains poorly understood how a fraction of tubulin is selected from its large cytoplasmic pool and the mechanisms that operate to deliver these specialized tubulin to construct defined lengths of centriolar- and ciliary-microtubules.

Since cilium templates from a centriole that resides within a centrosome, it is conceivable that a centrosomal protein that can directly interact with cytoplasmic tubulin could play a role in selective regulation of tubulin incorporation during centriolar- and ciliary-microtubule construction. Among the centrosomal proteins, CPAP and its ortholog Sas-4 plays roles in centriolar- and ciliary-microtubule elongation[9–14]. Data have shown that these functions require CPAP-tubulin interaction. Specifically, a CPAP/Sas-4 mutant that does not bind tubulin caused shortening of centrioles and primary cilia[9–11]. These data suggest the possibility that CPAP could play a role in delivering its bound tubulin at the site of centriole assembly and/or building centriolar-microtubules.

Free tubulin is ubiquitously present in high amounts in cells in contrast to CPAP, which has lower expression levels[9,15,16]. It is known that CPAP *via* its conserved PN2-3 domain (amino acids 319–394) sequesters free tubulin into a non-polymerizable 1:1 complex[17,18]. Thus at equilibrium, the amount of CPAP bound cytoplasmic tubulin that is unavailable for polymerization would only be a small fraction of the free tubulin. This suggests that the small fraction of CPAP-bound tubulin is required in certain CPAP-specific processes that are regulated in a spatiotemporal manner such as centriolar- and ciliary-microtubule size control. While recent studies have substantially improved our understanding on the significance of CPAP-tubulin interaction in centriole biogenesis and pericentriolar material recruitment, its significance in centriolar- and ciliary-microtubule construction remains unclear[9,11–14]. Thus, understanding the molecular basis of PN2-3-tubulin interaction is crucial in dissecting how cytoplasmic tubulin is sequestered by CPAP for the controlled delivery to define centriolar- and ciliary-microtubule lengths in cells.

In this study, we therefore investigated the structural basis of CPAP-tubulin interaction and identified that CPAP via its conserved PN2-3 domain forms a high affinity complex with GTP-tubulin and prevents it from polymerization. Our functional studies in human cells and flies then identified that, through the different facets of its PN2-3 domain, CPAP defines centriolar- and ciliary-microtubule lengths, firstly, through the sufficient binding of cytoplasmic tubulin and secondly by regulated release of its bound tubulin to define centriolar- and ciliary-microtubule lengths.

Results

Molecular basis for PN2-3-tubulin interaction. The PN2-3 domain, at the N-terminus of CPAP, is conserved from invertebrates to vertebrates (Fig. 1a). Using isothermal titration calorimetry (ITC), we determined a 25.6 nM binding affinity between PN2-3 and tubulin (Fig. 1b), and found PN2-3$_C$ (PN2-3's C-terminus, aa 372-394) is sufficient to bind tubulin (Fig. 1c). By adopting a DARPin strategy, in which DARPin molecule didn't affect binding of PN2-3$_C$ to tubulin, we solved the 2.1 Å crystal structure of bovine tubulin bound to PN2-3$_C$ (ref. 19) (Fig. 1d,e, Table 1 and Supplementary Fig. 1). In this structure, a loop-helix motif spanning residues 372–386 of PN2-3$_C$ targets an acidic microtubule outer surface on β-tubulin, although the last eight C-terminal residues (aa 387–394) were not traceable in the density map (Fig. 1e). A GTP molecule is identified in the β-tubulin nucleotide-binding pocket despite tubulin exhibiting a curved conformation (Fig. 1e and Supplementary Fig. 2). Recognition specificity arises from a number of water-mediated and direct interchain hydrogen bonds, and hydrophobic contacts between β-tubulin and PN2-3$_C$ (Fig. 2a). Key interacting residues within PN2-3$_C$ were then confirmed by structure-guided mutagenesis and ITC (Fig. 2b). Notably, F375A caused a drastic 109-fold drop in affinity from 25.6 nM to 2.8 μM, indicating its significance in forming a high-affinity CPAP-tubulin complex. We observed a perfect shape complementarity between the crouched PN2-3$_C$ loop-helix and its binding groove along the vertical axis for tubulin polymerization (Fig. 2c).

The N-terminal helical region of PN2-3 (PN2-3$_N$, aa 323–361) alone has weak tubulin binding affinity ($K_D = 68.0$ μM) (Fig. 1c). However, together with PN2-3$_C$, it contributes a ~140-fold increased binding affinity ($K_D = 25.6$ nM) (Fig. 1b). As the PN2-3$_N$-tubulin co-crystal structure could not be resolved, we used cross-linking mass spectrometry (CL-MS) to identify PN2-3$_N$ contacts with tubulin (Fig. 2d and Supplementary Fig. 3). CL-MS analysis indicates that PN2-3$_N$ wraps around the microtubule α-β-tubulin interface and makes contacts at the β-tubulin's microtubule-lumen surface, as a majority of cross-linking peaks were identified between PN2-3-N-terminal amine and lysine 372 in proximity to the β-tubulin M-loop (Fig. 2d). Such a binding mode is further supported by competition nuclear magnetic resonance spectroscopy (NMR) titration, where the weakly binding PN2-3$_N$ region can be displaced by the high affinity ligand vinblastine, which is known to bind to the microtubule α-β-tubulin interface, but not by colchicine, which binds to the β-α interface within a tubulin dimer (Fig. 2e and Supplementary Fig. 4). Arginine substitutions of the conserved PN2-3$_N$'s E343 and E344 (hereafter EE343RR) caused a 8-fold reduced interaction ($K_D = 194.2$ nM) (Fig. 2b).

We then compared the NMR spectra of wild type and mutant (PN2-3^{F375A} and PN2-3^{EE343RR}) PN2-3 fragments, which exhibited numerous chemical shift differences between PN2-3^{WT} and PN2-3^{EE343RR}. This suggests a potential disruption of the helix, which extends from residues F338-E368 (Supplementary Fig. 4c). On the other hand, we noticed similar spectra of PN2-3^{WT} and the PN2-3^{F375A}, which is further confirmed by the comparison of PN2-3^{F375A} and PN2-3^{EE343RR} spectra. Upon addition of unlabeled tubulin at equimolar ratio to ^{15}N-labeled PN2-3^{WT}, PN2-3^{F375A} and PN2-3^{EE343RR} mutants, we observed line broadening/disappearance of the peaks, which is suggestive of binding. Exchange broadening can become obvious in low affinity (μM K_D) binding events. Accordingly, we observed that line broadening increases from PN2-3^{WT} to PN2-3^{EE343RR} and is the highest with the PN2-3^{F375A} mutant, as the affinity for tubulin decreases in the same order agreeing with our ITC titrations (Figs 1b and 2b).

Together, our structural and mutagenesis data indicate that PN2-3 wraps around β-tubulin like a necklace with its PN2-3$_N$ covering the microtubule α-β and lumen surfaces of β-tubulin and its PN2-3$_C$ occluding the β-tubulin microtubule outer surface (Fig. 2c,d and Supplementary Fig. 3d). This unique binding mode suggests that PN2-3 could prevent the polymerization of its bound tubulin (Supplementary Fig. 3e).

PN2-3 prevents its bound tubulin from polymerization. To test if PN2-3 could bind tubulin and prevent the bound tubulin from polymerization, we performed microtubule-pelleting assays using

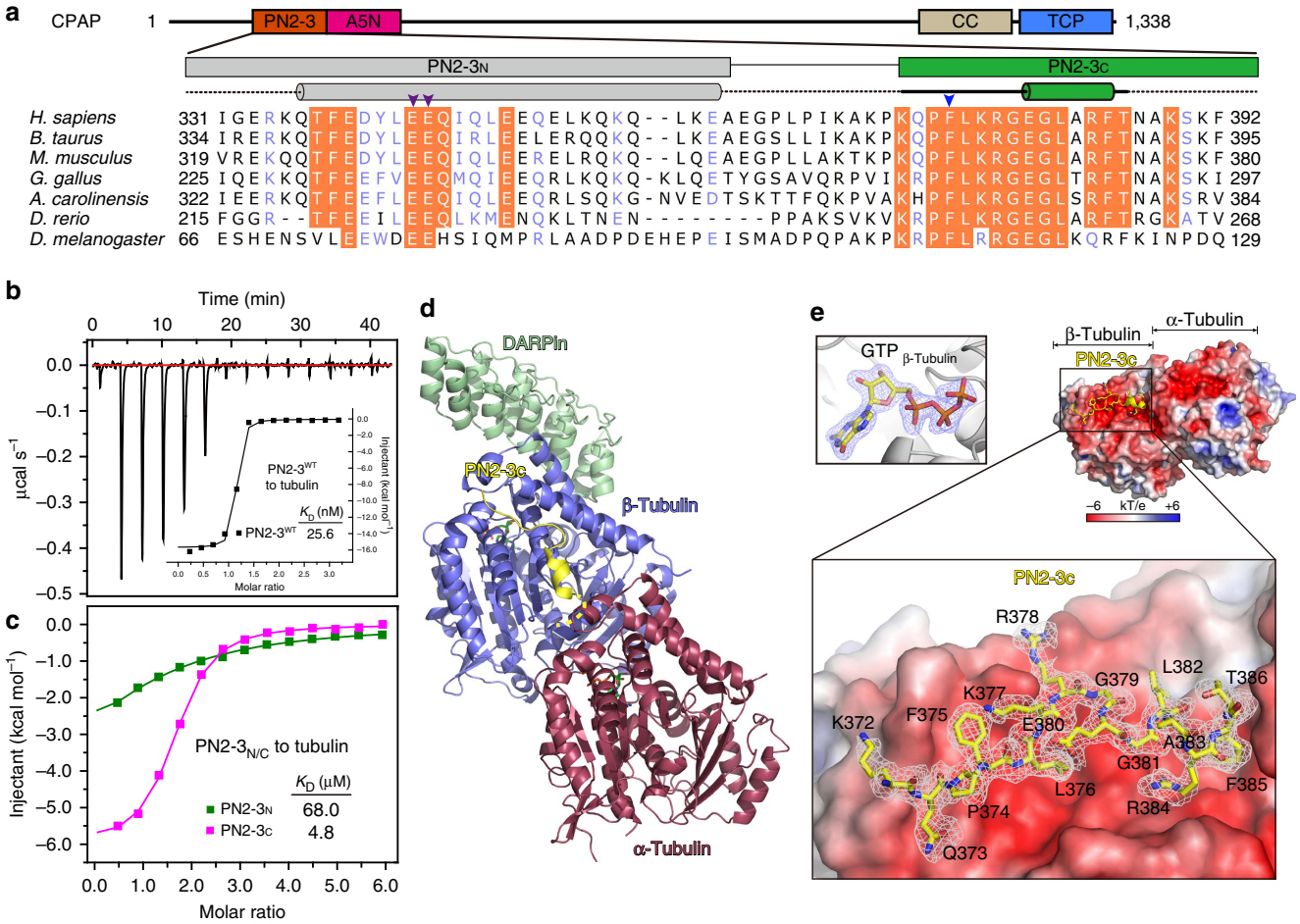

Figure 1 | Molecular basis for PN2-3-tubulin interaction. (**a**) Domain architecture of CPAP and sequence conservation analysis of PN2-3$_N$ and PN2-3$_C$. Arrowheads mark E343-E344 (purple) and F375 (blue). (**b**) ITC titration and fitting curve of wild type (WT) PN2-3 with tubulin. (**c**) Overlay of ITC fitting curves of PN2-3$_N$ (green) and PN2-3$_C$ (magenta) titrated into tubulin. (**d**) Ribbon view of PN2-3$_C$-GTP-tubulin-DARPin complex. Yellow dot line indicates the invisible region of PN2-3$_C$ in density map. GTP, green sticks. (**e**) Close-up view of PN2-3$_C$ loop-helix motif (yellow) docked onto β-tubulin outer surface colored by electrostatic potential (-6 kT e^{-1}, red; $+6$ kT e^{-1}, blue). Fo-Fc omit map (1.5 σ) of PN2-3$_C$ was shown as grey meshes. Top-left, Fo-Fc omit map (blue meshes, 4.5 σ) of GTP.

free tubulin and PN2-3 variants (Supplementary Fig. 5a). Tubulin at a high concentration self-polymerizes into microtubules. While polymerized tubulin could be pelleted by centrifugation, free tubulin remains in solution in the supernatant[17]. When we included PN2-3 variants in this assay, we found that in contrast to PN2-3^{WT}, PN2-3^{F375A} did not prevent tubulin polymerization (Supplementary Fig. 5b). This could be due to the presence of F375, which is required for the formation of high affinity CPAP-tubulin complex (Fig. 2b). In addition, F375-containing PN2-3$_C$ domain binds the β-tubulin at the microtubule outer surface, which might allosterically disrupt microtubule formation by inducing or stabilizing a curved tubulin dimer (Supplementary Fig. 2). Supporting this notion, PN2-3$_C$ alone was sufficient to prevent tubulin from polymerization (Supplementary Fig. 5c). PN2-3$_N$ caps β-tubulin and conceivably has intrinsic microtubule depolymerization activities. However, compared to PN2-3$_C$, PN2-3$_N$ is not sufficient to prevent microtubule polymerization (Supplementary Fig. 5c). This is likely due to the weak binding affinity observed for PN2-3$_N$ and tubulin ($K_D = 68\,\mu M$) as compared to the case of PN2-3$_C$ ($K_D = 4.8\,\mu M$) (Fig. 1c). Similarly, PN2-3$_C^{F375A}$ failed to prevent tubulin from polymerization due to loss of PN2-3-tubulin binding (Supplementary Figs 5c and 6a). We then tested the effects of PN2-3 variants in cytoplasmic microtubules by overexpressing green fluorescent protein (GFP)-tagged PN2-3 variants in HeLa cells. In contrast to PN2-3^{WT}, overexpression of PN2-3^{F375A} did not cause the collapse of cytoplasmic microtubules indicating that *in vitro*, the ability of PN2-3 to bind tubulin and prevent it from polymerization is F375-dependent (Supplementary Fig. 6b).

CPAP-tubulin regulates centriole and cilium lengths. First, we tested the functional significance of CPAP's F375-tubulin interaction in centrosome biogenesis. To test this, we established stable HeLa lines expressing RNAi-resistant GFP-tagged CPAP, and CPAP^{F375A} using bacterial artificial chromosome recombineering (BACs). This system allows expression of gene products under their own endogenous promoters[20,21]. As described previously, treating cells with CPAP-specific siRNA depleted endogenous protein, retaining the RNAi-resistant CPAP (Supplementary Fig. 7a). Expressing wild type siRNA-resistant CPAP completely rescued the effects of siRNA-mediated CPAP depletion as cells proliferated without centrosome duplication defects. In contrast, RNAi-resistant CPAP^{F375A} failed to rescue the centrosome duplication phenotype caused by wild type CPAP depletion. Specifically, when cultured for prolonged periods of time, we noticed a proportion of cells displaying less than two centrosomes reaffirming previous findings that CPAP-tubulin interaction is

Table 1 | Data collection and refinement statistics.

	DARPin-Tubulin-PN2-3_C
Data collection	
Space group	$P2_1$
Cell dimensions	
a, *b*, *c* (Å)	73.9, 91.1, 83.3
α, β, γ (°)	90, 97, 90
Wavelength (Å)	0.9792
Resolution (Å)	50–2.1 (2.17–2.10)*
R_{merge} (%)	12.8 (89.9)
$I/\sigma I$	16.8 (2.5)
Completeness (%)	99.1 (98.2)
Redundancy	4.6 (4.6)
Refinement (F>0)	
Resolution (Å)	50–2.1
No. reflections	63,551
R_{work}/R_{free} (%)	17.8/22.2
No. atoms	
Protein	8021
Ligand	66
Water	597
B-factors (Å^2)	
Protein	29.6
Ligand	21.5
Water	35.3
r.m.s. deviations	
Bond lengths (Å)	0.01
Bond angles (°)	1.26

*Values in parentheses are for highest-resolution shell.

required for centrosome duplication in cultured human cells[11,12] (Supplementary Fig. 7b)

Since, depleting endogenous CPAP perturbs centrosome duplication, we took an alternative approach to study the role of CPAP-tubulin interaction in regulating centriolar- and ciliary-microtubule lengths. We overexpressed GFP-tagged $CPAP^{WT}$ and $CPAP^{F375A}$ in RPE1 cells using lentiviral-transduction. We analyzed ciliated cells and determined daughter centrioles from mother centrioles by immunostaining CP110, a centrosomal protein that localizes to the distal end of daughter centrioles providing a cap-like structure[14,22]. CP110 predominantly localizes to the daughter centriole, which does not template the formation of cilium (Fig. 3a). Compared to $CPAP^{WT}$ expression, $CPAP^{F375A}$, which fails to efficiently bind tubulin, resulted in shorter centrioles. These data suggest the need of a high-affinity CPAP-tubulin interaction for centriolar-microtubule elongation (Fig. 3ai-ii).

We then expressed $CPAP^{EE343RR}$ that perturbs PN2-3's N-terminal helix, which caps the microtubule lumen surface of β-tubulin and possibly unmasks the β-tubulin surface for polymerization (Fig. 2d)[23,24]. To our surprise, $CPAP^{EE343RR}$ expression caused overly long mother and daughter centrioles. In contrast to most of the $CPAP^{F375A}$ centrioles, which were shorter in length, we could readily distinguish and measure the lengthy centrioles induced by $CPAP^{EE343RR}$. The finding that $CPAP^{EE343RR}$ causes longer daughter centrioles, suggests that $CPAP^{EE343RR}$ can affect newly forming microtubule-based structures (Fig. 3aiii-iv and Supplementary Fig. 8b).

Next, we analyzed the significance of CPAP-tubulin interaction in ciliogenesis. Although $CPAP^{F375A}$ expressing cells could assemble cilia, they were shorter in length. Serial sectioning-electron microscopy (EM) identified that they appear structurally normal until the transition zone where they displayed abnormal axonemes with distorted doublet-microtubules (Fig. 3b,c,e and Supplementary Fig. 9). On the other hand, expressing $CPAP^{EE343RR}$ resulted in structurally normal but overly long cilia also causing ~10% of cells to be biciliated (Fig. 3d,e, Supplementary Figs 9 and 10a). EM analyses revealed that biciliated cells contained four centrioles, in which two of them template cilium formation consistently displaying centriolar-appendages, indicating that they are either the mother and/or matured daughter centriole. This data suggests that $CPAP^{EE343RR}$ not only favors centriolar-microtubule elongation but also promotes daughter centrioles to form cilia (Fig. 3d,e and Supplementary Figs 9 and 10b,c).

To exclude that overly long cilia in cells expressing $CPAP^{EE343RR}$ is due to defective ciliary disassembly, we synchronized RPE-1 cells expressing doxycycline inducible $CPAP^{EE343RR}$ at G_0 by serum starvation for 96 h (ref. 25). The doxycycline inducible system prevented cells from forming long cilia caused by constitutive expression of $CPAP^{EE343RR}$. Upon serum stimulation and doxycycline induction, the percentages of cells expressing $CPAP^{WT}$ and $CPAP^{EE343RR}$ re-entering cell cycle concurrent with cilium disassembly did not differ. This excluded the involvement of defective ciliary disassembly in causing long cilia (Supplementary Fig. 11).

CPAP via PN2-3 controls dynamic release of its bound tubulin. Based on the above findings (Figs 1–3), we speculated that in the cytoplasm, CPAP binds GTP-tubulin forming a high-affinity cytoplasmic complex and prevents the bound-tubulin from spontaneous polymerization until targeted to centriolar- and ciliary-microtubule elongation sites during the early phase of centriole/cilium formation. The experiment that supports this idea is the finding of shorter centriolar- and ciliary-microtubules upon $CPAP^{F375A}$ expression, a variant with strongly reduced tubulin interaction (Fig. 3a). At the site of centriolar- and ciliary-microtubule elongation, a mechanism that operates to control tubulin release could then regulate microtubule growth. One factor that could contribute to this regulation to facilitate tubulin release is the uncapping of CPAP's $PN2\text{-}3_N$ from β-tubulin (Supplementary Fig. 12a). It is also known that CPAP/Sas-4 is a dynamically regulated cell cycle protein with cytoplasmic and centriolar pools[11,15]. Thus, centriolar CPAP could be an atypical centriolar-microtubule builder, regulating microtubule growth to define centriolar lengths. This is demonstrated by the overly long centrioles observed upon $CPAP^{EE343RR}$ expression, a variant with reduced tubulin affinity and unmasking β-tubulin surface making it available for tubulin polymerization (Fig. 3 and Supplementary Fig. 12). If this were true, $CPAP^{EE343RR}$ would exhibit an enhanced release of its bound-tubulin via a 'clutch-like' mechanism so as to favor microtubule growth at the onset of centriolar-microtubule assembly (Supplementary Fig. 12a).

To test PN2-3's bound-tubulin releasing ability *in vitro*, we performed microtubule-end tracking assays using GMPCPP (a non-hydrolysable GTP analog) stabilized microtubules and PN2-3 variants (Fig. 4a–c). PN2-3, which can bind tubulin dimers at high affinity but not microtubules, has a microtubule-destabilizing activity primarily harbored in $PN2\text{-}3_C$ (Supplementary Fig. 5)[17,18]. Thus, we measured the rate of PN2-3-mediated microtubule-destabilization as a function of its bound-tubulin releasing ability, with the assumption that PN2-3 is dynamically recycled for continuous microtubule disruption. Consistently, adding $PN2\text{-}3^{WT}$ destabilized microtubules at a slower rate compared to $PN2\text{-}3^{EE343RR}$, implying a faster rate of bound-tubulin release (Fig. 4b,c and Supplementary Movies 1–3). Importantly, these *in vitro* microtubule destabilization activities do not reflect how full-length CPAP functions in cells to regulate centriolar- and ciliary-microtubule growth with excess GTP-tubulin.

To directly analyze CPAP in elongating centrioles of living cells, we expressed inducible CPAP^{WT} and CPAP^{EE343RR} in RPE1 cells. Real time measurements reveal CPAP^{EE343RR} to have faster centriole elongation rates of $\sim 0.014\,\mu m\,min^{-1}$ (CPAP^{WT} $= 0.0017\,\mu m\,min^{-1}$) reaching up to $3.7\,\mu m$ in centriolar length. This suggests that CPAP regulates microtubule

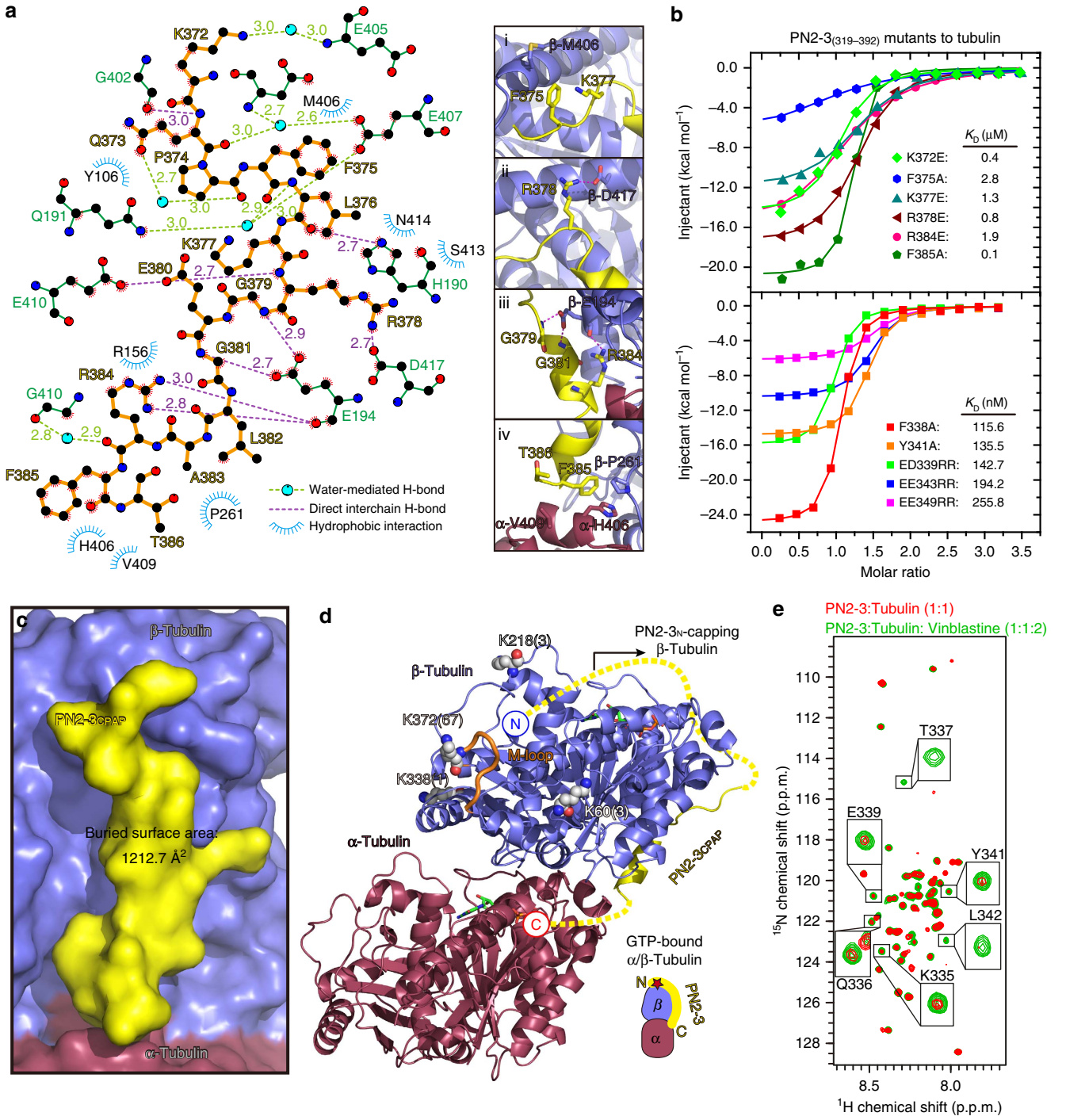

Figure 2 | Interaction details of PN2-3$_C$-tubulin and recognition mode for PN2-3$_N$. (**a**) Left, LigPlot diagram of PN2-3$_C$ and tubulin binding details. The PN2-3$_C$ was colored dark yellow and depicted as thick lines. Right, (i–iv) close-up view and structural illustration of key interaction pairs listed in the LigPlot diagram. Overall structures are in ribbon view and key residues are in stick view. Yellow, PN2-3$_C$; raspberry, α-tubulin; slate, β-tubulin. (**b**) ITC fitting curves of mutant PN2-3 titrated into tubulin dimer with the upper figure for mutations in PN2-3$_C$ and the lower figure for mutations in PN2-3$_N$. (**c**) Surface view of PN2-3$_C$ bound to a tubulin dimer. PN2-3$_C$, β-tubulin, α-tubulin are colored yellow, slate, and raspberry, respectively. Note, PN2-3$_C$ binds to the microtubule outer surface in an anti-parallel orientation along the longitudinal axis of microtubule. (**d**) Structural annotation of CL-MS results over a tubulin dimer. White spheres, lysine residues that cross-link with PN2-3N-terminal amine. Parenthesis, number of CL-MS peaks detected. (**e**) Overlay of ^{1}H,^{15}N-SOFAST HMQC spectra of tubulin-free PN2-3 (black, Supplementary Fig. 4) and tubulin-bound PN2-3 (red) at equimolar ratios. Disappearance/broadening of PN2-3 peaks indicate its binding to tubulin. Upon addition of 2-fold excess of vinblastine (green), some PN2-3 peaks reappear, indicating that vinblastine interferes with PN2-3-tubulin interaction.

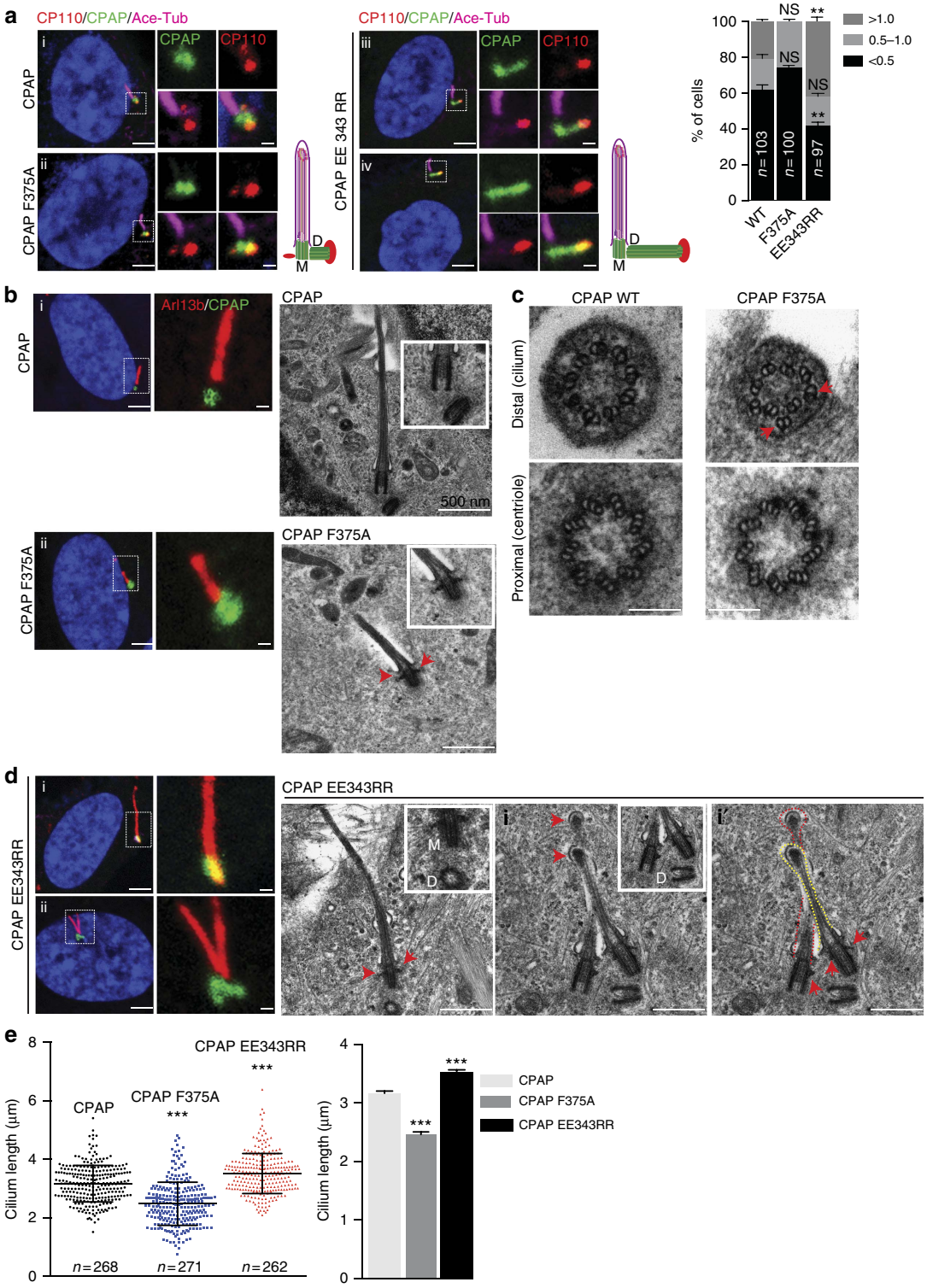

Figure 3 | Effects of CPAP-tubulin interaction on centriolar- and ciliary-microtubule formation in human cells. CPAP^{EE343RR} expression but not CPAP or CPAP^{F375A} (green) causes overly long daughter centriolar- (**a**) and ciliary-microtubules (**b**). The centrosomal protein CP110 (red) caps the distal end of daughter centrioles in (**a**), which does not template cilium formation. Schematic is given at right. Acetylated-α-tubulin (magenta) in (**a**) or Arl13b (red) in (**d**) labels cilia. A bar diagram at top right quantifies percentage of cells and their centriolar lengths ($n=103$ for WT, $n=100$ for CPAP^{F375A} and $n=97$ for CPAP^{EE343RR}), ANOVA, $^{**}P<0.001$. Error bars represent ± s.e.m. Number of experiments (N) = 3. Note that the exact lengths of CPAP^{F375A}, centrioles could sometimes not be measured due to their small size. EM-micrographs of cilia in cells expressing the respective CPAP variants are given at the sides of light microscopy images. Arrows mark centriolar-appendages. (**c**) Serial section-EM of centriole and cilium from cells expressing CPAP^{WT} or CPAP^{F375A}. Arrows mark the abnormally organized ciliary microtubule doublets ($n=32$). Scale bar 100 nm. (**d**) CPAP^{EE343RR} expression causes biciliation (i and i'). Serial sectioning-EM showing single- and double-cilia (arrowheads and red/yellow dotted lines). Red arrows mark centriolar-appendages. In biciliated cells, mother and/or matured daughter centrioles template the formation of cilia. M, mother centriole. D, daughter centriole. Scale bar 500 nm. (**e**) Ciliary-length quantifications. ANOVA, $^{***}P<0.0001$, $n>250$. The error bars represent ± s.e.m. Number of experiments (N) = 3. Scale bar 1 µm.

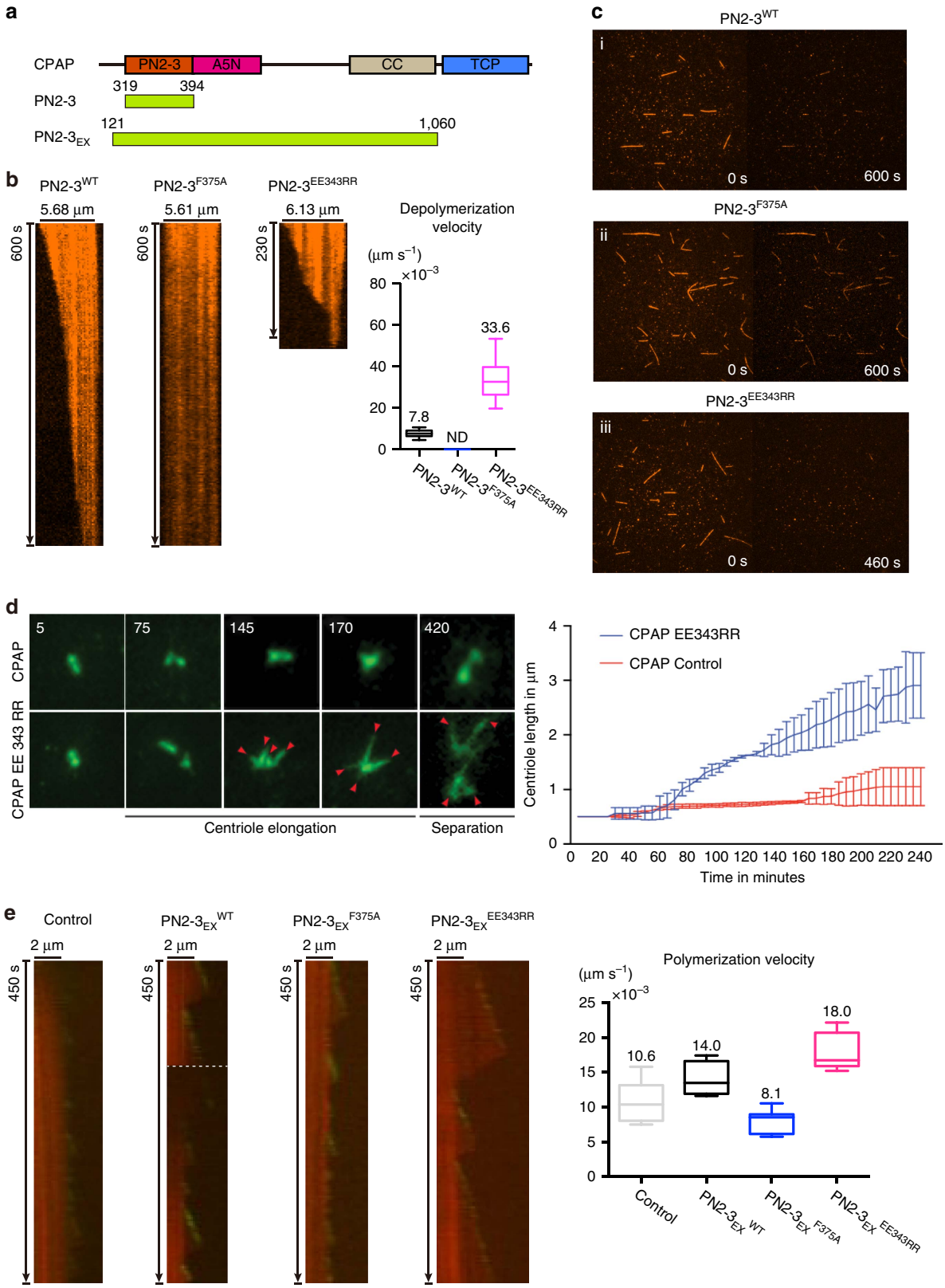

Figure 4 | Microtubule end-tracking and live-imaging measurements of centriolar growth rates. (**a**) Schematic view of PN2-3 and PN2-3$_{EX}$ constructs. (**b**) Kymographs and averaged depolymerization velocities of PN2-3^{WT}, PN2-3^{F375A} and PN2-3^{EE343RR} during microtubule end-tracking assay. (**c**) Snapshots of microtubule end-tracking assays of PN2-3^{WT} (i), PN2-3^{F375A} (ii), and PN2-3^{EE343RR} (iii) at different time points. (**d**) Expression of CPAP^{EE343RR}-GFP but not CPAP^{WT}-GFP causes a rapid centriolar-elongation that is distinct enough to measure in contrast to CPAP^{WT} expression. Arrowheads mark elongating (at 145th and 170th mins) and separating (at 420th mins) centrioles. Centriolar-growth rate curve is given ($n = 57$, CPAP^{EE343RR}; 50, CPAP^{WT}). The error bars represent ± s.d. Number of experiments (N) = 3. (**e**) Kymographs and averaged polymerization velocities of PN2-3$_{EX}^{WT}$, PN2-3$_{EX}^{F375A}$, and PN2-3$_{EX}^{EE343RR}$ during microtubule polymerization experiments.

growth for defined centriolar-microtubule lengths (Fig. 4c, Supplementary Fig. 12b and Supplementary Movies 4–7). Consistently, our fixed experiments also revealed that CPAP^{EE343RR} caused a faster rate of ciliary-microtubule growth (Supplementary Fig. 12c). It thus appears that CPAP regulates the growth of microtubule-based structures through controlled release of its bound tubulin and its ability to function as a centriolar-microtubule builder, both of which occur at the site of centriole assembly.

Extended PN2-3 promotes microtubule polymerization *in vitro*. In order to prove the microtubule polymerization activity of CPAP *in vitro*, we recombinantly prepared an extended CPAP frame spanning from PN2-3 to a C-terminal coiled coil (CC) motif (aa 121–1060, PN2-3$_{EX}$; Fig. 4a) using mammalian cell expression system and conducted microtubule polymerization assays (Fig. 4e and Supplementary Movies 8–11). In an optimized microtubule growth condition in the presence of 15 μM GTP-tubulin, we could observe background microtubule growth at an average rate of $\sim$0.0106 μm s^{-1} without PN2-3$_{EX}$. After adding 1 μM wild type PN2-3$_{EX}$, the microtubule growth rate was increased to $\sim$0.014 μm s^{-1}, suggesting a role of PN2-3$_{EX}$ in prompting microtubule polymerization. Interestingly, PN2-3$_{EX}^{F375A}$ caused slight inhibition of microtubule polymerization with a growth rate of $\sim$0.0081 μm s^{-1}. In consistence with our live imaging experiments of CAPA^{EE343RR}, PN2-3$_{EX}^{EE343RR}$ displayed an enhanced microtubule growth with a rate of $\sim$0.018 μm s^{-1}. In addition, GFP-tagged EB1 (refs 26,27) was used to trace the plus end of growing microtubule. We observed active and dynamic plus end microtubule growth in the presence of PN2-3$_{EX}$, especially in its EE343RR mutant form. These data suggest wild type and EE343RR mutant PN2-3$_{EX}$ may localize at the plus end during the process of microtubule polymerization (Fig. 4e and Supplementary Movies 8–11). PN2-3$_{EX}$ contains a tubulin-binding PN2-3 motif[28], a microtubule-binding A5N motif[17] and a dimerization CC motif[29] (Fig. 4a), which likely constitute as a key element for the observed microtubule polymerization activity. In summary, our *in vitro* microtubule growth studies support a critical role of CPAP in regulating centriolar and ciliary length.

Sas-4-tubulin controls centriole and cilium lengths *in vivo*. We then confirmed whether the Sas-4-tubulin interaction (the fly counterpart of CPAP) has a conserved function in controlling centriolar and ciliary length *in vivo*. To do this, we generated transgenic *Drosophila* expressing endogenous levels of GFP-tagged Sas-4^{WT}, Sas-4^{F112A} (corresponding to CPAP^{F375A}) and Sas-4^{EE78RR} (corresponding to CPAP^{EE343RR}) in Sas-4 null flies (Supplementary Fig. 12d). In contrast to Sas-4^{WT} and Sas-4^{EE78RR}, Sas-4^{F112A} failed to rescue the uncoordination and sterile phenotypes of null flies indicating that Sas-4^{F112}-tubulin interaction is required to form functional sensory cilia and sperm flagella[9,30].

However, Sas-4^{F112A} flies displayed correct centrosome numbers in spermatogonia indicating that Sas-4-tubulin interaction in flies is dispensable for centrosome duplication (Fig. 5a). This allowed us to specifically study the significance of Sas-4-tubulin interaction in centriole length determination *in vivo*. Analyzing mature spermatocytes of Sas-4^{F112A} flies, we found centrioles with significantly reduced lengths. On the other hand, Sas-4^{EE78RR} flies displayed overly elongated centrioles, consistent with observations in human cells (Fig. 5b,d). Examining Sas-4's localization at the elongating centrioles of spermatocytes, we consistently found a concentrated proximal localization of Sas-4^{WT}. In contrast, Sas-4^{EE78RR} that causes elongated centrioles displayed an extended localization along the length of its overly elongated centrioles, coherent with our *in vitro* experiments suggesting that CPAP binds at the plus end of microtubule during polymerization (Figs 4e and 5b,c).

We then performed EM analyzes of Sas-4^{F112A} centrioles to analyze centriolar architecture when Sas-4-tubulin interaction is significantly perturbed. In contrast to Sas-4^{WT} and Sas-4^{EE78RR}, the spermatogonium and spermatocyte centrioles of Sas-4^{F112A} mostly contained doublet instead of triplet centriolar-microtubules (Fig. 6a,b). This finding indicated that Sas-4^{F112}-tubulin interaction is not required for nucleating centriolar-microtubules *per se* but for the formation of third centriolar-microtubules suggesting insufficient tubulin delivery by perturbed Sas-4-tubulin interaction. Indeed, γ-TuRC has been suggested to nucleate the A-microtubule that subsequently templates B-and C-microtubule elongation[31].

When analyzing primary cilia of spermatocytes, we identified that flies expressing Sas-4^{EE78RR} resulted in long cilia. In contrast, spermatocyte cells expressing Sas-4^{F112A} displayed shorter cilia (Fig. 6c). Furthermore, EM analyses revealed that Sas-4^{F112A} cilia displayed incomplete and distorted ciliary microtubules (Fig. 6e). These findings indicate that Sas-4-tubulin interaction is required to form structurally stable and defined lengths of ciliary microtubules. Taken together, these studies indicate that via interacting with tubulin, CPAP/Sas-4 proteins have a conserved function to define centriolar- and ciliary-microtubule lengths.

Discussion

In cells, how a fraction of specialized tubulin from a large cytoplasmic pool is specifically recognized and licensed to form defined numbers and lengths of centriolar- and ciliary-microtubules is poorly understood. In this work, we have undertaken an integrated approach to dissect the conserved function of CPAP-tubulin interaction, which represents a crucial step in understanding centriolar- and ciliary-microtubule length control. Our results support a model in which CPAP/Sas-4 through the different facets of its PN2-3 domain, defines centriolar- and ciliary-microtubule lengths. Our structural studies reveal that PN2-3 embraces a 'necklace-like' mode for tubulin recognition, in which, CPAP via its PN2-3$_N$ targets the lumen surface of β-tubulin, and PN2-3$_C$ loop-helix motif occupies the β-tubulin microtubule outer surface (Fig. 2d). This unique binding mode practically approves the formation of a high-affinity CPAP-GTP-tubulin complex and simultaneously prevents the polymerization of its bound GTP-tubulin, which is reactive, unstable, and ready for microtubule build-up once released. Noticeably, the last eight C-terminal residues of PN2-3$_C$ were not visible in the electron density map. However, these residues together with F385, seem to play important roles in microtubule depolymerization, as the PN2-3$_{C2}$ variant with truncation of its last ten residues, almost failed to depolymerize GTP-stabilized microtubules, when compared with full length PN2-3$_C$ (Supplementary Fig. 6a).

To our knowledge, CPAP is the first centrosomal protein shown to form a high-affinity complex with tubulin, making it unavailable for polymerization. Although, we do not yet fully understand the mechanisms by which how the CPAP-bound tubulin is released at the sites of centriole assembly, it appears that controlled delivery of tubulin is essential for constructing defined numbers and lengths of centriolar- and ciliary-microtubules (Figs 3,5 and 6). One of the potential mechanisms that could facilitate tubulin release at the site of centriole assembly is perhaps uncapping of CPAP's PN2-3$_N$ from the β-tubulin surface. Thus, the cleared tubulin surface is then

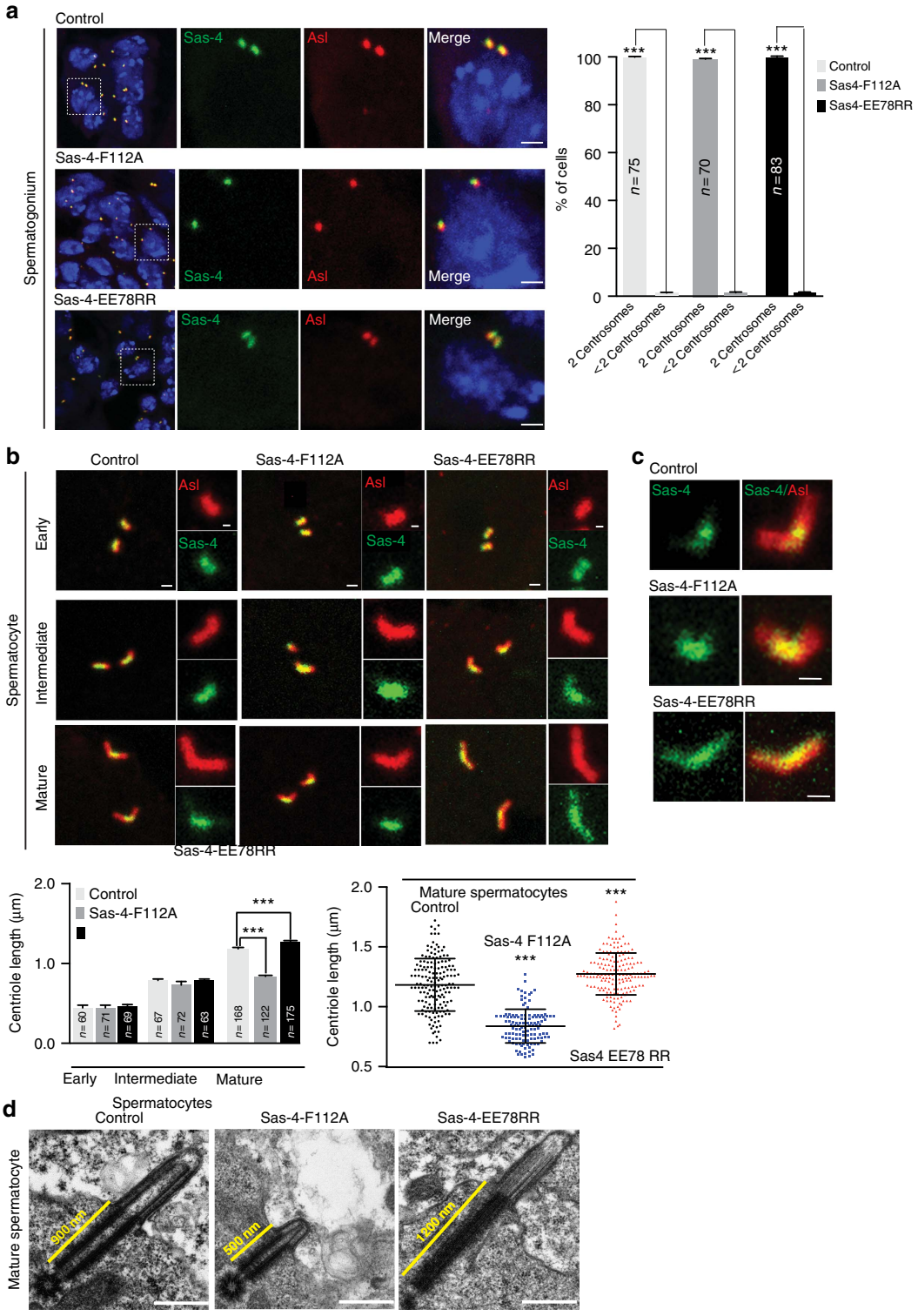

Figure 5 | Effects of Sas-4-tubulin interaction on centriolar- and ciliary-microtubule formation in *Drosophila*. (**a**) Sas-4-tubulin interaction is dispensable for centrosome duplication in spermatogonium cells. Neither Sas-4 variant prevents centrosome duplication as numerically normal numbers of centrosomes were found in *Drosophila* expressing GFP tagged Sas-4^{WT}, Sas-4^{F112A}, or Sas-4^{EE78RR} in Sas-4 null flies. Quantification is shown at top right. Centrosomes are co-labeled with Asl (red) ($n \geq 70$), ANOVA, ***$P < 0.0001$. Error bars represent ± s.e.m. Number of experiments (N) = 3. Scale bar, 1 µm. (**b**) Mature but not early or intermediate spermatocyte centrioles of *Drosophila* expressing Sas-4^{EE78RR} (green) display long centrioles. Asl (red) labels the elongating centrioles. Scale bar 1 µm (insets 0.5 µm). (**c**) Sas-4 localization in mature spermatocyte centrioles. In contrast to Sas-4^{WT} (control) and Sas-4^{F112A}, Sas-4^{EE78RR} displays an extended localization all along the centriole length. Length measurements are given at bottom. ANOVA, ***$P < 0.0001$, ($n > 120$). The error bars represent ± s.e.m. Scale bar 1 µm. (**d**) Longitudinal EM-sections of mature spermatocytes expressing Sas-4^{WT} (control), Sas-4^{F112A} and Sas-4^{EE78RR}. Sas-4^{EE78RR} expression causes long centrioles. In contrast, Sas-4^{F112A} fails to elongate centrioles. Scale bar 500 nm.

available for polymerization into micrometer scale centriolar-microtubules. This is supported by our experiments with CPAP^{EE343RR} / Sas-4^{EE78RR} and CPAP PN2-3$^{EE343RR}_{EX}$ variants with reduced tubulin affinity and unmasking of the β-tubulin surface causing overly long centriolar-microtubules (Figs 3d,4c, 5b and 6d).

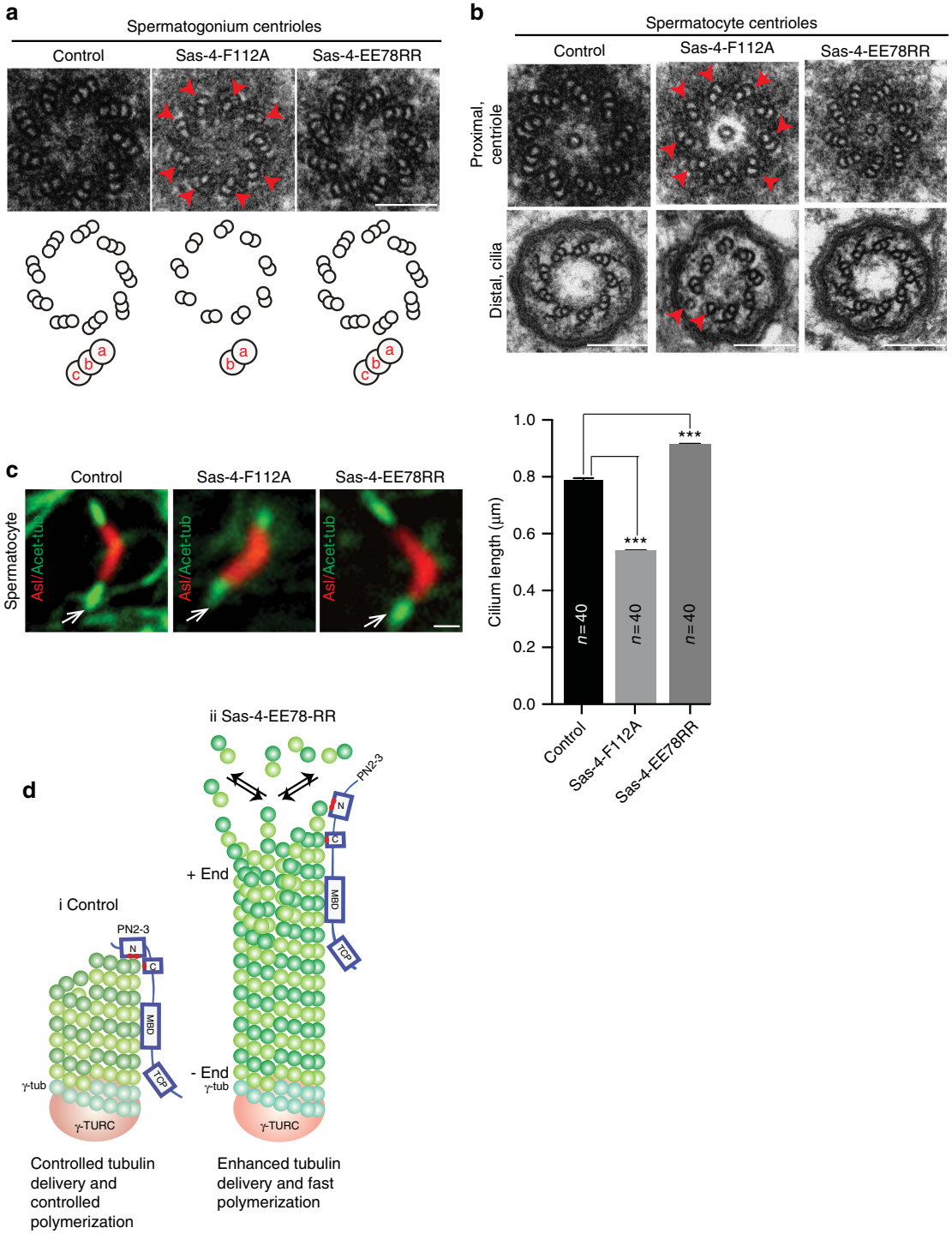

Figure 6 | Effects of Sas-4-tubulin interaction on centriolar and ciliary architecture *in vivo*. EM-micrographs displaying centrioles of spermatogonium. Scale bar 100 nm. (**a**) and matured spermatocyte cells (**b**). In contrast to Sas-4^{WT} and Sas-4^{EE78RR}, Sas-4^{F112A} centrioles contain doublet- instead of triplet-microtubules and aberrant ciliary microtubules (arrowheads and cartoon). (**c**) Primary cilia of matured spermatocytes expressing Sas-4^{WT}, Sas-4^{F112A} and Sas-4^{EE78RR}. Compared to Sas-4^{WT}, Sas-4^{EE78RR} spermatocytes display long cilia (arrows). In contrast, Sas-4^{F112A} spermatocytes form cilia with reduced lengths. Asl (red) labels elongating centrioles and acetylated α-tubulin (green and arrows) labels primary cilia. Bar diagrams at right show the ciliary length measurements ($n = 40$). ANOVA, $^{***}P < 0.0001$. Error bars represent ± s.e.m. Scale bar, 1 μm. Number of experiments (N) = 3. Scale bar, 1 μm (**d**) Hypothetical model depicts how Sas-4^{EE78RR} differs from Sas-4^{WT} in promoting centriolar microtubule growth. Various domains of Sas-4 are shown. Red dots mark the mutations studied at the N- and C-terminus of PN2-3. Microtubule-binding domain (MBD) and TCP domain that are C-terminus to PN2-3 are shown.

The finding that CPAP^{EE343RR} causes overly long daughter centrioles and enhances ciliary lengths without affecting mother centrioles suggests that CPAP specifically acts on growing microtubule-based structures. Although, these experiments indirectly suggest that CPAP could function as a centriolar-microtubule builder, currently we are unable to dissect centriole-specific CPAP functions. Thus, it is unknown how CPAP spatiotemporally exerts both its tubulin binding and polymerization activities. Since CPAP is a cell cycle regulated protein, it is likely that cell cycle-dependent posttranslational modifications and its interaction partners including centriolar-microtubule length determining factors are required to modulate CPAP's tubulin binding and polymerization activities[9–11,14,32,33] As centriolar-microtubules markedly differ from cytoplasmic microtubules, experiments employing tools that allow inducible expression of centriole-specific CPAP or its microtubule bound atomic structure are additionally required to solve the puzzle of how CPAP acts on centriolar-microtubules.

CPAP^{EE343RR} expression causes enhanced ciliogenesis. This finding is strikingly similar to phenotypes observed when Kif24, a centriolar kinesin is depleted[33]. Interestingly, Kif24 specifically acts on mother centrioles and possesses microtubule-depolymerizing activity. Thus, it is tempting to speculate that an enhanced expression of CPAP^{EE343RR} could counteract endogenous Kif24 to promote ciliogenesis. Taken together, several questions remain, requiring future studies.

Although, our *in vitro* experiments suggest a possible role for CPAP functioning as an atypical centriolar-microtubule builder, our *in vivo* experiments in flies seem to support Sas-4's role mainly as a regulator of tubulin release at the onset of centriolar-microtubule elongation. The experiment that highlights this aspect is the proximal localization of endogenous Sas-4 at the elongating spermatocyte centrioles (Fig. 5b)[34,35]. This finding supports an idea that Sas-4 has a tendency to release tubulin to control centriolar-microtubule growth independent from its localization at the distal end of centrioles. CPAP at the distal end of the centriole could play a role in regulating the growing end of centriolar-microtubules (Figs 5c and 6d). The tubulin incorporation ability of Sas-4 is further supported by our EM experiments revealing doublet instead of triplet centriolar-microtubules in flies expressing Sas-4^{F112A}, a variant that strongly reduces its interaction with tubulin. These findings not only support the tubulin incorporation aspect of Sas-4 but also highlight the requirement of other factors for centriolar-microtubule growth.

How does CPAP/Sas-4 play a role in ciliary microtubule growth control? It is known that during cilium construction, IFT machineries transport ciliary building blocks of tubulin from the cytoplasmic ciliary base to the tip[6–8]. As CPAP/Sas-4 mainly localizes to the ciliary base, it rules out a direct role for CPAP in ciliary microtubule elongation at the ciliary tip. Thus, CPAP/Sas-4 likely controls cilia growth indirectly by regulating the available pool of unpolymerized soluble tubulin at the ciliary base. This diffusible tubulin is then concentrated and transported by intraflagellar transport proteins for cilia elongation[6–8]. If this is true, there could be an interaction between CPAP-tubulin complex and a subset of IFT particles. Future experiments revealing these molecular interactions will help in linking cytoplasmic tubulin recognition and their subsequent transport within the cilium by IFTs.

As free tubulin is ubiquitously present in cells, this raises the possibility of forming increased numbers and lengths of centriolar and ciliary structures. However, cells have strict mechanisms to prevent this. One such mechanism is CPAP/Sas-4-tubulin in the cytoplasm. Under physiological conditions, CPAP/Sas-4 has lower expression levels in contrast to free tubulins in cells[15]. Thus, at equilibrium, the amount of cytoplasmic tubulin bound by CPAP/Sas-4 making it unavailable for polymerization would only be a small fraction of the free tubulin pool. Therefore, it makes sense that CPAP/Sas-4 has a dedicated function in binding limited amounts of cytoplasmic tubulin and licenses them for centriolar- and ciliary-microtubules, which is then spatiotemporally regulated for constructing defined numbers and lengths of centriolar and ciliary structures.

Methods

Protein and peptide preparation. The cDNA encoding human CPAP (UniProtKB: Q9HC77) PN2-3 domain (aa 319-394) was cloned into a modified pRSFDuet vector with an N-terminal 10xHis tag followed by a PreScission^{Tm} protease cleavage site. Recombinant wild type and mutant PN2-3 proteins were overexpressed in *E. coli* BL21 (DE3). After overnight induction by 0.2 mM isopropyl β-D-thiogalactoside (IPTG) at 20 °C in LB medium, cells were harvested and suspended in buffer: 20 mM Tris, 200 mM NaCl, pH 8.0. Then cells were lysed with an Emulsiflex C3 (Avestin) high-pressure homogenizer. After centrifugation at 32,000 × *g*, the supernatant was applied to a HisTrap column (GE Healthcare), and the protein was eluted with a linear imidazole gradient from 50 to 500 mM. The resultant protein was digested overnight by PreScission protease to remove 10xHis tag, and further purified by HiTrap Heparin HP and Superdex 200 columns (GE Healthcare). Both wild type and mutant PN2-3 proteins were concentrated to 1 mM in 1xBRB80 buffer (80 mM PIPES-K, 1 mM $MgCl_2$, 1 mM EGTA, pH 6.8), and stored at −80 °C for future use.

Human CPAP PN2-3$_{EX}$ (aa 121-1060) was cloned into the pMlink vector (gifted from Yigong Shi's lab) with an N-terminal 2xStrep-Flag tag, and point mutations were further introduced following the same method described above. Recombinant wild type and mutant PN2-3$_{EX}$ proteins were expressed in HEK 293F cells (Invitrogen), which cultured in SMM 293 T-I medium (Sino Biological Inc.) with shaking (3.5 × *g*) at 37 °C under 5% CO_2 and 75% humidity. When cell density reached 1.5×10^6 cells per ml, wild type or mutant PN2-3$_{EX}$ plasmids were transfected into cells using titrated concentration of 25-KDa linear polyethylenimines (PEIs) (Polysciences). After 60 h from transfection, cells were harvested by centrifuge at 800 × *g* and resuspended in a lysis buffer containing 20 mM Tris, 200 mM NaCl, pH 8.0, and protease inhibitor cocktails (Amresco). Cell lysis was conducted by sonication on ice, and the suspension was centrifuged at 38,000 × *g* for 1 h to remove any cell debris. The supernatant was incubated with Strep-Tactin Superflow (IBA BioTAGnology) beads for 30 min at 4 °C. The resin was washed three times, each with 10 ml lysis buffer, and wild type or mutant PN2-3$_{EX}$ proteins were finally eluted with lysis buffer supplied with 10 mM d-Desthiobiotin (Sigma).

The codon-optimized DARPin cDNA was assembled from a dozen of DNA oligos following a reported method[36], and then cloned into the pRSFDuet vector (Novagen) with an N-terminal 6xHis tag. Recombinant DARPin was overexpressed in *E. coli* BL21 (DE3) by overnight induction using 0.2 mM IPTG at 20 °C. After cell harvest and lysis, the 6xHis DARPin protein was purified to homogeneity over successive HisTrap, anion exchange Q, and Superdex 200 columns (GE Healthcare). The protein was concentrated to 1 mM in 1xBRB80 buffer and stored at −80 °C for future use.

Recombinant GFP-tagged fly EB1 protein was expressed in *E. coli* Bl21 (DE3) and prepared following the method reported previously[26] with minimum modifications.

Peptides of PN2-3$_N$ (aa 323-361), PN2-3$_C$ (aa 372-394), and other PN2-3$_C$ variants were synthesized in >95% purity by SciLight Biotechnology.

Complex reconstitution and crystallization. Porcine/bovine brain tubulin was purified by modified procedures of two cycles of polymerization and depolymerization[37]. The purified tubulin was stored at −80 °C in 1xBRB80 buffer until use.

DARPin-tubulin complex was assembled by mixing DARPin and tubulin in a 1.5:1 molar ratio (DARPin to tubulin). The sample was incubated at 4 °C for 1 h and then loaded onto a pre-equilibrated Superdex 200 column (GE Healthcare) using 1xBRB80 buffer. Fractions responding to DARPin-tubulin complex were pooled and concentrated for future use.

DARPin-tubulin-PN2-3$_C$ complex was reconstituted by mixing PN2-3$_C$ with DARPin-tubulin complex in the molar ration of 1.2:1 (PN2-3$_C$ to DARPin-tubulin) at a total concentration of 20 mg ml^{-1}. After incubation at 4 °C for 1 h, crystallization screen was performed using an Art Robbins Gryphon crystallization robot by mixing equal volumes of DARPin-tubulin-PN2-3$_C$ complex with different screening conditions from the commercial crystallization kits. Crystals appeared three days after tray set-up under 9 °C from the Hampton Research PEG/Ion crystallization screen kit. Manual crystallization and optimization were then conducted via the sitting-drop vapor diffusion method, and diffraction quality crystals were finally obtained under the reservoir condition of 0.2 M potassium sodium tartrate, 20% (w/v) polyethylene glycol 3,000, and 4% polypropylene glycol P 400.

Data collection and structure determination. Crystals were briefly soaked in a cryo-protectant composed of reservoir solution supplemented with 20% glycerol, and were flash frozen in liquid nitrogen for data collection at 100 K. Data collection was performed at beamline BL17U at the Shanghai Synchrotron Radiation Facility under the wavelength of 0.9792 Å. Diffraction data were indexed, integrated and merged using the HKL2000 software package (http://www.hkl-xray.com/).

The structure of DARPin-tubulin-PN2-3_C was solved by the molecular replacement using MOLREP[38,39] with the published DARPin-tubulin structure (PDB code: 4DRX) as search model. Structure refinement was performed using PHENIX[40] with iterative manual model building using COOT[41]. In the final structure, PN2-3_C residues 372–386 were modelled. The last eight residues (387–394) are invisible due to flexibility. Data collection and structure refinement statistics were shown in Table 1. All structural figures were prepared using PYMOL (http://www.pymol.org/).

Isothermal titration calorimetry. Calorimetric experiments were conducted at 15 °C with a MicroCal iTC200 instrument (GE Healthcare). All proteins and peptides, including tubulin, wild type and mutant PN2-3 proteins/peptides, were dialyzed against the 1 × BRB80 buffer (80 mM PIPES-K, 1 mM $MgCl_2$, 1 mM EGTA, pH 6.8) prior to titration. Concentration of tubulin and PN2-3 proteins were determined by their respective absorbance at 280 nm. Peptides were quantified by weighing on a large scale and further confirmed and adjusted by their respective absorbance at UV_{205} *(14)*. Acquired calorimetric titration data were analyzed using Origin 7.0 (GE Healthcare) using the 'One Set of Binding Sites' fitting model. In order to avoid microtubule formation, tubulin sample was kept under low temperature (< 15 °C) and low concentration (< 15 μM) during wild type and mutant PN2-3 titrations. Specifically, for ITC curves in Fig. 1d and Supplementary Fig. 3c, a sample cell tubulin concentration of 9 μM was used with resultant titration *C*-values ranging from 3.2 (PN2-3^{F375A}) to 360 (PN2-3^{WT}). For ITC titrations in Supplementary Fig. 1, a tubulin or DARPin-tubulin concentration of 36 μM was used to ensure reasonable titration *C*-value (0.5–10) and measurable heat signal.

Microtubule pelleting assays. For microtubule co-sedimentation pelleting assays in Supplementary Figs 6 and 7, tubulin polymerization was first conducted at 37 °C using either GMPCPP or 33% (v/v) glycerol-containing buffer (80 mM PIPES-K, 5 mM $MgCl_2$, 0.5 mM EGTA, 33% (v/v) glycerol). After centrifugation at room temperature, microtubules were harvested and re-suspended in warm 1 × BRB80 buffer. Different amount of PN2-3 proteins/peptides were then added and incubated at 37 °C for 20 min. After centrifugation under 100,000 × *g* at room temperature, all supernatant and pellet fractions were analyzed using SDS-PAGE.

Cross-linking mass spectrometry. Equal molar of prepared PN2-3 and tubulin proteins were mixed and incubated at 25 °C for 10 min. 5- to 80-fold excess BS^3 was used to perform cross-linking reaction between PN2-3 and tubulin. After incubate reaction systems at 25 °C for 1 h, final concentration of 1 mM Tris base was added to stop reaction. The resultant sample was then applied to SDS-PAGE, and the cross-linked band was excised for trypsin digestion with or without prior reduction and alkylation in 50 mM ammonium bicarbonate at 37 °C overnight.

The peptides were extracted twice with 1% trifluoroacetic acid in 50% acetonitrile aqueous solution for 30 min. The extractions were then centrifuged in a speedvac to reduce the volume. For LC-MS/MS analysis, the digestion product was separated by a 65 min gradient elution at a flow rate 0.25 μl min^{-1} with the EASY-nLCII integrated nano-HPLC system (Proxeon, Denmark), which was directly interfaced with the Thermo Q Exactive mass spectrometer. The analytical column was a home-made fused silica capillary column (75 μm ID, 150 mm length; Upchurch, Oak Harbor, WA) packed with C-18 resin (300 A, 5 μm, Varian, Lexington, MA). Mobile phase A consisted of 0.1% formic acid, and mobile phase B consisted of 100% acetonitrile and 0.1% formic acid. The Q Exactive mass spectrometer was operated in the data-dependent acquisition mode using the Xcalibur 2.0.7 software and there is a single full-scan mass spectrum in the Orbitrap (400–1800 m z^{-1}, 30,000 resolution) followed by 20 data-dependent MS/MS scans at 35% normalized collision energy. The MS/MS spectra for cross-linked peptides from each LC-MS/MS run were searched against the selected database using the pLink program[42].

Data availability. Coordinates have been deposited at the Protein Data Bank under accession code 5EIB. The data that support the findings of this study are available from the corresponding author upon request.

References

1. Azimzadeh, J. & Marshall, W. F. Building the Centriole. *Current biology: CB* **20,** R816–R825 (2010).
2. Marshall, W. F. What is the function of centrioles? *J Cell Biochem.* **100,** 916–922 (2007).
3. Avidor-Reiss, T. & Gopalakrishnan, J. Building a centriole. *Current opinion in cell biology* **25,** 72–77 (2013).
4. Nachury, M. V. How do cilia organize signalling cascades? *Philosophical transactions of the Royal Society of London. Series B, Biological sciences* **369,** 369–378 (2014).
5. Nigg, E. A. & Raff, J. W. Centrioles, centrosomes, and cilia in health and disease. *Cell* **139,** 663–678 (2009).
6. Ishikawa, H. & Marshall, W. F. Ciliogenesis: building the cell's antenna. *Nature reviews. Molecular cell biology* **12,** 222–234 (2011).
7. Bhogaraju, S. *et al.* Molecular basis of tubulin transport within the cilium by IFT74 and IFT81. *Science* **341,** 1009–1012 (2013).
8. Craft, J. M., Harris, J. A., Hyman, S., Kner, P. & Lechtreck, K. F. Tubulin transport by IFT is upregulated during ciliary growth by a cilium-autonomous mechanism. *The Journal of cell biology* **208,** 223–237 (2015).
9. Gopalakrishnan, J. *et al.* Tubulin nucleotide status controls Sas-4-dependent pericentriolar material recruitment. *Nature cell biology* **14,** 865–873 (2012).
10. Lin, Y. N. *et al.* CEP120 interacts with CPAP and positively regulates centriole elongation. *The Journal of cell biology* **202,** 211–219 (2013).
11. Tang, C. J., Fu, R. H., Wu, K. S., Hsu, W. B. & Tang, T. K. CPAP is a cell-cycle regulated protein that controls centriole length. *Nature cell biology* **11,** 825–831 (2009).
12. Wu, K. S. & Tang, T. K. CPAP is required for cilia formation in neuronal cells. *Biology open* **1,** 559–565 (2012).
13. Kohlmaier, G. *et al.* Overly long centrioles and defective cell division upon excess of the SAS-4-related protein CPAP. *Current biology: CB* **19,** 1012–1018 (2009).
14. Schmidt, T. I. *et al.* Control of centriole length by CPAP and CP110. *Current biology: CB* **19,** 1005–1011 (2009).
15. Dammermann, A., Maddox, P. S., Desai, A. & Oegema, K. SAS-4 is recruited to a dynamic structure in newly forming centrioles that is stabilized by the gamma-tubulin-mediated addition of centriolar microtubules. *The Journal of cell biology* **180,** 771–785 (2008).
16. Zheng, Y., Wong, M. L., Alberts, B. & Mitchison, T. Nucleation of microtubule assembly by a gamma-tubulin-containing ring complex. *Nature* **378,** 578–583 (1995).
17. Hsu, W. B. *et al.* Functional characterization of the microtubule-binding and -destabilizing domains of CPAP and d-SAS-4. *Experimental cell research* **314,** 2591–2602 (2008).
18. Cormier, A. *et al.* The PN2-3 domain of centrosomal P4.1-associated protein implements a novel mechanism for tubulin sequestration. *The Journal of biological chemistry* **284,** 6909–6917 (2009).
19. Pecqueur, L. *et al.* A designed ankyrin repeat protein selected to bind to tubulin caps the microtubule plus end. *Proceedings of the National Academy of Sciences of the United States of America* **109,** 12011–12016 (2012).
20. Poser, I. *et al.* BAC TransgeneOmics: a high-throughput method for exploration of protein function in mammals. *Nature methods* **5,** 409–415 (2008).
21. Zheng, X. *et al.* Conserved TCP domain of Sas-4/CPAP is essential for pericentriolar material tethering during centrosome biogenesis. *Proceedings of the National Academy of Sciences of the United States of America* **111,** E354–E363 (2014).
22. Kobayashi, T. & Dynlacht, B. D. Regulating the transition from centriole to basal body. *The Journal of cell biology* **193,** 435–444 (2011).
23. Howard, J. & Hyman, A. A. Dynamics and mechanics of the microtubule plus end. *Nature* **422,** 753–758 (2003).
24. Desai, A. & Mitchison, T. J. Microtubule polymerization dynamics. *Annual review of cell and developmental biology* **13,** 83–117 (1997).
25. Pugacheva, E. N., Jablonski, S. A., Hartman, T. R., Henske, E. P. & Golemis, E. A. HEF1-dependent Aurora A activation induces disassembly of the primary cilium. *Cell* **129,** 1351–1363 (2007).
26. Li, W. *et al.* EB1 promotes microtubule dynamics by recruiting Sentin in Drosophila cells. *The Journal of cell biology* **193,** 973–983 (2011).
27. Bieling, P. *et al.* Reconstitution of a microtubule plus-end tracking system *in vitro*. *Nature* **450,** 1100–1105 (2007).
28. Hung, L. Y., Chen, H. L., Chang, C. W., Li, B. R. & Tang, T. K. Identification of a novel microtubule-destabilizing motif in CPAP that binds to tubulin heterodimers and inhibits microtubule assembly. *Molecular biology of the cell* **15,** 2697–2706 (2004).
29. Zhao, L. *et al.* Dimerization of CPAP orchestrates centrosome cohesion plasticity. *The Journal of biological chemistry* **285,** 2488–2497 (2010).
30. Basto, R. *et al.* Flies without centrioles. *Cell* **125,** 1375–1386 (2006).
31. Guichard, P., Chretien, D., Marco, S. & Tassin, A. M. Procentriole assembly revealed by cryo-electron tomography. *The EMBO journal* **29,** 1565–1572 (2010).
32. Tang, C. J. *et al.* The human microcephaly protein STIL interacts with CPAP and is required for procentriole formation. *The EMBO journal* **30,** 4790–4804 (2011).
33. Kobayashi, T., Tsang, W. Y., Li, J., Lane, W. & Dynlacht, B. D. Centriolar kinesin Kif24 interacts with CP110 to remodel microtubules and regulate ciliogenesis. *Cell* **145,** 914–925 (2011).

34. Blachon, S. *et al.* Drosophila asterless and vertebrate Cep152 Are orthologs essential for centriole duplication. *Genetics* **180,** 2081–2094 (2008).
35. Gopalakrishnan, J. *et al.* Sas-4 provides a scaffold for cytoplasmic complexes and tethers them in a centrosome. *Nature communications* **2,** 359 (2011).
36. Stemmer, W. P., Crameri, A., Ha, K. D., Brennan, T. M. & Heyneker, H. L. Single-step assembly of a gene and entire plasmid from large numbers of oligodeoxyribonucleotides. *Gene* **164,** 49–53 (1995).
37. Mitchison, T. & Kirschner, M. Dynamic instability of microtubule growth. *Nature* **312,** 237–242 (1984).
38. Vagin, A. A. & Teplyakov, A. MOLREP: an Automated Program for Molecular Replacement. *J Appl Crystallogr* **30,** 1022–1025 (1997).
39. Vagin, A. & Teplyakov, A. Molecular replacement with MOLREP. *Acta crystallographica. Section D, Biological crystallography* **66,** 22–25 (2010).
40. Adams, P. D. *et al.* PHENIX: a comprehensive Python-based system for macromolecular structure solution. *Acta crystallographica. Section D, Biological crystallography* **66,** 213–221 (2010).
41. Emsley, P. & Cowtan, K. Coot: model-building tools for molecular graphics. *Acta crystallographica. Section D, Biological crystallography* **60,** 2126–2132 (2004).
42. Yang, B. *et al.* Identification of cross-linked peptides from complex samples. *Nature methods* **9,** 904–906 (2012).

Acknowledgements

We thank the staff members at beamline BL17U of the Shanghai Synchrotron Radiation Facility and Dr S. Fan at Tsinghua Center for Structural Biology for his assistance in data collection. We thank Drs. Y. Wang and C. Chen for technical support in TIRF-based microtubule end-tracking assays and the China National Center for Protein Sciences Beijing for providing facility support. This work was supported by grants from the Human Frontier Science Program (HFSP) RGY0064/2015 to J.G. and H.L., the Natural Science Foundation of China General Program 31470720 to H.L., the Major State Basic Research Development Program in China 2015CB910503 to H.L., and Deutsche Forschungsgemeinschaft (DFG) GO 2301/2-1 to J.G.

Author contributions

H.L. and J.G. conceived and supervised this study; X.Z., A.R., J.G. and H.L. designed the experiments; X.Z. and S.Z. performed the X-ray crystallography, cross-linking mass spectrometry, microtubule pelleting assays, ITC and TIRF studies under the guidance of H.L.; A.R. and L.M.G. performed the cell culture, western blot, transgenic flies, immunofluorescence and light microscopy with help from A.M. and A.W.; K.S. and M.S. performed NMR spectroscopy; M.G., M.R., and G.C. performed electron microscopy; S.F. and H.D. performed mass spectrometry; W.L. and G.O. helped with TIRF study; P.W., A.P. I.P. and A.A.H. provided expertise in molecular biology and critical feedback; X.Z., A.R., J.G. and H.L. wrote the manuscript. All authors reviewed the results and approved the final version of the manuscript.

Additional information

Supplementary Information accompanies this paper at http://www.nature.com/naturecommunications

Competing financial interests: The authors declare no competing financial interests.

Reprints and permission information is available online at http://npg.nature.com/reprintsandpermissions/

How to cite this article: Zheng, X. *et al.* Molecular basis for CPAP-tubulin interaction in controlling centriolar and ciliary length. *Nat. Commun.* 7:11874 doi: 10.1038/ncomms11874 (2016).

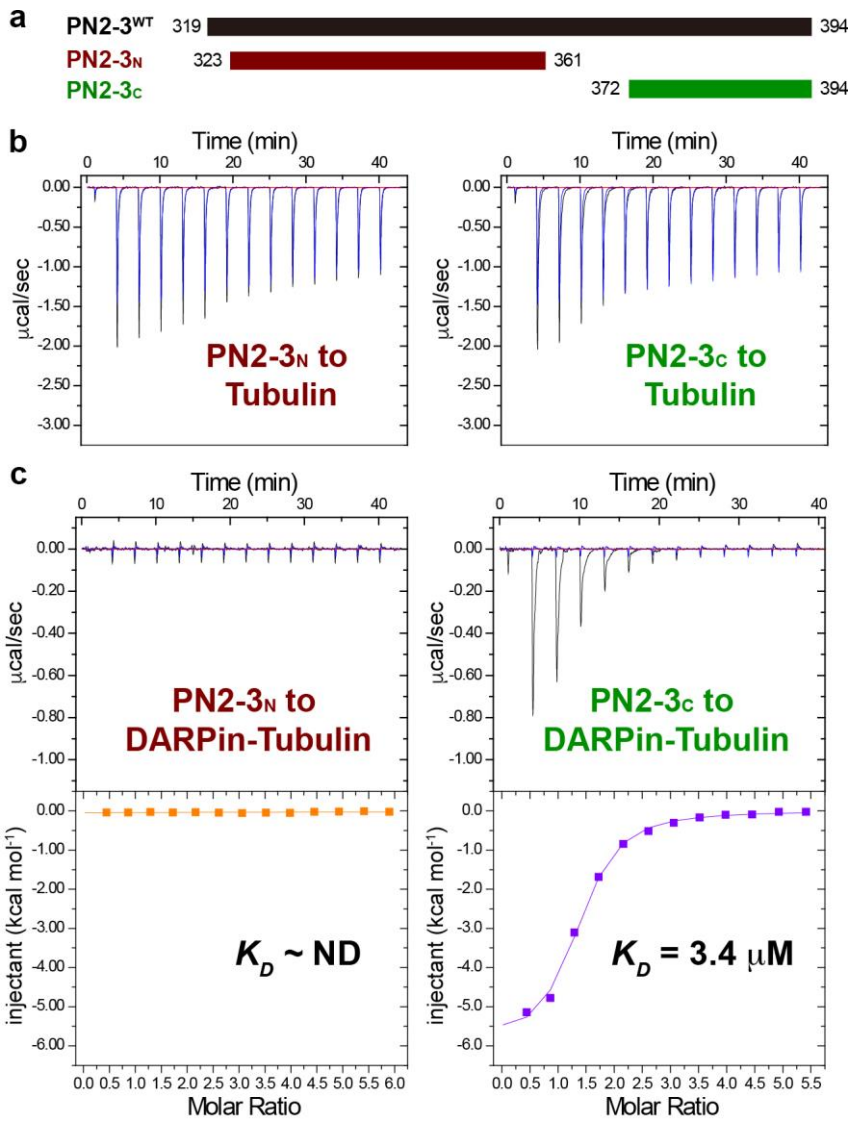

Supplementary Figure 1. DARPin and PN2-3$_C$ are compatible for tubulin dimer binding. (a) Diagrams of wild type PN2-3 (PN2-3$_{WT}$), PN2-3$_N$ and PN2-3$_C$. **(b)** ITC titration curves of PN2-3$_N$ (1 mM) and PN2-3$_C$ (1mM) titrated into tubulin dimer (36 µM). **(c)** ITC titration and fitting curves PN2-3$_N$ (1 mM) and PN2-3$_C$ (1mM) titrated into DARPin-tubulin dimer (36 µM). Background titrations of buffer to tubulin in **(b)** and **(c)** were shown as blue curves and overlaid to their respective peptide sample titrations. Peptide to buffer titrations yielded no heat signal (data not shown). The background heat signals were subtracted for ITC curve fitting. The presence of DARPin completely inhibited PN2-3$_N$-tubulin but did not affect PN2-3$_C$-tubulin interactions, thus leading to the strategy of co-crystallization of the PN2-3$_C$-DARPin-tubulin complex.

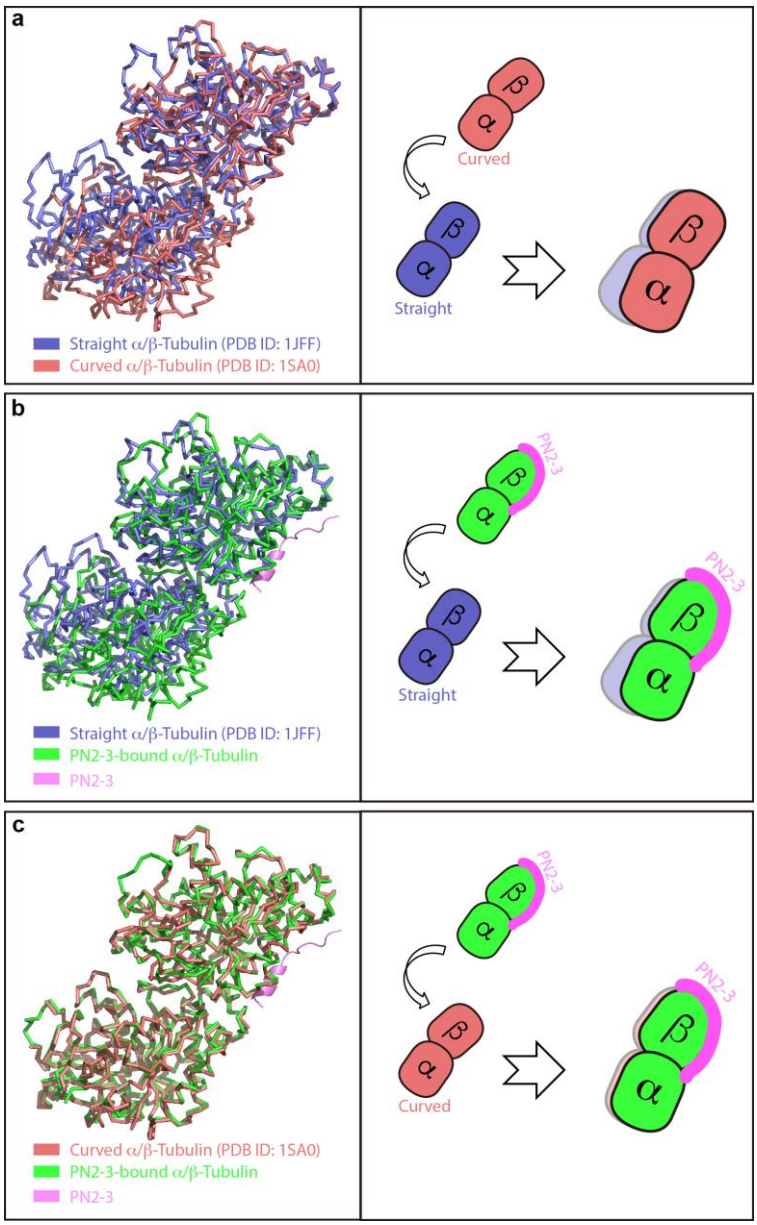

Supplementary Figure 2. Curved tubulin dimer is captured by PN2-3. (a) Left, structural alignment of a straight tubulin dimer (blue) as part of microtubule (PDB 1JFF) and a curved tubulin dimer (deep salmon) stabilized by a stathmin-like domain (PDB 1SA0). Structural superimposition is based on β-tubulin. Right, a cartoon diagram highlighting the imperfect superimposition between curved and straight tubulin dimers. **(b)** Structural alignment and cartoon diagram of the PN2-3_C–bound tubulin (green) superimposed with straight tubulin dimer (blue). Structural superimposition is based on β-tubulin. **(c)** Structural alignment and cartoon diagram of the PN2-3_C–bound tubulin (green) superimposed with curved tubulin dimer (deep salmon). The perfect superimposition suggests that PN2-3_C binding to tubulin dimer favors a curved conformation.

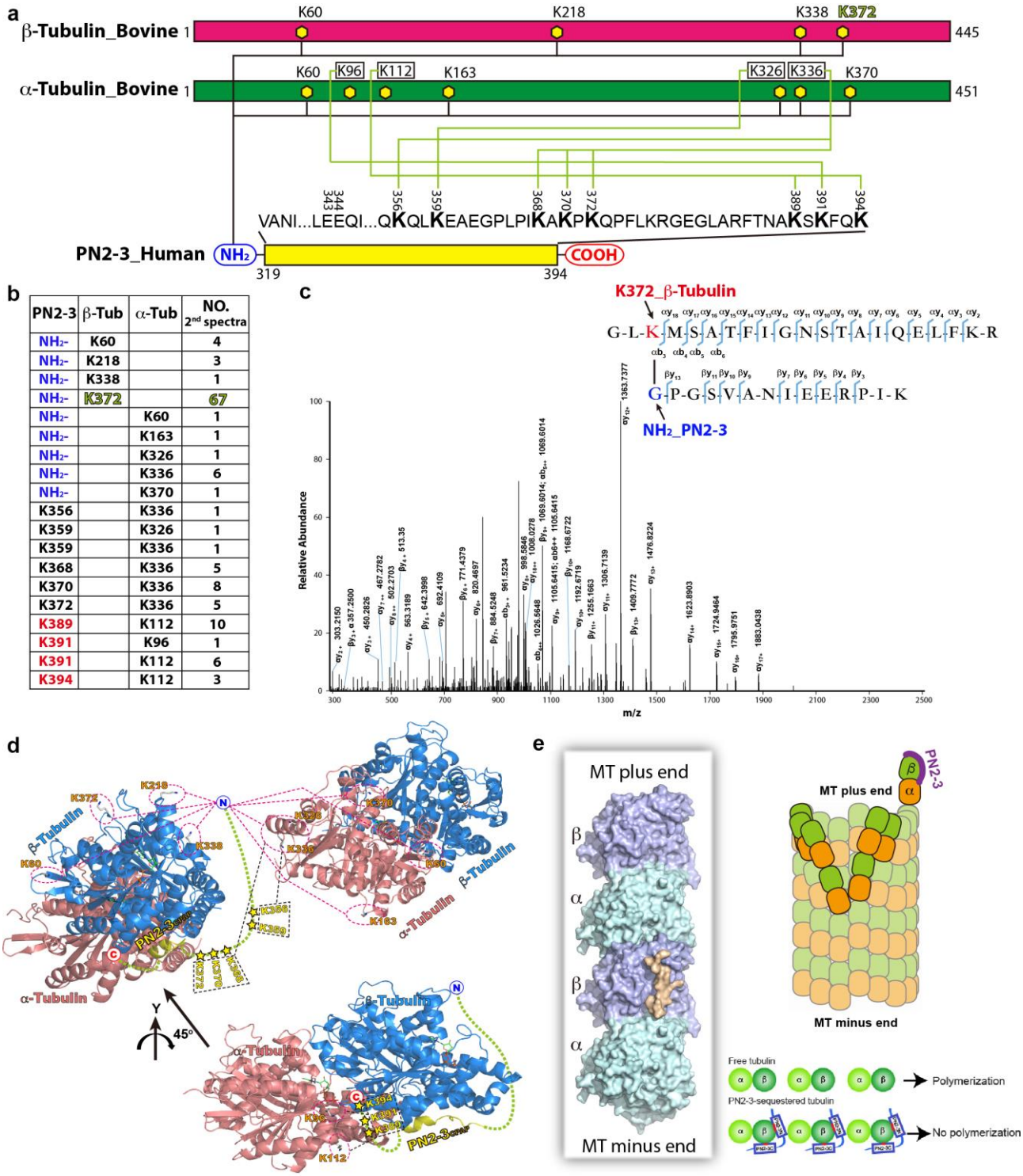

PN2-3	β-Tub	α-Tub	NO. 2nd spectra
NH_2-	K60		4
NH_2-	K218		3
NH_2-	K338		1
NH_2-	K372		67
NH_2-		K60	1
NH_2-		K163	1
NH_2-		K326	1
NH_2-		K336	6
NH_2-		K370	1
K356		K336	1
K359		K326	1
K359		K336	1
K368		K336	5
K370		K336	8
K372		K336	5
K389		K112	10
K391		K96	1
K391		K112	6
K394		K112	3

Supplementary Figure 3. Cross-linking mass spectrometry analysis of the PN2-3-tubulin complex. (a) Cross-link map for PN2-3 in complex with tubulin. The observed links from PN2-3 to tubulin dimer are denoted by direct lines. The identified cross-linking events within PN2-3_N are mainly mediated by its N-terminal amine (black lines). A large number of links were identified between lysine residues within the PN2-3 "linker-PN2-3_C" region and tubulin (green lines). **(b)** Summary of

cross-links identified by MS. Number of the secondary mass spectra is also listed to indicate a relative abundance of the cross-links. Lysine residues highlighted in red belong to PN2-3_C C-terminal segment that is invisible in the crystal structure. **(c)** Example secondary mass spectrum of cross-linked NH2_PN2-3 and K372_β-tubulin. **(d)** Mapping of the cross-links over the structure of tubulin dimers. α-tubulin, β-tubulin, and PN2-3 are colored coded salmon, blue, yellow, respectively. Cross-links mediated by the N-terminal amine of PN2-3 map to the microtubule-lumen surface of β-tubulin within a tubulin dimer as well as the α-tubulin of an adjacent tubulin dimer, likely due to dynamic association of tubulin dimer with a tendency of microtubule formation. Despite invisible in crystal structure, the C-terminal lysine cluster of PN2-3_C forms multiple cross-links with α-tubulin lysine residues near the α-β-tubulin interface within a tubulin dimer, which is consistent with our crystal structure study and in part validates the cross-linking MS strategy. **(e)** Surface view of PN2-3_C bound to a tubulin dimer. PN2-3_C, β-tubulin, α-tubulin are colored wheat, light blue and pale cyan, respectively. PN2-3_C buries a solvent accessible surface area of 1212.7 $Å^2$ upon complex formation. On the right, positioning of PN2-3_C in the context of microtubule. Note, PN2-3_C binds to the microtubule outer surface in an anti-parallel orientation along the longitudinal axis of microtubule. Cartoon highlights how PN2-3 wraps around β-tubulin from microtubules outer surface as well as capping the β-tubulin surface, thus blocking its bound cytoplasmic tubulin dimer from polymerization.

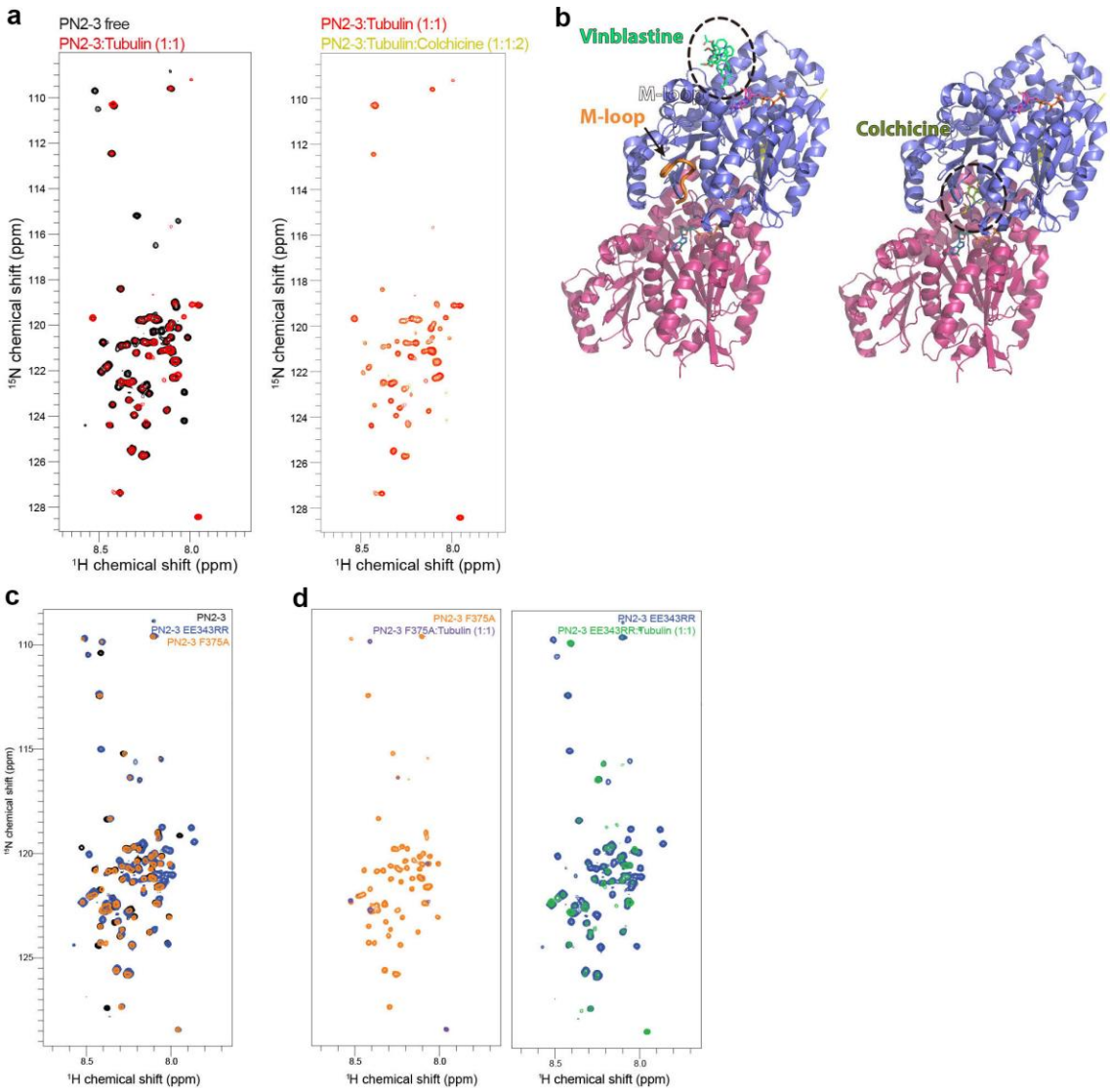

Supplementary Figure 4. Competitive NMR titration experiment to analyze PN2-3 and tubulin using vinblastine and colchicine. (a) Overlay of $^{1}H,^{15}N$-SOFAST HMQC spectra of PN2-3-tubulin complex (red) alone, in the presence of 3-fold excess of Colchicine (golden), no detectable perturbation of PN2-3-tubulin interaction was observed as opposed to that of vinblastine **(Fig. 2f). (b)** Models display taxol, vinblastine and colchicine bound to tubulin dimers. **(c)** Overlay of $^{1}H,^{15}N$ SOFAST-HMQC spectra of PN2-3^{WT} (black), PN2-3^{F375A} (orange) and PN2-$3^{EE343RR}$ (blue). Notably, the NMR spectra of PN2-3^{WT} and PN2-3^{F375A} are overall very similar while that of PN2-$3^{EE343RR}$ is different. **(d)** Overlay of $^{1}H,^{15}N$ SOFAST-HMQC spectra of PN2-3^{F375A} and PN2-$3^{EE343RR}$ in complex with tubulin at equimolar ratios are shown in purple (left panel) and green (right panel). The overall spectral quality of the complexes decreases in the order PN2-3^{WT} > PN2-$3^{EE343RR}$ > PN2-3^{F375A} due to line broadening that is consistent with decreasing in affinity, where micromolar interactions may induce line-broadening of the NMR signals.

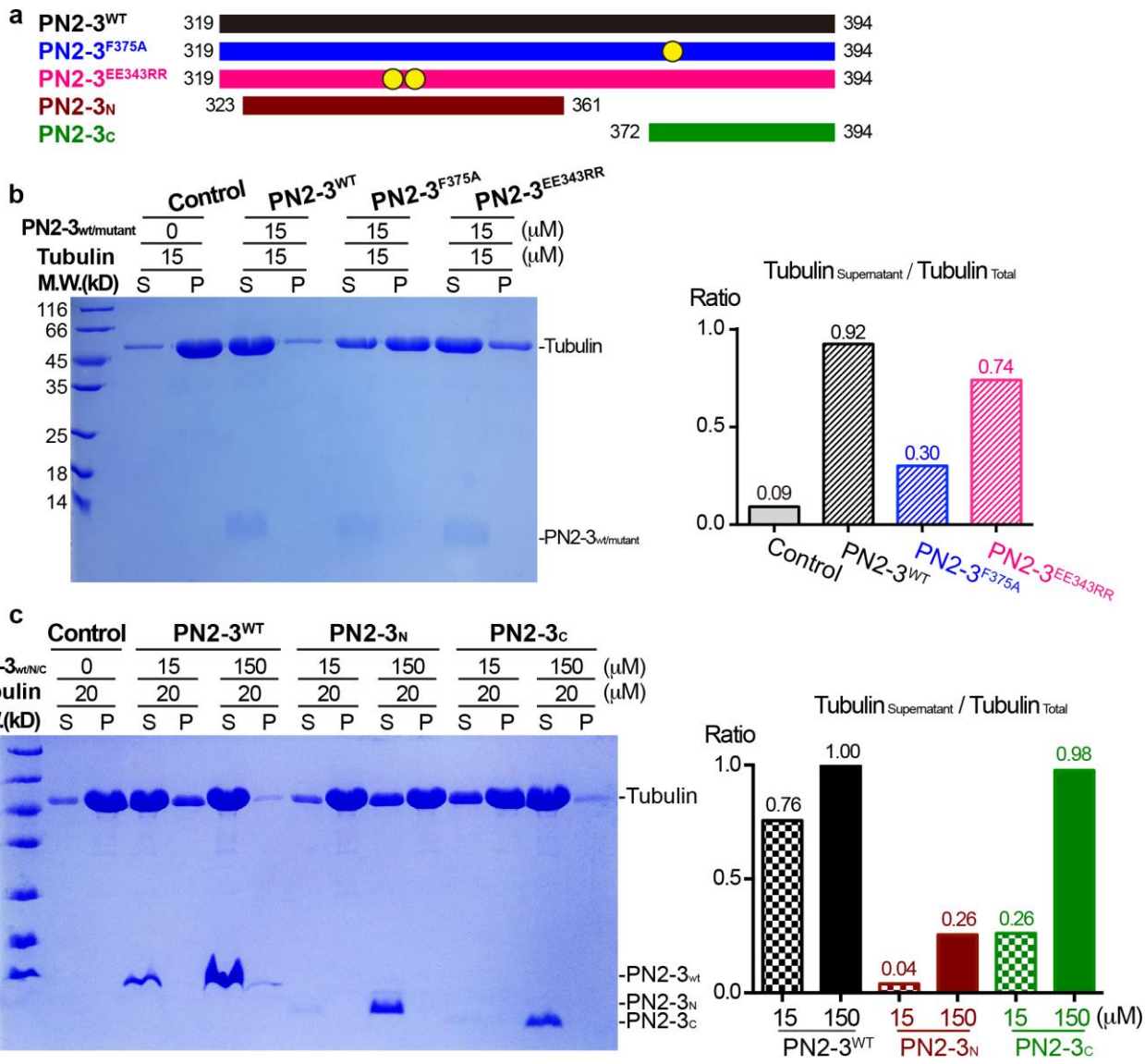

Supplementary Figure 5. CPAP PN2-3$_C$ via its F375 residue is sufficient to sequester tubulin from polymerization. (a) Diagram representing the PN2-3$_N$ and PN2-3$_C$ domain of CPAP. **(b)** PN2-3^{WT} and PN2-3^{EE343RR} prevents tubulin from polymerization. In contrast, PN2-3^{F375A} fails to do so indicating that the PN2-3's tubulin sequestering activity is F375 dependent. The ratio of tubulin in the supernatant to the total tubulin is represented in the right as a bar diagram. **(c)** Microtubule pelleting assay with PN2-3^{WT}, PN2-3$_N$ and PN2-3$_C$ domains. PN2-3$_C$ is sufficient to prevent tubulin from polymerization. The ratio of tubulin in the supernatant (S) to the total tubulin (S+P) is represented in the right as a bar diagram based on the densitometric quantification of the SDS-PAGE gel bands. The inhibitory efficiency of PN2-3$_{WT}$ at 150 μM is normalized to 1.

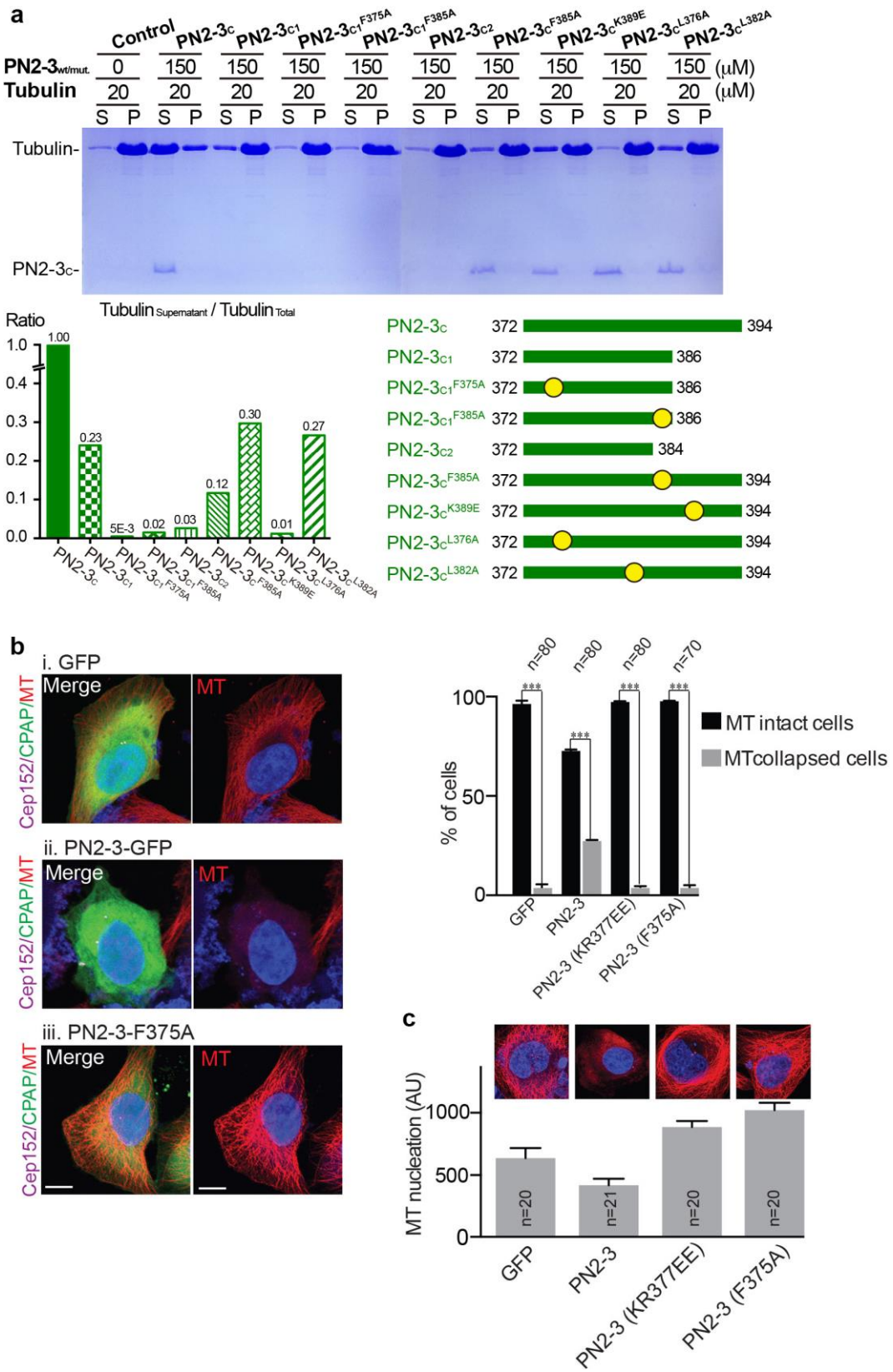

Supplementary Figure 6. PN2-3^{F375A} residue is essential for tubulin sequestration. (a) Microtubule pelleting assay with several truncated versions of the PN2-3$_C$ domain shows the significance of F375 residue in tubulin sequestration. The ratio of tubulin in the supernatant to the

total tubulin is represented in the right as a bar diagram. Note that while PN2-3_C exhibits the maximum tubulin sequestration activity (normalized to 1), PN2-3_{C1}^{F375A} displays the least activity. **(b)** Overexpression of GFP-tagged PN2-3^{WT} and PN2-3^{F375A} fragments in Hela cells. While PN2-3^{WT} fragment collapses the cytoplasmic microtubules, PN2-3^{F375A} prevents microtubules from collapsing eventually causing enhanced microtubule-nucleation in cells microtubules are labeled with anti-α-tubulin antibodies (red). Scale bar, 1 μm. Quantifications for percentages of cells with intact and collapsed microtubules (n>80 for all constructs except for PN2-3^{F375A}, where n=70, ANOVA, ***P<0.0001. Error bars represent ± s. e. m and the microtubules-nucleating intensities are given at right (n=20) **(c)**. Error bars represent ± s. e. m. Number of experiments (N)=3.

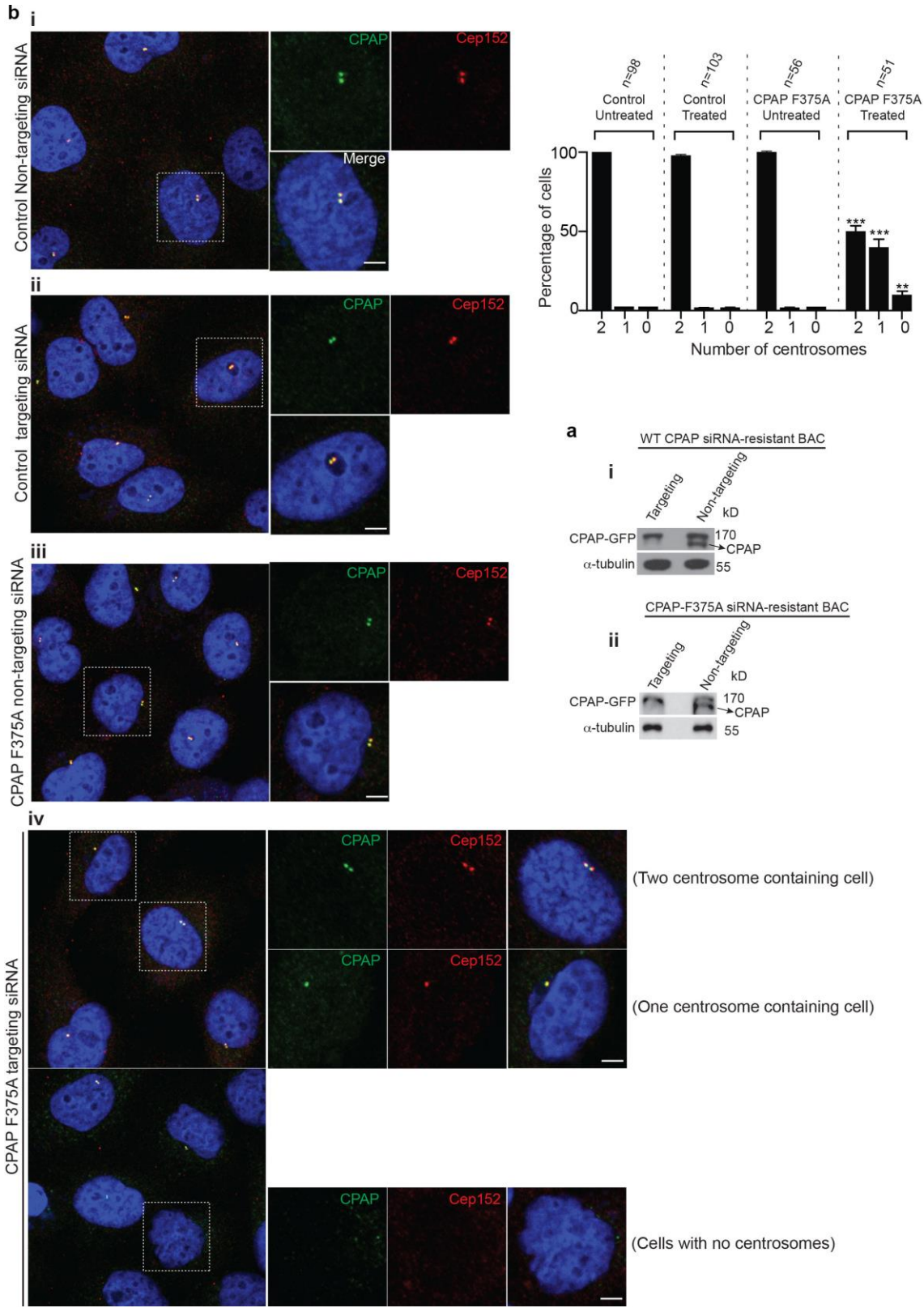

Supplementary Figure 7. CPAP-tubulin interaction is required for centrosome duplication in HeLa cells. (a) Western blots showing both wild type **(i)** and CPAP^{F375A} **(ii)** BACs are resistant for CPAP targeting siRNA, Note that endogenous CPAP is depleted in treatments with CPAP-targeting

siRNA. **(b)** Stable HeLa lines expressing RNAi-resistant GFP-tagged $CPAP^{WT}$ **(i-ii)**, and $CPAP^{F375A}$ **(iii-iv)** using artificial chromosome recombineering (BACs), a system that allows expressing gene products under their own endogenous promoters. As described previously, treating cells with CPAP-specific siRNA depleted endogenous protein, retaining the RNAi-resistant CPAP[1]. Expressing wild type siRNA-resistant $CPAP^{WT}$ completely rescued the effect of siRNA-mediated CPAP depletion as cells proliferated without centrosome duplication defects **(i-ii)**. In contrast, RNAi-resistant $CPAP^{F375A}$ failed to rescue the centrosome duplication phenotype caused by CPAP depletion **(iii-iv).** Specifically, when cultured for prolonged period of time, a proportion of cells displaying less than two centrosomes were noticed. Centrosomes are marked with CPAP (green) and Cep152 (red). Bar diagram quantifications showing percentages of cells showing centrosome numbers. ($n>100$ for $CPAP^{WT}$, $n>50$ for $CPAP^{F375A}$), ANOVA, , ***$P<0.0001$, , **$P<0.001$.Error bars represent ± s. e. m. Group of cells at low-magnifications are shown at left. Scale bar, 1 μm.

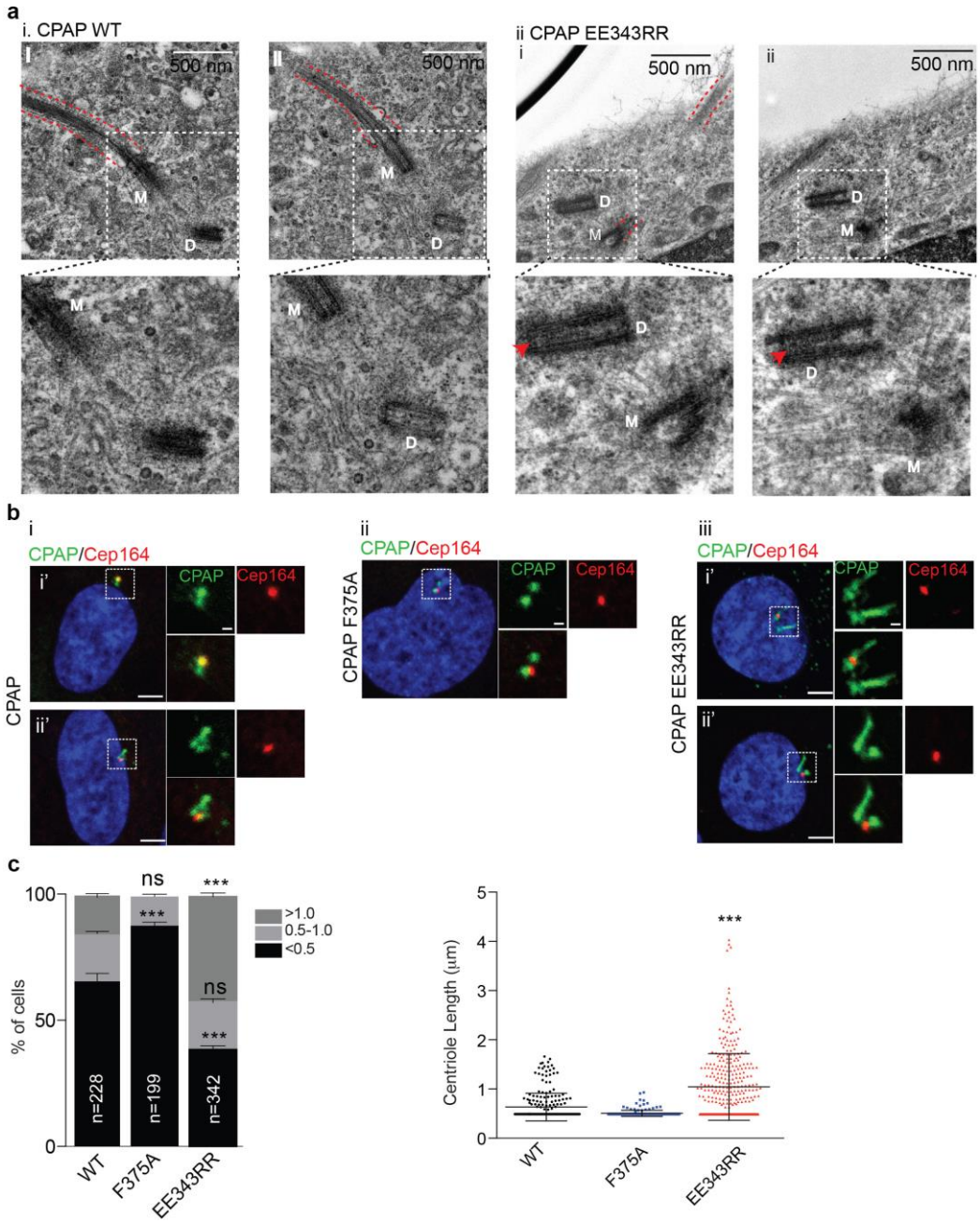

Supplementary Figure 8. CPAP^{EE343RR} expression causes overly long daughter centrioles. (a) Longitudinal serial sectioning EM-micrographs of RPE1 cells expressing CPAP^{WT} **(i)** and CPAP^{EE343RR} **(ii)**. In contrast to CPAP expression CPAP^{EE343RR} specifically causes lengthening of daughter centrioles (arrows). n>15. **(b)** RPE-1 cells expressing CPAP^{WT} **(i),** CPAP^{F375A} **(ii)** and CPAP ^{EE343RR} **(iii).** The CPAP variants are expressed as GFP (green), the mother centriole is labeled by centriolar appendage protein Cep164 (red) that specifies mother centrioles. Scale bar, 1 µm (insets 0.5 µm). **(c)** Quantification of mother centriole lengths. n=228 for WT, n=199 for CPAP^{F375A} and n=342 for CPAP^{EE343RR}. ANOVA, ***P<0.001, *P<0.05, Error bars represent ± s. e. m. Number of experiments (N)=3.

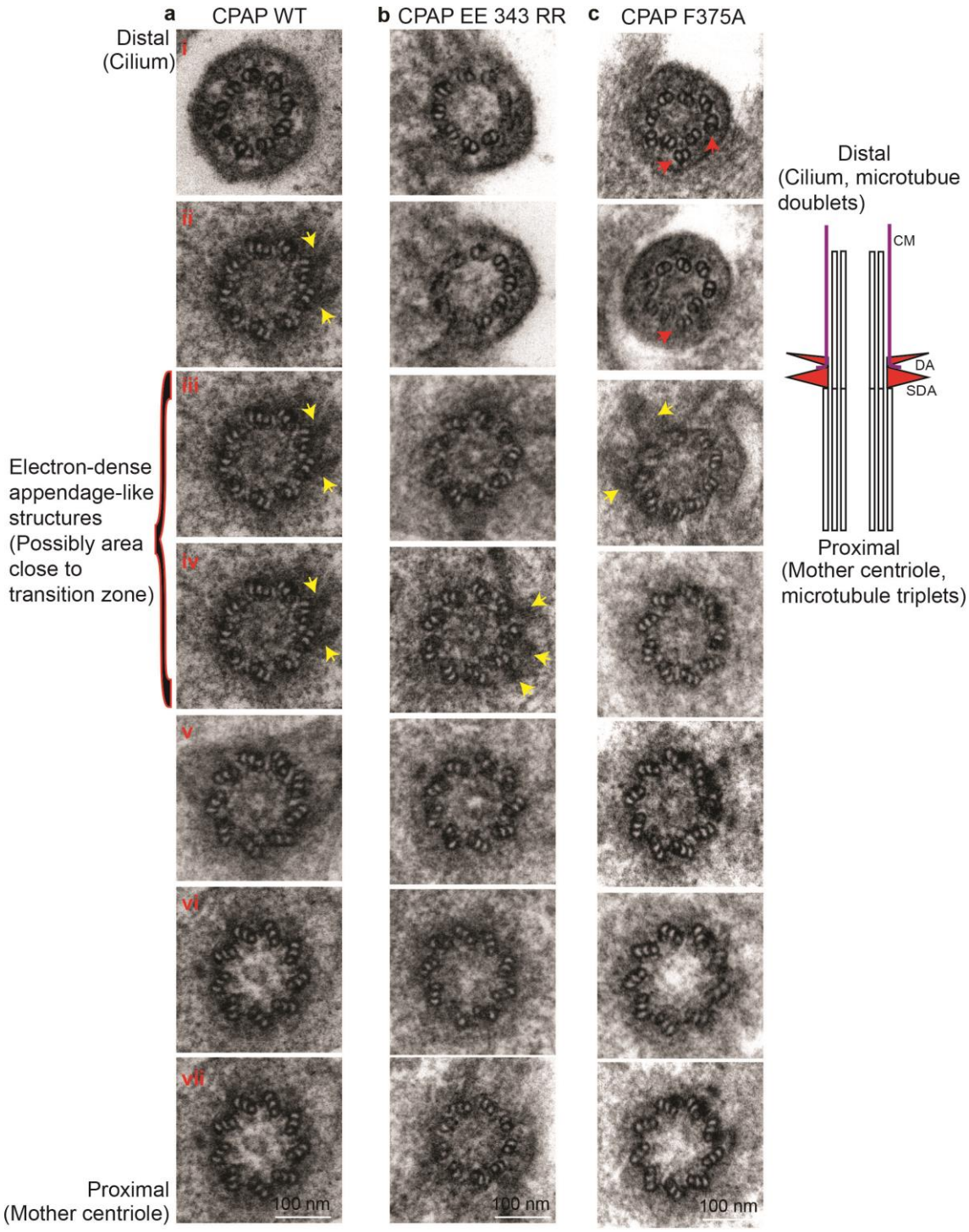

Supplementary Figure 9. CPAP^{EE343RR} expression causes overly long cilia. Cross serial sectioning EM-micrographs of RPE1 cells expressing CPAP^{WT} **(a),** CPAP^{EE343RR} **(b)** and CPAP^{F375A} **(c)**. Serial sections spans from proximal mother centriole (triplet microtubules) until the distal cilium (doublet microtubules). Electron dense area (yellow arrows) marks the region of ciliary transition zone. In contrast to CPAP^{WT} and CPAP^{EE343RR}, CPAP^{F375A} expression causes aberrant ciliary-microtubule organization. Scheme at right depicts centriolar and ciliary regions. (n=32)

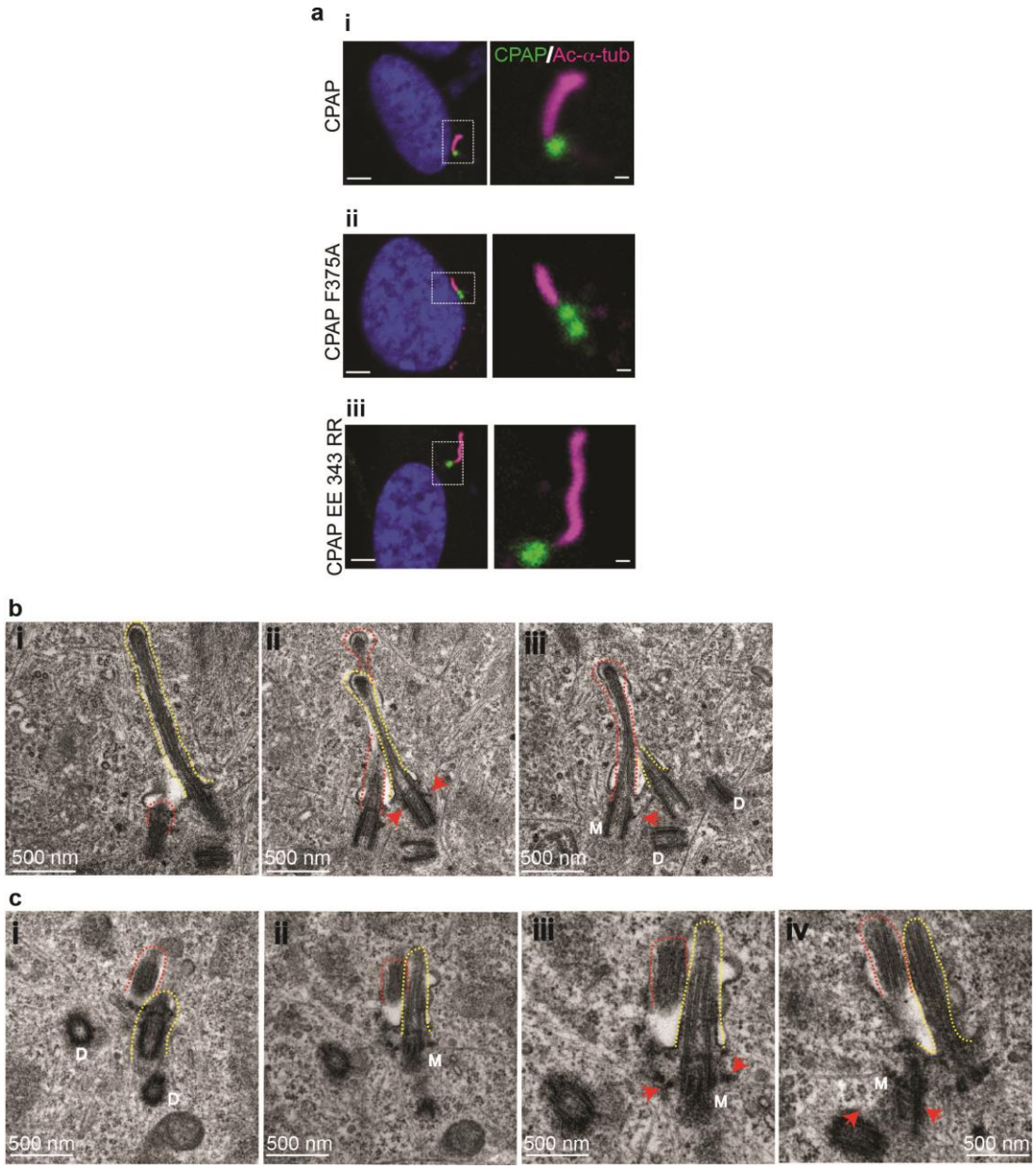

Supplementary Figure 10. CPAP^{EE343RR} expression causes overly long cilia and promotes daughter centrioles to form cilia. (a) RPE1 cells expressing CPAP^{WT} **(i),** CPAP^{F375A} **(ii)** and CPAP^{EE343RR} **(iii).** In contrast to CPAP^{WT} expression, CPAP^{EE343RR} causes cells to form long cilia. In contrast, CPAP^{F375A} expression causes cells to form short cilia. Cilia are labeled by acetylated α-tubulin (magenta). Scale bar, 1 μm (insets 1.0 μm). **(b-c)** Longitudinal serial sectioning-EM of at least two biciliated cells (dotted red and yellow lines). Four centrioles were observed and two of them constantly contained centriolar appendages (arrows) indicating that they are mother and matured daughter centrioles capable of forming cilia. (n=5).

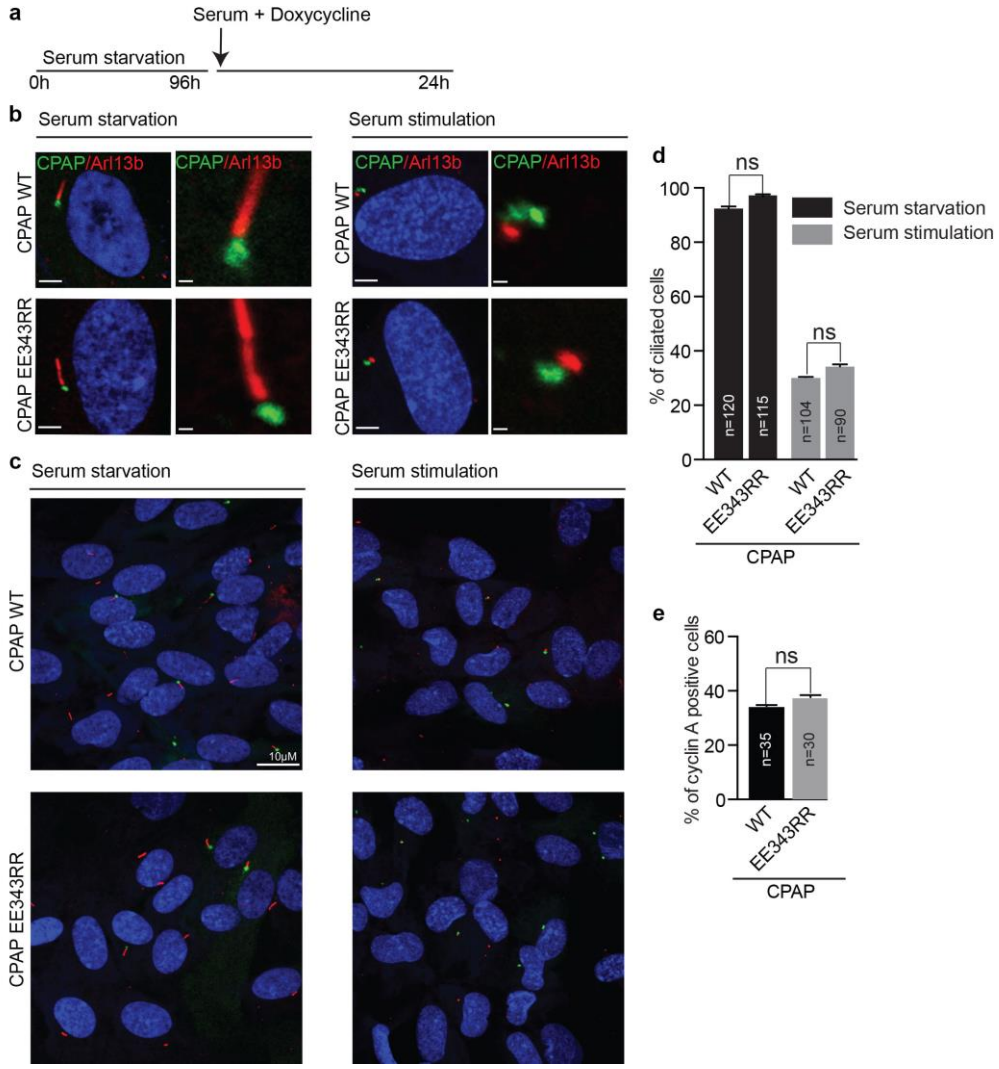

Supplementary Figure 11. Long cilia caused by CPAP^{EE343RR} expression is not due to defective cilia disassembly. (a) Experimental plan. RPE1 cells expressing doxycycline-inducible CPAP^{WT} or CPAP^{EE343RR} were synchronized at G_0-phase of cell cycle by serum starvation. A prolonged period of serum starvation for 96 hrs causes cells to have equivalent ciliary lengths. **(b)** Serum stimulation simultaneously with doxycycline-induction causes cells to disassemble cilia concurrent with cell cycle-re-entry. Scale bar, 1 μm (insets 1 μm). **(c)** Low-magnification overview of cells expressing CPAP^{WT} or CPAP^{EE343RR} cells after serum starvation and serum stimulation. Arl13b labels (red) cilia and ciliary remnants. Scale bar, 10 μm. **(d)** Quantification shows that CPAP^{EE343RR} cells disassemble cilia similar to CPAP^{WT} expressing cells and thus, there is no delay in cell cycle re-entry as measured by cyclin-A immunoreactivity **(e)**, a G1-S transition cell cycle marker. For cilia disassembly experiment: ANOVA, Error bars represent ± s. e. m. (n>100), number of experiments (N)=3. For Cyclin A experiment: (n>30), t-test, Error bars represent ± s. e. m. Scale bar, 1 μm.

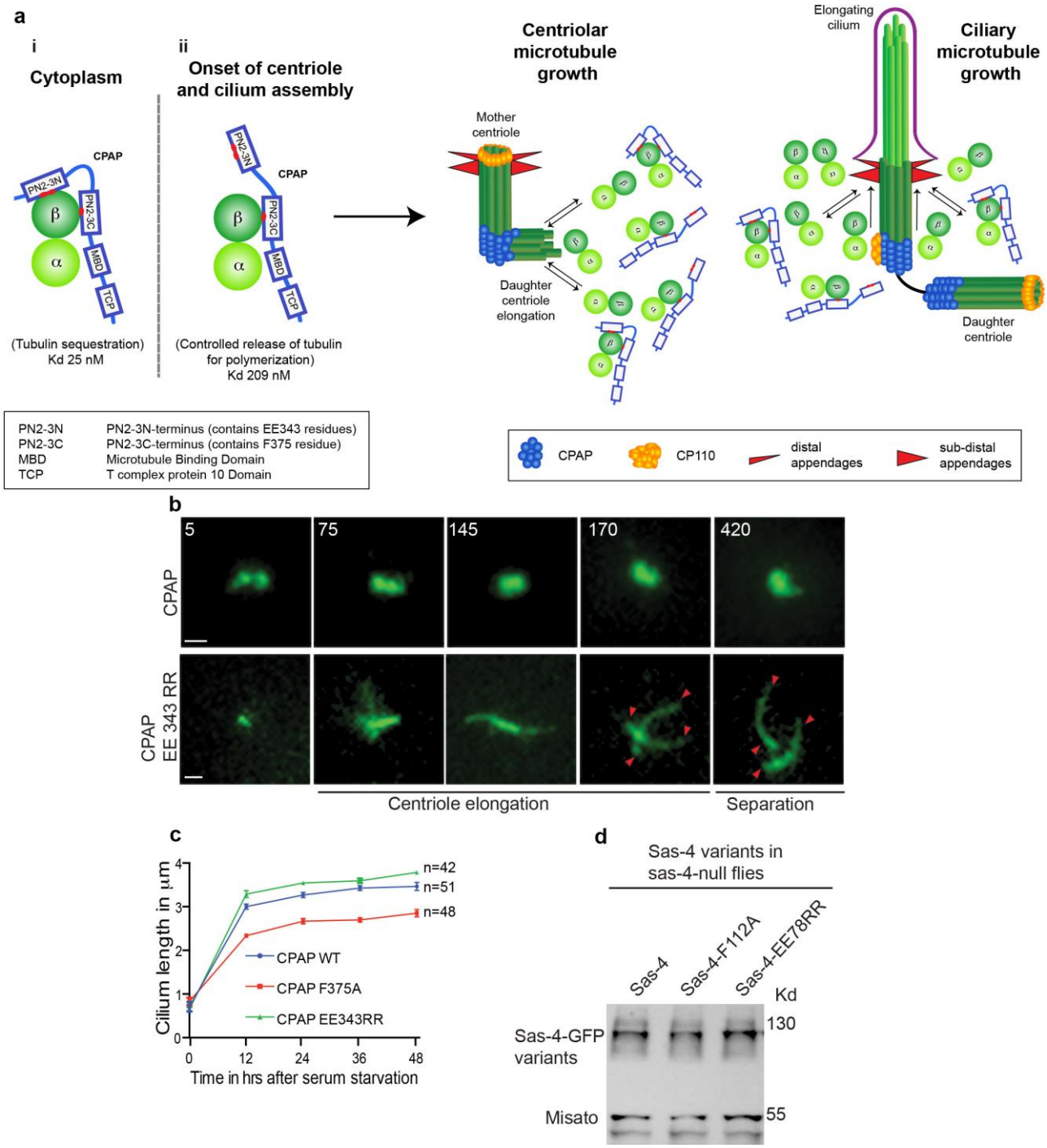

Supplementary Figure 12. A hypothetical model depicting how CPAP could control the delivery of its bound tubulin during centriolar and ciliary microtubule formation. (ai) In the cytoplasm, CPAP sequesters tubulin through its PN2-3 domain and forms a high affinity complex with a K_D of 25 nM. As given in **Fig. 1e**, while PN2-3_N caps the β–tubulins' lumen surface for polymerization, its PN2-3_C tethers β–tubulins from its outer surface. Different domains of CPAP are shown. **(aii)** At the onset of centriole and cilium assembly, CPAP delivers its sequestered tubulin by unmasking β–tubulin surface via its PN2-3N with a simultaneous reduction in binding affinity (K_D=209

nM). This could favor delivering of CPAP-bound tubulin available for centriolar and ciliary microtubule formation. CPAP's tubulin delivery could be regulated by cell cycle kinases, its interaction partners including centriolar- microtubule length determining factors [2-4]. Graphical depiction of centriolar appendages, CPAP and centriolar capping protein CP110 are painted in colors. **(b)** Time lapse imaging measurements of centriolar growth rate. A second example of RPE1 expressing $CPAP^{WT}$ and $CPAP^{EE343RR}$-GFP. While the CPAP expressing cell displays a controlled centriolar growth, $CPAP^{EE343RR}$, a mutation that perturbs PN2-3_N-mediated capping of β–tubulins' polymerization surface causes a rapid centriolar-elongation. In contrast to $CPAP^{WT}$-induced structures, elongating centriolar structures caused by $CPAP^{EE343RR}$ expression is distinct and measurable. Arrowheads mark fully elongated (at 170^{th} mins) and separated (at 420^{th} mins) centrioles. Scale bar is 1 μM. **(c)** Ciliary growth rate of RPE1 cells expressing $CPAP^{WT}$, $CPAP^{F375A}$ or $CPAP^{EE343RR}$. Ciliary lengths were measured at various time points after serum starvation. Note, experiments began with asynchronously growing cells. Compared to $CPAP^{WT}$, cells expressing $CPAP^{EE343RR}$ display an enhanced ciliary growth rate and cells expressing $CPAP^{F375A}$ display a reduced ciliary growth rate (n>40), Error bars represent ± s. e. m. **(d)** Western blots showing nearly same level of Sas-4 variants are expressed in Sas-4 null flies. Each lane contains equivalent numbers of testes. Misato is used as a loading control.

Supplementary Table 1

Summary of thermodynamic parameters from ITC

Tubulin	PN2-3$^{WT/mut.}$	ΔH (kcal mol^{-1})	ΔS (cal mol^{-1} deg^{-1})	*K*a (M^{-1})	N
Tubulin	PN2-3^{WT}	-15.7±0.2	-19.6	3.9±1.6 E7	1.08±0.01
	PN2-3^{F338A}	-24.9±0.1	-54.5	8.7±0.6 E6	0.97±0.00
	PN2-3^{Y341A}	-14.6±0.1	-19.2	7.4±0.5 E6	1.19±0.00
	PN2-3^{ED339RR}	-15.9±0.1	-23.7	7.0±0.7 E6	0.98±0.01
	PN2-3^{EE343RR}	-10.9±0.1	-7.1	5.2±0.5 E6	1.20±0.01
	PN2-3^{EE349RR}	-6.4±0.1	8.0	3.9±0.3 E6	1.23±0.01
	PN2-3^{K372E}	-14.7±0.7	-21.9	2.4±0.7 E6	1.01±0.03
	PN2-3^{F375A}	-6.9±0.3	1.64	3.6±0.5 E5	1.00±0.00
	PN2-3^{K377E}	-14.0±0.2	-21.7	7.6±0.5 E5	1.13±0.01
	PN2-3^{R378E}	-16.4±0.3	-29.1	1.2±0.1 E6	1.20±0.02
	PN2-3^{R384E}	-17.1±0.6	-33.1	5.3±0.6 E5	1.19±0.03
	PN2-3^{F385A}	-20.8±0.3	-40.2	1.0±0.2 E7	1.13±0.01
	PN2-3$_N$	-6.0±1.0	-1.6	1.5±0.2 E4	1.25±0.18
	PN2-3$_C$	-8.0±0.1	-3.3	2.1±0.2 E5	1.28±0.02
DARPin-Tubulin	PN2-3$_N$	N.D.			
	PN2-3$_C$	-6.6±0.2	2.2	3.0±0.4 E5	1.13±0.02

PN2-3^{WT}: VANIEERPIKAAIGERKQTFEDYLEEQIQLEEQELKQKQLKEAEGPLPIKAKPKQPFLKRGEGLARFTNAKSKFQK

PN2-3$_N$: IQLEEQELKQKQLKEAEGPLPIKAKP

PN2-3$_C$: KQPFLKRGEGLARFTNAKSKFQK

N.D. not detected

Supplementary Methods

Microtubule end-tracking assay

Microtubule depolymerization assay was performed at room temperature by monitoring the catastrophe of GMPCPP-stabilized microtubules seeds, which were immobilized on coverslips using biotin-streptavidin links as previously described [5]. For preparation the reaction chambers, microscope slides and biotin-coated coverslips were assembled using double-side tape. After blocking reaction chambers with 1% Pluronic F127 and 0.5 mg ml^{-1} κ-casein for 5 min, 50 μg ml^{-1} streptavidin was flowed in and incubate for 5 min. Microtubule seeds assembled from 50 μM tubulin mixed with 10% rhodamine-labeled tubulin and 10% biotin-labeled tubulin under 1 mM GMPCPP were then specifically attached to the functionalized surface by previously bound streptavidin. After wash the chamber with 1xBRB80 buffer, microtubule severing was initiated by flowing in 15 μM PN2-3^{WT}/PN2-3^{F375A}/PN2-$3^{EE343RR}$ protein, which was diluted in 1xBRB80 buffer in presence of oxygen scavenger system (50 mM glucose, 400 μg ml^{-1} glucose-oxidase, 200 μg ml^{-1} catalase, and 4 mM DTT). After immediately seal the reaction chamber with candle wax, images were collected every 3 sec within 10 min using a TIRF (total internal reflection fluorescence) microscope (NikonEclipse Ti). ImageJ software (http://rsbweb.nih.gov/ij/) was used for kymograph presentation and image analysis[5].

Microtubule polymerization assay was conducted following the same method described above. Briefly, after pre-assembled microtubule seeds were attached to the functionalized reaction chambers, tubulin polymerizing was initiated by flowing in 1 μM PN2-$3_{EX}{}^{WT}$/PN2-$3_{EX}{}^{F375A}$/PN2-$3_{EX}{}^{EE343RR}$, 20 nM GFP-tagged EB1, 15 μM tubulin and 1.5 μM rhodamine-labeled tubulin, which were diluted in oxygen scavenger system supplied tubulin polymerizing buffer (80 mM PIPES-K, 150 mM KCl, 1 mM EGTA, 5 mM GTP, 4 mM $MgCl_2$ and 5% glycerol, pH 6.8). After seal the reaction chamber with candle wax, images were collected every 3 sec within 7.5min. A control of PN2-3_{EX}-null buffer was used to detect the autonomous tubulin polymerization in this assay.

NMR spectroscopy

All NMR spectra, to compare the WT with the mutant PN2-3 proteins were recorded at 298K on 800MHz or 900MHz Bruker spectrometer with concentrations PN2-3 (35μM):Tubulin (35 μM) for wildtype and PN2-3 mutant proteins (F375A, EE343RR). The inhibitors (vinblastine

and colchicine) were added in 3-fold molar excess. The buffer used in all experiments is 50mM sodium phosphate, 100mM NaCl, 1mM EGTA, 1mM $MgCl_2$, 1mM GDP pH 6.8.

Plasmids and cloning for cell culture experiments

$PN2\text{-}3^{WT}$, $PN2\text{-}3^{KR377EE}$ and $PN2\text{-}3^{F375A}$ encompassing the regions (aa 317-394) were cloned into pEGFP-C1 vector for transient transfection in HeLa cells. $CPAP^{WT}$, $CPAP^{F375A}$ and $CPAP^{EE343RR}$ genes were cloned into pSinEF-2-GFP vector (addgene Plasmid #16578) between BamH1 cloning sites for transiently expressing the genes in Retinal pigment epithelial cells (RPE1) cells. For inducible expression of the genes, the CPAP-GFP constructs were cloned into PLIX backbone using gateway cloning (PLIX403 was a gift from David Root- addgene plasmid 41395). RNAi-resistant CPAP BACs were prepared and described as previously described [1, 6].

Lentiviral production

For carrying out lentiviral transductions, the GFP tagged $CPAP^{WT}$, $CPAP^{F375A}$ and $CPAP^{EE343RR}$ were cloned into the pSinEF-2-GFP vector. For packaging the virus, pMD2, pRSV and pMDL plasmids were used. Further, HEK293T cells were transfected with the packaged products along with the pLenti plasmids using calcium chloride. After 24 hrs of transfection, the first batch of virus was collected followed by the second batch that was collected after 36 hrs.

Cell Culture, transfection and viral transduction

Wild type RPE1 and HeLa cells were cultured in a medium containing Dulbecco's modified Eagle's medium (DMEM), 10% (v/v) fetal bovine serum (FBS), 0.1 mM MEM non-essential amino acids (NAA), 100 µg ml^{-1} streptomycin, 100 U ml^{-1} penicillin (from life Technologies GmbH, Dermstadt, Germany). The cells were incubated at 37^0C and split after they reached a confluency of 70-80%. For induction of cilium in RPE1, the cells were serum starved for different time periods by growing them in a medium that lacks serum. For cilium resorption experiments, 10 % FBS was added to the serum starved medium and incubated for 24 to 48 hrs. RPE1 cells were seeded on coverslips and transduced with lentiviral particles (1:10 dilution), harboring GFP tagged $CPAP^{WT}$, $CPAP^{F375A}$ and $CPAP^{EE343RR}$ genes. The transduced cells were incubated for a minimum of 48 hrs before further treatment. For the inducible lentiviral system, 2µg ml^{-1} of doxycycline was added to the cultures to induce the expression of CPAP. The cells were incubated for 2 hrs before taking measurements to

ensure sufficient protein expression. For RNAi experiments, the siRNA-resistant versions of CPAP with the above mentioned point mutations were generated as described previously [6].

Immunofluorescence and light microscopy

For immunofluorescence, mouse anti-CPAP (1:25) *(2),* rat anti-α-tubulin (1:50 chemicon), rabbit anti-Cep 152 (1:500 provided by the Nigg laboratory), rabbit anti-Arl13b (1:100, Proteintech, Manchester, UK), mouse anti-acetylated tubulin (1:500, Sigma-Aldrich), rabbit anti-CP110 (1:500 Proteintech), rabbit anti-cep 164 (1:1000 provided by Nigg laboratory), rabbit anti-Asl (1:5000) were used. Secondary antibodies, Alexa fluor dyes (goat or donkey anti-mouse/ anti-rabbit) were used at 1:1000 dilution (Life technologies). DAPI (1 μg ml^{-1}. Sigma) was used to stain DNA.

For light microscopy, the required amount of cells were seeded on coverslips and allowed to adhere. After experimental treatment, the cells were either fixed using 3.7% para-formaldehyde (PFA) or ice-cold methanol. After fixation, the specimens were permeabilized with 0.5% triton X-100 in PBS for 10 mins. 0.5% fish gelatin in PBS was used to block the permeabilized samples at room temperature for 2 hrs. Primary antibody labeling was carried out either at RT for 1 hr or overnight at 4ºC. After labeling, the antibody was removed and the samples were washed thrice with PBS. Further, the respective secondary antibodies along with DAPI were used against the primary antibody and incubated at room temperature for 1 hr. Confocal images were obtained using an Olympus Fluoview FV 1000 scanning confocal microscope. The images were further processed using Image J and Adobe Photoshop. For the live cell imaging of RPE1, the cells were grown on ibidi microscopic chamber (Cat.No.80296) was performed with Leica DMI 6000B using 40X water objective and 63X oil objective.

For light microscopy of fly testes, the dark pupae testes were dissected in PBS and permeabilized with 0.1% Triton X-100 in PBS for 10 mins. The samples were blocked with 2 % BSA, 0.1% tritonX-100 in PBS for 1 hr at room temperature. The samples were labeled with primary antibodies at RT for 1-2hr or overnight at 4ºC. The samples were further washed and labeled with secondary antibodies for 1 hr at RT along with DAPI. Analyses of the samples were carried out as described earlier.

Electron microscopy

For EM of RPE1 cells stably expressing the CPAP mutants, the cells were seeded onto

coverslips and allowed to adhere. The cells were further serum starved for 48 hrs to induce cilium formation. 2% glutaraldehyde (Electron Microscopy Sciences) was used to fix the cells. The fixed cells were further processed and then used for electron microscopy as described earlier [6].

For EM of drosophila testes, the testes from the different Sas-4 transgenic flies were dissected and fixed using 2% glutaraldehyde. The fixed samples were then processed and used for electron microscopy. The images obtained were processed using Adobe photoshop.

Western Blotting

Protein samples in 4x laemlli buffer were heated at 98ºC for 10 mins before use. The samples were resolved using 8% acrylamide gels and transferred to nitrocellulose membranes. The blots were further blocked with 5% non-fat dried milk powder in TBST for 1 hr and incubated overnight at 4ºC with the primary antibodies. The blots were later treated with the respective secondary antibodies at RT for 1 hr. Super signal west pico/ femto chemilluminescent substrates were used to detect the peroxidase activity in the samples.

Generation of transgenic flies

Genomic Sas-4^{WT} (control), Sas-4^{F112A} and Sas-4^{EE78RR} were cloned into PattB-GFP between AscI and NotI sites. The plasmids were injected into the larvae as described [7]. All the genes were expressed under Sas-4 endogenous promoter and were inserted at the identical sites at the third chromosome using PattB vectors. The flies were balanced to generate a stable stock. For rescue experiments, Sas-4^{WT}, Sas-4^{F112A} and Sas-4^{EE78RR} were expressed in the background of Sas-4 null homozygous flies, and analyzed for their fly co-ordination, centriole and cilium length.

Statistical Analysis

Statistical analysis was carried out using Graph Pad Prism software (version 6.0). Student's T- test or one-way ANOVA followed by Tukey's multiple comparison tests were used to analyze the results.

Supplementary References

1. Zheng, X. *et al.* Conserved TCP domain of Sas-4/CPAP is essential for pericentriolar material tethering during centrosome biogenesis. *Proceedings of the National Academy of Sciences of the United States of America* **111**, E354-363 (2014).
2. Schmidt, T.I. *et al.* Control of centriole length by CPAP and CP110. *Current biology : CB* **19**, 1005-1011 (2009).
3. Kobayashi, T., Tsang, W.Y., Li, J., Lane, W. & Dynlacht, B.D. Centriolar kinesin Kif24 interacts with CP110 to remodel microtubules and regulate ciliogenesis. *Cell* **145**, 914-925 (2011).
4. Lin, Y.N. *et al.* CEP120 interacts with CPAP and positively regulates centriole elongation. *The Journal of cell biology* **202**, 211-219 (2013).
5. Bieling, P., Telley, I.A., Hentrich, C., Piehler, J. & Surrey, T. Fluorescence microscopy assays on chemically functionalized surfaces for quantitative imaging of microtubule, motor, and +TIP dynamics. *Methods in cell biology* **95**, 555-580 (2010).
6. Poser, I. *et al.* BAC TransgeneOmics: a high-throughput method for exploration of protein function in mammals. *Nature methods* **5**, 409-415 (2008).
7. Fish, M.P., Groth, A.C., Calos, M.P. & Nusse, R. Creating transgenic Drosophila by microinjecting the site-specific phiC31 integrase mRNA and a transgene-containing donor plasmid. *Nature protocols* **2**, 2325-2331 (2007).

Chapter II

Plk1/Polo Phosphorylates Sas-4 at the Onset of Mitosis for an Efficient Recruitment of Pericentriolar Material to Centrosomes.

Journal: Cell Reports
Year: 2018

Relevant publication:

Ramani A, Mariappan A, Gottardo M, Mandad S, Urlaub H, Avidor-Reiss T, Riparbelli M, Callaini G, Debec A, Feederle R, Gopalakrishnan J*. Plk1/Polo Phosphorylates Sas-4 at the Onset of Mitosis for an Efficient Recruitment of Pericentriolar Material to Centrosomes. ***Cell Reports***. 25(13): 3618-3630 (2018).

Link to publication: https://doi.org/10.1016/j.celrep.2018.11.102

My contribution to this work

- Design and execution of experiments
- Molecular biology for Sas-4 genes.
- Biochemical analysis of Sas-4 peptides and proteins.
  Functional significance of Sas-4 activation and the analysis of pericentriolar material recruitment in mitotic cells of *Drosophila*

Article

Cell Reports

Plk1/Polo Phosphorylates Sas-4 at the Onset of Mitosis for an Efficient Recruitment of Pericentriolar Material to Centrosomes

Graphical Abstract

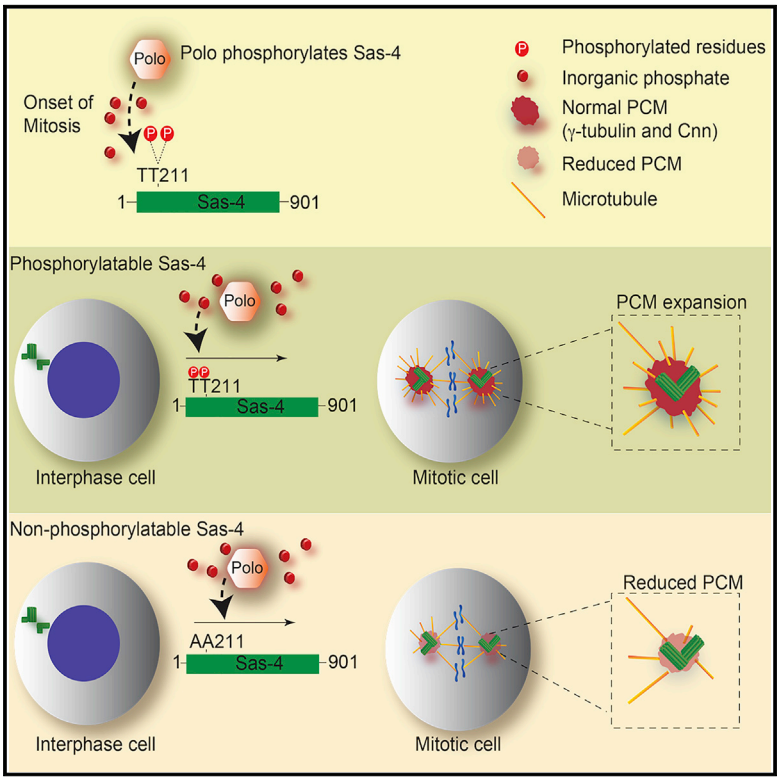

Highlights

- *Drosophila* Sas-4 is phosphorylated by Plk1/Polo at the onset of mitosis
- Cell-cycle-specific Sas-4 antibodies identify spatiotemporal dynamics of Sas-4
- Sas-4 phosphorylation at TT211 site is required for recruitment of Cnn and g-tubulin
- Phosphorylation status of Sas-4 determines the PCM size of mitotic centrosomes

Authors

Anand Ramani, Aruljothi Mariappan, Marco Gottardo, ..., Alain Debec, Regina Feederle, Jay Gopalakrishnan

Correspondence

jay.gopalakrishnan@hhu.de

In Brief

Ramani et al. show that Plk1/Polo phosphorylates *Drosophila* Sas-4 at the onset of mitosis. Cell-cycle-specific modification of Sas-4 determines the spatiotemporal localization of Sas-4 in centrosomes, which is required for an efficient recruitment of PCM proteins in mitosis.

Ramani et al., 2018, Cell Reports *25*, 3618–3630
December 26, 2018
https://doi.org/10.1016/j.celrep.2018.11.102

CellPress

OPEN ACCESS
CellPress

Cell Reports
Article

Plk1/Polo Phosphorylates Sas-4 at the Onset of Mitosis for an Efficient Recruitment of Pericentriolar Material to Centrosomes

Anand Ramani,[1,2,3] Aruljothi Mariappan,[1,2] Marco Gottardo,[1,2] Sunit Mandad,[4,5,6] Henning Urlaub,[4,5] Tomer Avidor-Reiss,[7] Maria Riparbelli,[8] Giuliano Callaini,[8] Alain Debec,[9] Regina Feederle,[10] and Jay Gopalakrishnan[1,2,3,11,*]

[1]Institute of Human Genetics, Universitätsklinikum Heinrich-Heine-Universität Düsseldorf, Universität Str. 1, 40225 Düsseldorf, Germany
[2]Center for Molecular Medicine Cologne, University of Cologne, Robert-Koch-Str. 21, 50931 Cologne, Germany
[3]IUF–Leibniz-Institut für umweltmedizinische Forschung gGmbH, Auf'm Hennekamp 50, 40225 Düsseldorf, Germany
[4]Bioanalytical Mass Spectrometry Group, Max Planck Institute for Biophysical Chemistry, Am Fassberg 11, 37077 Göttingen, Germany
[5]Bioanalytics, University Medical Center Goettingen, Robert-Koch-Strasse 40, 37075 Goettingen, Germany
[6]Department of Neuro- and Sensory Physiology, University Medical Center Göttingen, Göttingen, Germany
[7]Department of Biological Sciences, College of Natural Sciences and Mathematics, University of Toledo, Toledo, OH 43606
[8]Department of Life Sciences, University of Siena, 53100 Siena, Italy
[9]Polarity and Morphogenesis Group, Institut Jacques Monod, Centre National de la Recherche Scientifique, University Paris Diderot, 75013 Paris, France
[10]Helmholtz Zentrum München, German Research Center for Environmental Health, Institute for Diabetes and Obesity, Core Facility, 81377 Munich, Germany
[11]Lead Contact
*Correspondence: jay.gopalakrishnan@hhu.de
https://doi.org/10.1016/j.celrep.2018.11.102

SUMMARY

Centrosomes are the major microtubule-organizing centers, consisting of centrioles surrounded by a pericentriolar material (PCM). Centrosomal PCM is spatiotemporally regulated to be minimal during interphase and expands as cells enter mitosis. It is unclear how PCM expansion is initiated at the onset of mitosis. Here, we identify that, in *Drosophila*, Plk1/Polo kinase phosphorylates the conserved centrosomal protein Sas-4 *in vitro*. This phosphorylation appears to occur at the onset of mitosis, enabling Sas-4's localization to expand outward from meiotic and mitotic centrosomes. The Plk1/Polo kinase site of Sas-4 is then required for an efficient recruitment of Cnn and γ-tubulin, bona fide PCM proteins that are essential for PCM expansion and centrosome maturation. Point mutations at Plk1/Polo sites of Sas-4 affect neither centrosome structure nor centriole duplication but specifically reduce the affinity to bind Cnn and γ-tubulin. These observations identify Plk1/Polo kinase regulation of Sas-4 as essential for efficient PCM expansion.

INTRODUCTION

Centrosomes have many important cellular functions. Among them is serving as the major microtubule-organizing center (MTOC) in regulating the organization of bipolar spindles for accurate cell division (Conduit and Raff, 2015; Tang and Marshall, 2012). At their core, centrosomes are composed of a pair of centrioles surrounded by pericentriolar material (PCM) formed by various multiprotein complexes (Avidor-Reiss and Gopalakrishnan, 2013; Nigg, 2004; Nigg and Raff, 2009) (Conduit et al., 2014) (Nigg and Holland, 2018). During cell division, centrosomes undergo a strict duplication cycle so that each daughter cell receives a centrosome. At interphase of the cell cycle, when centrioles duplicate, the centrosome contains a basal level of PCM and is incompetent to nucleate robust microtubules. However, as cells enter into mitosis, duplicated centrosomes recruit PCM and expand in size (Conduit et al., 2010; Gopalakrishnan et al., 2012). The process of PCM recruitment enabling centrosomes to be functional organelles in mitosis is called centrosome maturation. Centrosome maturation is not only essential for MTOC function of centrosomes but also critical for newborn daughter centriole-to-centrosome conversion (Fu et al., 2016; Novak et al., 2016).

Mechanisms of PCM recruitment have been studied in various organisms. As an example, in fly embryos, Spd-2 recruits Cnn, a bona fide PCM protein, which is phosphorylated by Polo kinase and is required for expanding PCM during mitosis (Conduit and Raff, 2010; Dix and Raff, 2007; Giansanti et al., 2008). Likewise, in worms, spindle-defective protein 5 (SPD-5), a distant ortholog of Cnn, is recruited to centrioles in an SPD-2-dependent manner, which is then phosphorylated by Plk1/Polo kinase, allowing SPD-5 to assemble mitotic centrosomes (Woodruff et al., 2015; Wueseke et al., 2016). Cnn recruitment in flies also seems to be initiated by Asterless (Asl), another centrosomal protein that functions at early stages of centrosome duplication (Blachon et al., 2008; Novak et al., 2014). Recently, it has been shown that Asl recruitment to the daughter centrioles of fly embryos is

directly dependent on the Cdk1-mediated phosphorylation status of the conserved centrosomal protein Sas-4 (Novak et al., 2016).

Earlier studies revealed that Plk1/Polo kinase, Cnn, and Asl interact with Sas-4 (Conduit et al., 2015; Gopalakrishnan et al., 2011). Thus, it appears that during PCM recruitment to a centrosome, Sas-4 functions upstream to Asl and Cnn. First, because Sas-4 provides a scaffold for S-CAP complexes (Sas-4 and components of PCM proteins such as Cnn, Asl, and PLP) (Conduit et al., 2015; Gopalakrishnan et al., 2011) and second, Sas-4 closely associates with the centriolar wall, providing an interface to mediate PCM tethering to the centriole (Fu and Glover, 2012; Gopalakrishnan et al., 2011; Zheng et al., 2014). However, how the timing and amount of PCM recruitment is determined has yet to be critically analyzed.

Our biochemical studies have identified that tubulin negatively affects Sas-4's ability to form cytoplasmic protein complexes (Gopalakrishnan et al., 2011, 2012; Zheng et al., 2016). *Drosophila* expressing a Sas-4 variant that does not bind tubulin exhibited abnormal PCM recruitment. In this mutant fly, the major PCM protein Cnn, normally abundant in mitotic centrosomes, was observed in interphase centrosomes, while mitotic centrosomes recruited at least twice the amount of Cnn as control centrosomes (Gopalakrishnan et al., 2012). These results suggested that tubulin present in wild-type Sas-4 complexes spatiotemporally regulates the amount of PCM recruitment (i.e., tubulin can function as a molecular switch in regulating Sas-4-mediated PCM recruitment). While these studies have substantiated the S-CAP complexes as components of PCM, at what stage of the cell cycle the S-CAP components are sequentially recruited to distinct domains of the centrosome has remained unclear.

With an application of advanced light microscopy techniques, a recent study using fluorescently tagged centrosomal proteins has elegantly shown distinct patterns of Sas-4, Asl, and Cnn recruitment to interphase centrioles (Conduit et al., 2015). The localization patterns of these proteins in a centrosome reaffirm the findings by the original super-resolution studies that imaged native centrosomal proteins in *Drosophila* and human centrosomes (Fu and Glover, 2012; Mennella et al., 2014) (Lawo et al., 2012). Although these studies provide greater insights into PCM recruitment, the crucial steps that initiate PCM growth, in particular, the upstream events that prime PCM recruitment to centrosomes at the onset of mitosis, remain unclear.

Here, by generating cell-cycle-specific Sas-4 antibodies, we identify that in *Drosophila*, Sas-4 can be phosphorylated by Plk1/Polo kinase. This phosphorylation appears to occur at the onset of mitosis, enabling Sas-4 to expand its localization, growing outward from meiotic and mitotic centrosomes. The Sas-4 residues that can be phosphorylated by Plk1/Polo are then required for an efficient recruitment of Cnn and γ-tubulin for PCM expansion during cell division. Cnn and γ-tubulin recruitments were independent from Asl recruitment. Thus, Plk1/Polo kinase regulation of Sas-4 appears to be a critical step at the early events of PCM expansion in building meiotic and mitotic centrosomes.

RESULTS

Sas-4 Is Post-translationally Modified at the Onset of Mitosis

To identify potential cell-cycle-dependent post-translational modification sites in Sas-4, we took an antibody-based approach using our mouse monoclonal antibodies generated against amino acids 1–350 of Sas-4 (Figure 1A). One of the clones (hereafter anti-Sas-4) recognized Sas-4 at centrosomes of *Drosophila* cells (Schneider cells) throughout the cell cycle (Figure 1B, i). The epitope-containing region for this antibody is present within the PN2-3 domain at the N terminus of Sas-4 (Figure 1A) (Gopalakrishnan et al., 2011, 2012; Hung et al., 2004). Another clone for which the epitope-containing region is 190-LIGKNACSSTPDLKS SYASSTTASSTSPRV-220 recognized Sas-4 at both centrosomal pairs of the interphase and prophase, similar to anti-Sas-4. However, using this antibody, we could not detect Sas-4 in either of the centrosomes of mitosis (hereafter non-mitotic anti-Sas-4) (Figure 1B, ii).

To investigate the localization pattern of Sas-4 recognized by the non-mitotic anti-Sas-4 at subdiffraction resolution, we performed stimulated emission depletion (STED) microscopy with ~50 nm lateral, 120 nm axial resolution (Fu et al., 2016). It is known that Sas-4 preferentially localizes to the daughter centrioles, which in turn then recruits another centrosomal protein Asl (Novak et al., 2014, 2016). Asl is recruited to daughter centrioles only after the centrosomes are disengaged at the end of mitosis (Novak et al., 2014). Thus, in our analysis, we used Asl labeling to distinguish mother centrioles from daughter centrioles. Notably, the non-mitotic anti-Sas-4 preferentially recognized Sas-4 at daughter centrioles at interphase and prophase (Figure 1C, i and ii). Even at this subdiffraction resolution, we could not detect Sas-4 in either of the metaphase centrosomes (Figure 1C, iii). This finding suggests that the epitope for non-mitotic anti-Sas-4 appears to be post-translationally modified at the onset of metaphase.

Sas-4-TT211 Can Be Phosphorylated at the Onset of Mitosis

We then aimed to identify whether there are phosphorylatable residues within the epitope-containing region (190-LIGK NACSSTPDLKSSYASSTTASSTSPRV-220) of the non-mitotic anti-Sas-4 antibody. We noticed that there are at least two regions, namely -P1 and -P2 sites, containing threonine and serine residues that can be phosphorylated (Figure 2A). To identify the responsible residues for the non-mitotic anti-Sas-4, we expressed recombinant Sas-4 proteins (amino acids 1–350) containing deletions or replacements and probed them using the non-mitotic anti-Sas-4 (Figures S1A and S1B). This antibody failed to recognize the protein in which both -P1 and -P2 sites were deleted (Figure S1C). However, this antibody recognized the replacement of the -P1 but not the -P2 site, suggesting that the -P2 site harboring -SSTT211 (we number the first threonine) is a responsible residue for the non-mitotic anti-Sas-4. It has been recently shown that Cdk1 phosphorylates Sas-4's threonine at 200 (Sas-4-T200) of the -P1 site at the onset of mitosis (Novak et al., 2016).

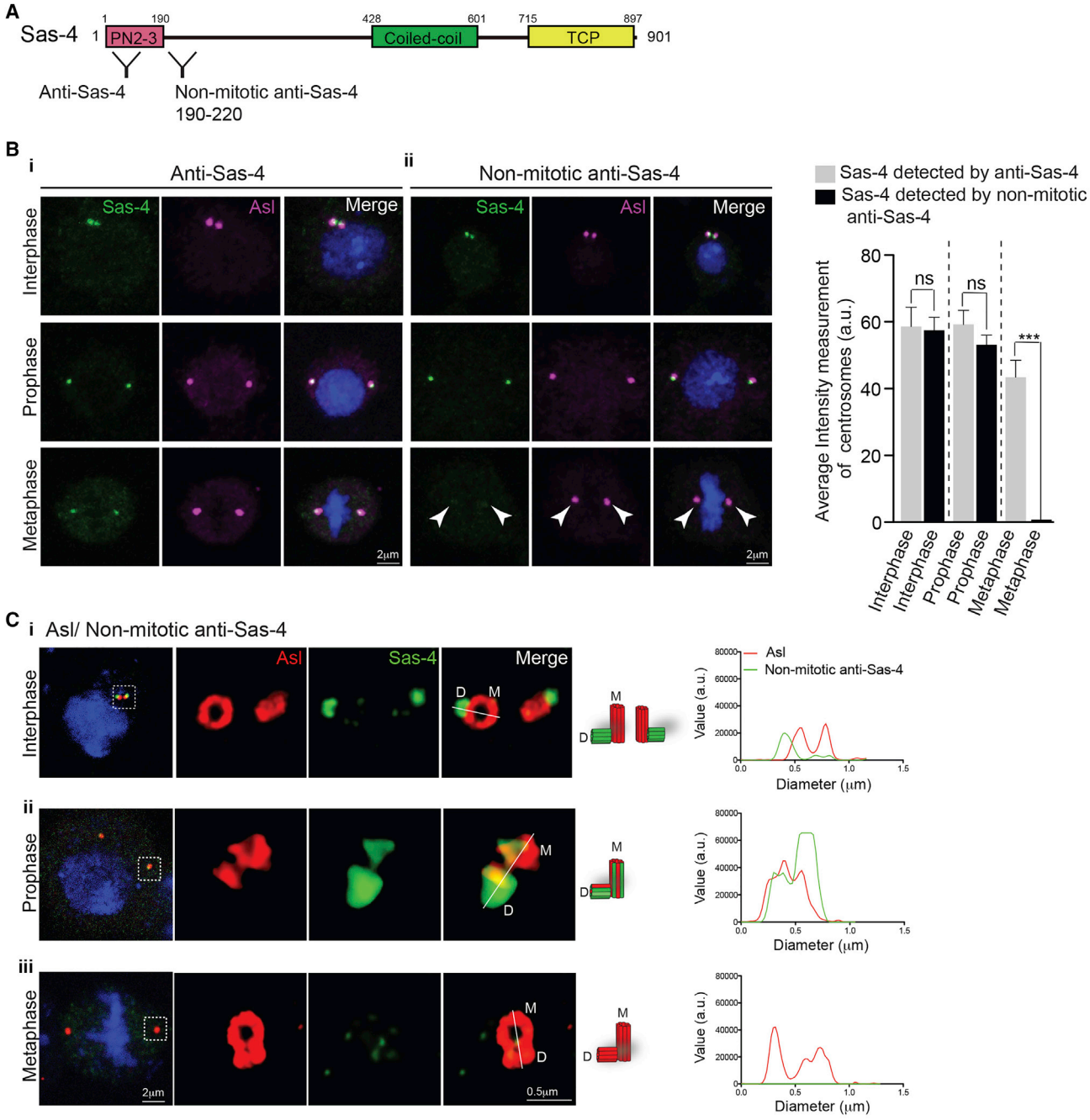

Figure 1. Non-mitotic Anti-Sas-4 Recognizes Centrosomal Sas-4 from Interphase through Prophase but Not at Metaphase

(A) Schematic of Sas-4 protein indicating epitope regions for anti-Sas-4 and non-mitotic anti-Sas-4 antibodies.

(B) Anti-Sas-4 antibody (green) recognizes Sas-4 at centrosomes of *Drosophila* cells (Schneider cells) throughout the cell cycle. Asl (magenta) labels centrosomes (i). In contrast, non-mitotic anti-Sas-4 does not recognize metaphase Sas-4 (arrowheads) (ii). Bar graph at right represents the average intensity measurements of centrosomes (labeled by anti-Sas-4 and non-mitotic anti-Sas-4). At least 60 centrosomes (n = 60) were analyzed from 3 independent experiments. ANOVA, ***$p < 0.0001$. Error bars represent means ± SEMs. See also Figure S1.

(C) Characterization of non-mitotic anti-Sas-4 using stimulated emission depletion (STED) microscopy. At interphase (before centrosomes disengage), non-mitotic anti-Sas-4 preferentially recognizes Sas-4 at the daughter centrioles (green). Note that Asl (red) labels only mother centrioles at interphase (i). At prophase (after centrosomes disengage), non-mitotic anti-Sas-4 also recognizes mother centrioles. Note that Asl starts to label daughter centrioles where Sas-4 is abundant (ii). At metaphase, non-mitotic anti-Sas-4 recognizes neither of the centrioles. At this stage, Asl (red) labels both mother and daughter centrioles. Illustrations of centrioles containing Asl and Sas-4 are at right. Line graph representing the relative distribution of proteins at the mother and daughter centrioles of various cell-cycle stages is at right. At least 30 mitotic centrosomes (n = 30) were analyzed for each antibody.

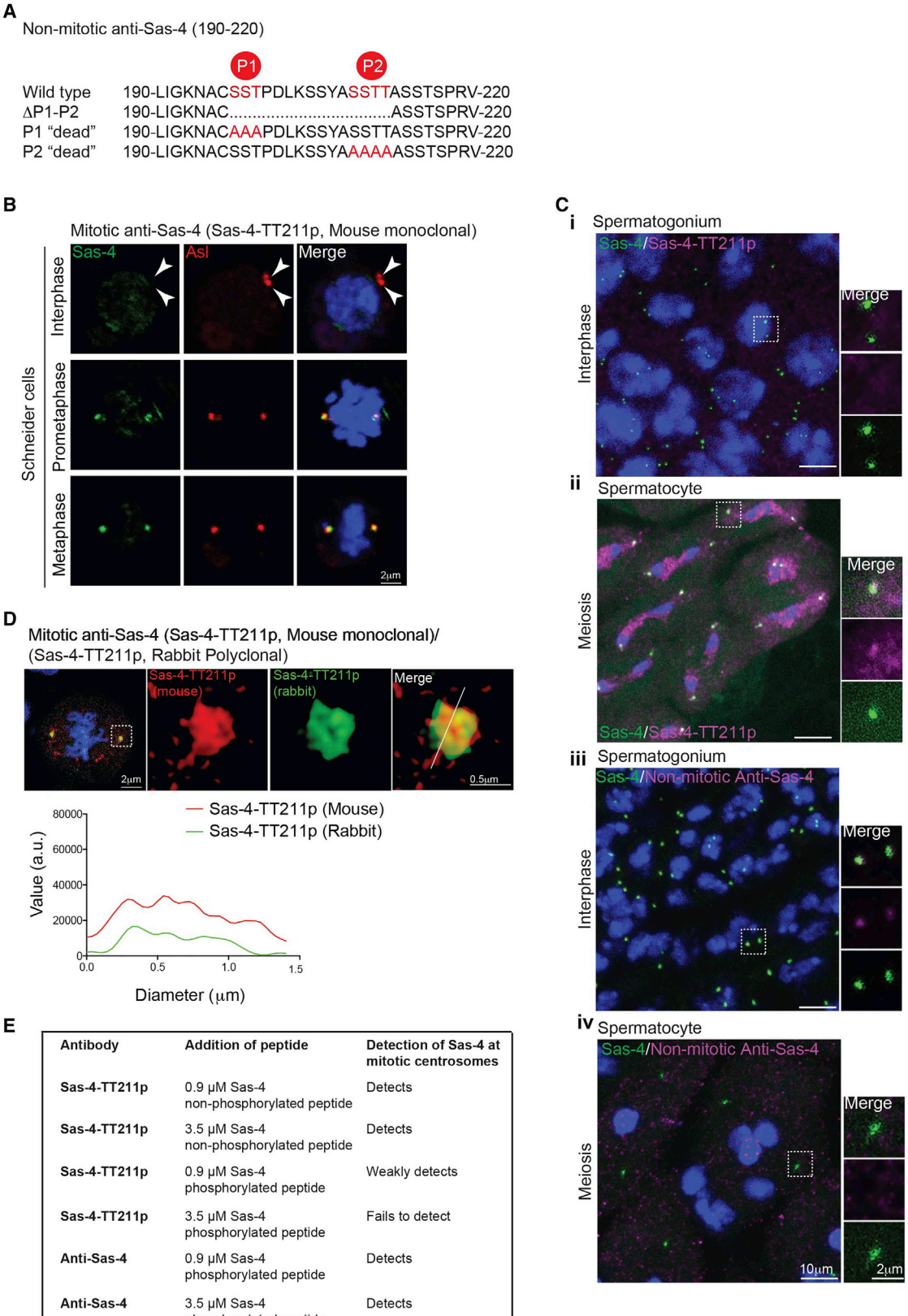

E

Antibody	Addition of peptide	Detection of Sas-4 at mitotic centrosomes
Sas-4-TT211p	0.9 μM Sas-4 non-phosphorylated peptide	Detects
Sas-4-TT211p	3.5 μM Sas-4 non-phosphorylated peptide	Detects
Sas-4-TT211p	0.9 μM Sas-4 phosphorylated peptide	Weakly detects
Sas-4-TT211p	3.5 μM Sas-4 phosphorylated peptide	Fails to detect
Anti-Sas-4	0.9 μM Sas-4 phosphorylated peptide	Detects
Anti-Sas-4	3.5 μM Sas-4 phosphorylated peptide	Detects

(legend on next page)

To further narrow down the epitope residues, we generated peptides with single amino acid replacements within the -P2 site (-SSTT211) and performed dot blots. The non-mitotic anti-Sas-4 recognized all of the single amino acid replacements with alanine (Figure S1D). However, replacing double amino acids with two-alanine -SSTT211 to -SSAA211 narrowed down the responsible residues for the non-mitotic anti-Sas-4 to be -TT211 (Figure S1E).

We then generated mouse monoclonal and rabbit polyclonal antibodies using a peptide (207-YASS**TT**ASSTSPRV-220) as an antigen in which both of the threonine -TT211s are phosphorylated. The resulting antibodies are called mitotic anti-Sas-4 (Sas-4-TT211p, where TTp denotes phosphorylated threonine residues). These antibodies specifically recognize a peptide that harbors two-phosphorylated threonine at -TT211 (Figure S1F). Although the mitotic anti-Sas-4 (Sas-4-TT211p) did not satisfactorily detect the protein in the western blots, both of these antibodies recognized Sas-4 not at the interphase but starting from prometaphase, suggesting that -TT211s are phosphorylated at the onset of mitosis (Figure 2B). Similarly, these antibodies did recognize only dividing sperm cells in *Drosophila* testes (Figure 2C). The labeling patterns of both of these antibodies at mitotic centrosomes were nearly identical, as demonstrated by STED microscopy (Figure 2D).

To validate the specificity of Sas-4-TT211p antibodies, we used Schneider cells (C131), which lack endogenous Sas-4 and centrosomes. Sas-4-TT211p antibodies could recognize centrosomes only when these cells were transfected with the Sas-4-GFP construct (Figure S1G). To further test whether Sas-4-TT211 is phosphorylated in cells, we performed a competition experiment with increasing concentrations of phosphorylated peptide (207-YASS**TT**ASSTSPRV-220), which could hinder the Sas-4-TT211p antibody from binding to the phosphorylated version of endogenous Sas-4 (Figure S2). In control experiments, we used a non-phosphorylated peptide (207-YASSTTASS TSPRV-220). At 0.9 μM phosphorylated peptide, the antibody could faintly recognize Sas-4 at mitotic centrosomes. However, at 3.5 μM phosphorylated peptide, the antibody nearly failed to recognize Sas-4 at mitotic centrosomes (Figures S2A and S2B). In contrast, in the presence of the non-phosphorylated peptide (both at 0.9 and 3.5 μM), Sas-4-TT211p could recognize Sas-4 normally at mitotic centrosomes (Figures S2C and S2D). Neither of these peptides prevented anti-Sas-4 (which labels Sas-4 throughout the cell cycle) from recognizing Sas-4 at mitotic centrosomes (Figures S2E and S2F). The schematic of this experiment and the results are summarized in Figures S2G and 2E. It is noteworthy that centrosome maturation begins with PCM recruitment, which occurs at the onset of mitosis.

In summary, we have obtained three different anti-Sas-4 antibodies, namely (1) anti-Sas-4, which recognizes centrosomal Sas-4 throughout the cell-cycle phases (Figure 1Bi); (2) non-mitotic anti-Sas-4, which recognizes Sas-4 only up to the prophase-like stage (Figures 1B, ii, and 1C); and (3) mitotic anti-Sas-4 (Sas-4-TT211p), which recognizes Sas-4 only at the onset of mitosis (Figures 2B, 2C, and S1H).

Plk1/Polo Can Phosphorylate Sas-4-TT211 *In Vitro*

At interphase, Sas-4 is incorporated into newly forming centrioles (Dammermann et al., 2008) (Figure 1C). In mitotic centrosomes where no centriole duplication occurs, Sas-4 is stably incorporated within mother centrioles, and no new Sas-4 is synthesized or exchanged from the cytoplasmic pool (Dammermann et al., 2008; Novak et al., 2014). This finding has possibly precluded the idea of Sas-4 being involved in mitotic PCM recruitment. However, a recent work showed that Cdk1 phosphorylates Sas-4's T200 at the onset of mitosis, providing a Polo docking site, which in turn recruits the PCM protein Asl to daughter centrioles of mitotic centrosomes (Novak et al., 2016). In addition, it is known that Plk1/Polo is required for the dramatic increase in PCM that occurs before mitotic entry in Schneider cells (Riparbelli et al., 2014; Asteriti et al., 2015; Haren et al., 2009). From these, we hypothesized that Plk1/Polo docking could phosphorylate Sas-4, which triggers the further recruitment of PCM components such as Cnn and γ-tubulin, which determine centrosome size.

It is known that Plk1/Polo kinase co-immunoprecipitates with Sas-4 (Gopalakrishnan et al., 2011) (Figure 3A). To determine whether Plk1/Polo can phosphorylate Sas-4's TT211, we tested whether Plk1/Polo kinase can directly interact with Sas-4. We found that wild-type recombinant Sas-4 1–350 could bind recombinant Plk1/Polo kinase. Deleting both -P1 and -P2 sites significantly reduced the binding capacity of Sas-4 to Plk1/Polo kinase (Figure 3B). To analyze whether Plk1/Polo kinase can specifically phosphorylate Sas-4-TT211, we extended our *in vitro* kinase assay on a Sas-4 peptide (207-YASSTTA SSTSPRV-220) that contained the epitope region for the non-mitotic anti-Sas-4 (Figure 3C). We took this peptide-based approach to avoid non-specific phosphorylation in sites other than the epitope-containing region. In positive controls, we used a Sas-4 phosphopeptide in which -TT211s are phosphorylated. In negative controls, we used an Sas-4 mutant peptide in which two of the threonines is replaced with non-phosphorylatable

Figure 2. Sas-4-TT211 Is Phosphorylated at the Onset of Mitosis

(A) Epitope-containing region (190-LIGKNACSSTPDLKSSYASSTTASSTSPRV-220) of the non-mitotic anti-Sas-4 displaying -P1 and -P2 sites (red). Different peptides used in this study are given.

(B) Mitotic anti-Sas-4 (Sas-4-TT211p) specifically recognizes centrosomal Sas-4 at prometaphase and metaphase (green). Note that mitotic anti-Sas-4 (Sas-4-TT211p) does not recognize interphase centrosomes (arrowheads). Asl (red) labels centrosomes. At least 60 mitotic centrosomes (n = 60) were analyzed for each condition. See also Figures S1 and S2.

(C) Sas-4-TT211p (i and ii, magenta) specifically labels mitotic centrosomes of *Drosophila* spermatocytes expressing Sas-4-GFP (green). The non-mitotic anti-Sas-4 (iii and iv, magenta) fails to recognize mitotic centrosomes, but specifically recognizes interphase centrosomes expressing Sas-4-GFP (green). At least 40 mitotic centrosomes (n = 40) were analyzed for each condition.

(D) STED imaging of mitotic centrosomes labeled by both mouse monoclonal and rabbit polyclonal mitotic anti-Sas-4 (Sas-4-TT211p). Line graphs representing the relative distributions of Sas-4 recognized by these antibodies are provided below. At least 20 mitotic centrosomes (n = 20) were analyzed for each condition.

(E) The table provides a summary of the Sas-4 peptide-based competition experiment in Schneider cells to confirm the specificity of Sas-4-TT211p antibody.

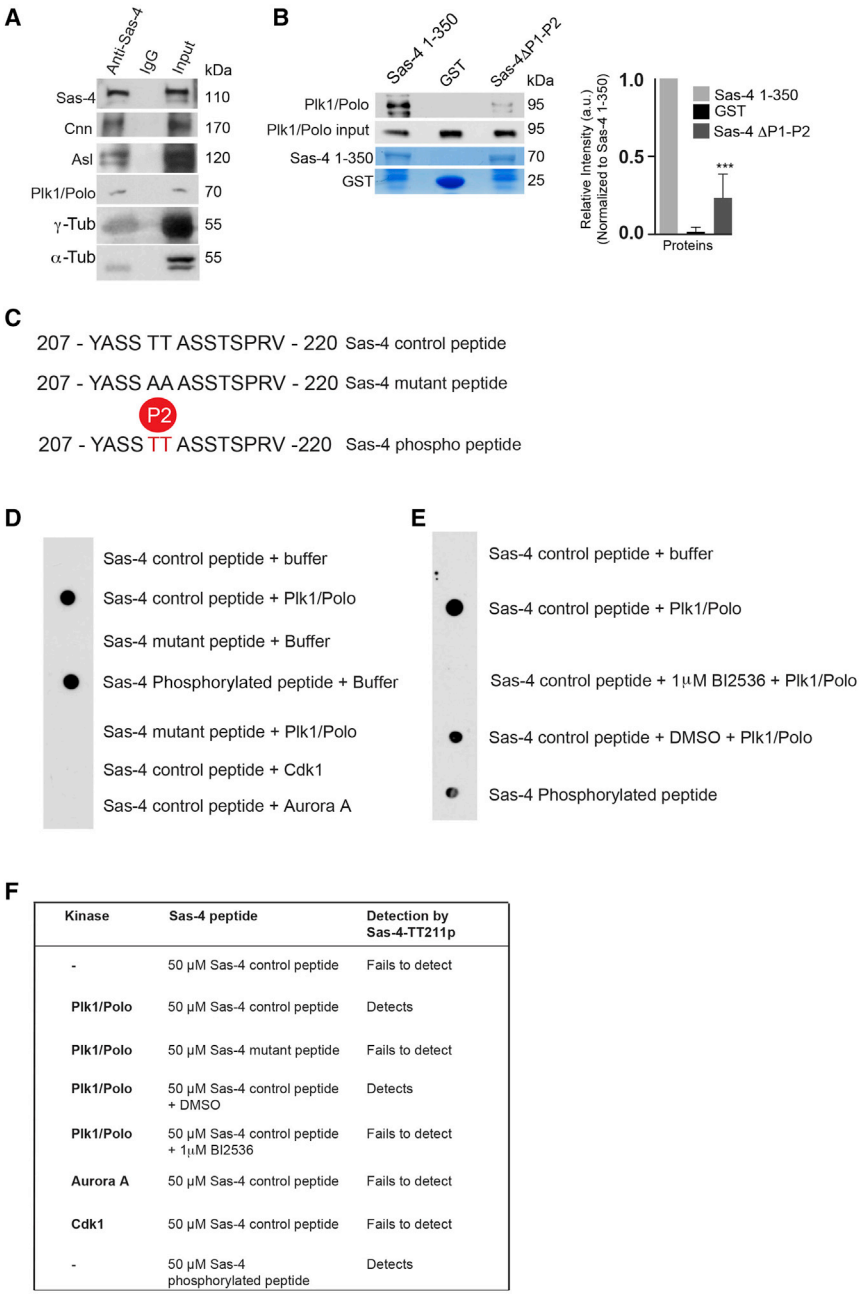

F

Kinase	Sas-4 peptide	Detection by Sas-4-TT211p
-	50 μM Sas-4 control peptide	Fails to detect
Plk1/Polo	50 μM Sas-4 control peptide	Detects
Plk1/Polo	50 μM Sas-4 mutant peptide	Fails to detect
Plk1/Polo	50 μM Sas-4 control peptide + DMSO	Detects
Plk1/Polo	50 μM Sas-4 control peptide + 1μM BI2536	Fails to detect
Aurora A	50 μM Sas-4 control peptide	Fails to detect
Cdk1	50 μM Sas-4 control peptide	Fails to detect
-	50 μM Sas-4 phosphorylated peptide	Detects

Figure 3. Plk1/Polo Can Bind and Phosphorylate Sas-4-TT211 *In Vitro*

(A) Immunopurification of Sas-4 complexes from *Drosophila* embryonic extracts using the anti-Sas-4 antibody. Plk1/Polo along with the S-CAP components co-immunoprecipitate with Sas-4. Immunoglobulin G (IgG)-coated beads are used as the control.

(B) Plk1/Polo directly interacts with Sas-4 1–350. Note that the deletion version of Sas-4 1-350 (190-LIGKNACSSTPDLKSSYASSTTASSTSPRV-220), in which the epitope region for the non-mitotic and mitotic anti-Sas-4 antibodies are eliminated, exhibits a reduced binding capacity. Coomassie blue staining of recombinant Sas-4 1–350 is given at bottom. The bar graph at right represents the relative intensity of Plk1/Polo interaction with Sas-4 variants. ANOVA, ***$p < 0.0001$. Error bars represent means ± SEMs from 3 independent experiments. See also Figure S3.

(C) Various peptides spanning the epitope for the mitotic anti-Sas-4 antibody (Sas-4-TT211p). Note that Sas-4 control peptide is wild-type (207-YASSTTASSTSPRV-220); Sas-4 mutant peptide carries two amino acid replacements TT211AA (207-YASSAAASSTSPRV-220), and Sas-4 phosphorylated peptide carries two phosphorylated threonine residues -TT211p (207-YASS**TT**ASSTSPRV-220).

(D) *In vitro* kinase assays. Plk1/Polo but not other cell-cycle kinases could phosphorylate Sas-4 control peptide used in this experiment. Note that Sas-4 mutant peptide is used in negative control experiments and phosphorylated peptide is used in positive control experiments. In control experiments, buffer replaces candidate kinases. Mitotic anti-Sas-4 antibodies (Sas-4-TT211p) were used to recognize the phosphorylation status of peptides. See also Figure S2.

(E) Plk1/Polo-mediated kinase activity is specific as revealed by the use of Plk1/Polo-kinase inhibitor BI2536, which inhibits the phosphorylation of the Sas-4 control peptide. In control experiments, the solvent DMSO replaces the inhibitor.

(F) The table summarizes the *in vitro* kinase assay using various Sas-4 peptides and mitotic kinases.

alanine. We probed these peptides using the mitotic anti-Sas-4 (Sas-4-TT211p) that is raised against two-phosphorylated threonine of Sas-4, which labels centrosomal Sas-4 only at the onset of mitosis. We noticed that the peptide (207-YASSTTASSTSPRV-220) could be phosphorylated by Plk1/Polo kinase as detected by the mitotic anti-Sas-4 (Sas-4-TT211p) (Figure 3D).

Furthermore, we could identify that Sas-4-TT211 is specifically phosphorylated by Plk1/Polo, since the antibody did not recognize the control peptide when the kinase assays used Cdk1 and aurora A (Figure 3D). The mitotic anti-Sas-4 (Sas-4-TT211p) did not recognize the peptide when -TT211 of the peptide was replaced with alanine (-TT211AA) or when the kinase assays included 1 μM BI2536, a specific Plk1/Polo inhibitor (Figure 3E). These results demonstrate that Plk1/Polo can phosphorylate Sas-4's TT211 and that mitotic anti-Sas-4 (Sas-4-TT211p) is specific for phosphorylated threonine at TT211 of Sas-4. A summary of this experiment is given in Figure 3F.

Sas-4-TT211 Seems to Be Phosphorylated at the Onset of Mitosis for an Efficient Interaction with Cnn and γ-Tubulin

To further corroborate our findings that Sas-4-TT211 is phosphorylated in cells at the onset of mitosis, we treated Schneider cells with 0.5 μM BI2536 and performed immunostaining using

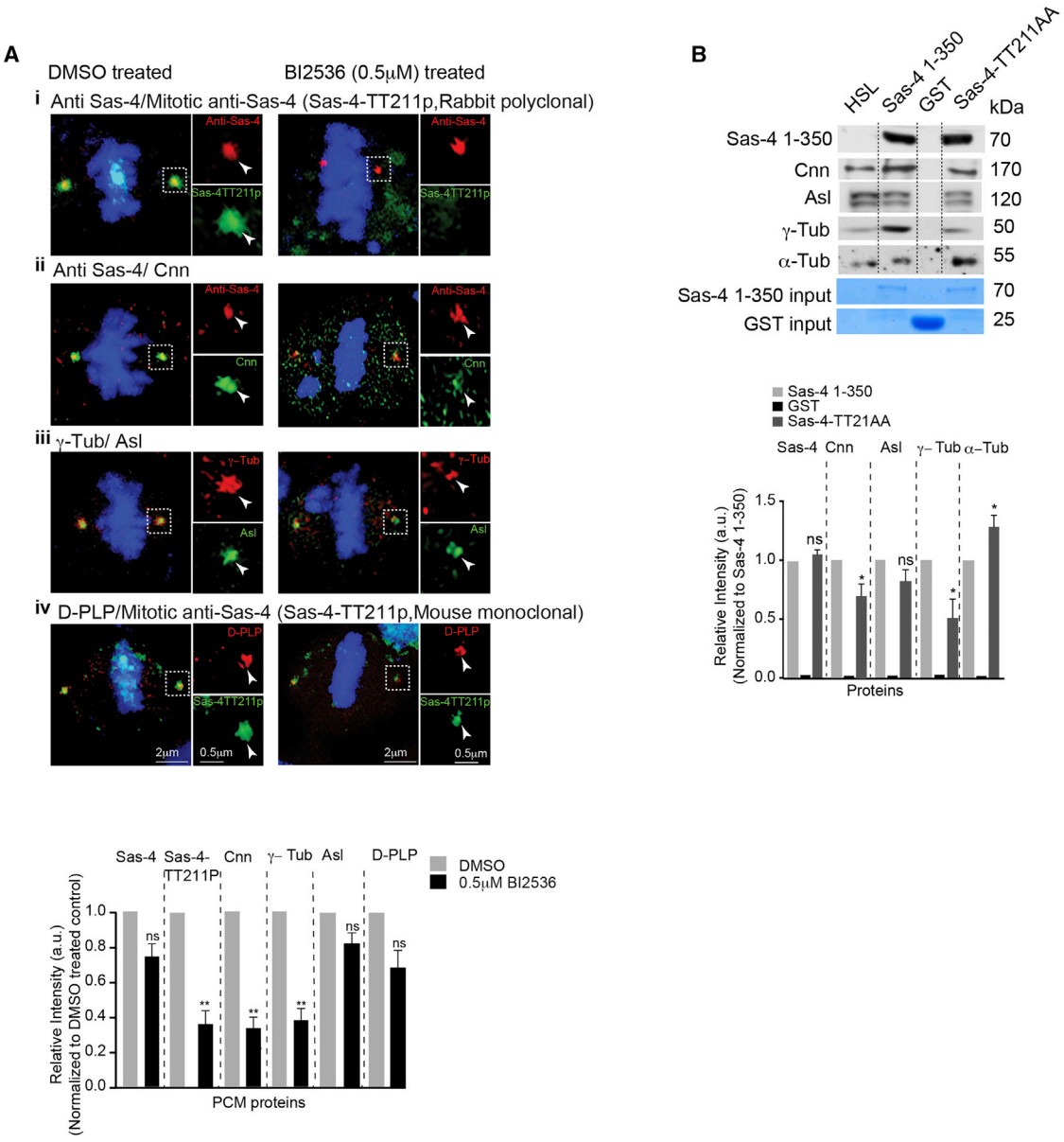

Figure 4. Phosphorylation of Sas-4-TT211 by Plk1/Polo Is Required for Efficient Binding of PCM Proteins

(A) Fraction of Schneider cells exhibiting bipolar spindles in the presence of Plk1/Polo-kinase inhibitor BI2536. In the presence of inhibitor, the mitotic anti-Sas-4 antibody (Sas-4-TT211p) fails to recognize mitotic Sas-4 (green). Note that the inhibitor BI2536 does not have the same effect on Sas-4 population that is recognized by anti-Sas-4 (red) that labels Sas-4 in all phases of the cell cycle (i). Mitotic recruitment of Cnn (green) and γ-tubulin (red) but not Asl (green) and D-PLP (red) are significantly perturbed in the presence of Plk1/Polo-kinase inhibitor BI2536 (ii–iv). The bar graph below represents the relative intensities of Sas-4, Cnn, γ-tubulin, Asl, and D-PLP recruitments to mitotic centrosomes in the presence of Plk1/Polo-kinase inhibitor BI2536. At least 60 mitotic centrosomes (n = 60) were analyzed for each condition from 3 independent experiments. Student's t test, $^{**}p < 0.001$. Error bars represent means ± SEMs.

(B) GST-pull down assay (i). Sas-4-TT211 is required for efficient binding of Cnn and γ-tubulin in the absence of endogenous Sas-4. Recombinant GST-tagged Sas-4 protein variants were used to capture its interaction partners from C131 cell extracts that lack endogenous Sas-4. HSL, high-speed cell extract that contains only cytoplasmic fractions. The bar graph at bottom represents the relative intensity of PCM proteins bound to GST-tagged Sas-4 1-350, GST, and Sas-4-TT211AA. ANOVA, $^{*}p < 0.05$. Error bars represent means ± SEMs from 3 independent experiments. See also Figure S4.

the mitotic anti-Sas-4 (Sas-4-TT211p) and anti-Sas-4 antibody. In the presence of BI2536, the mitotic anti-Sas-4 (Sas-4-TT211p) failed to strongly recognize Sas-4. In contrast, BI2536 treatment did not affect the anti-Sas-4 antibody, which labels centrosomal Sas-4 throughout the cell cycle. These data suggest that Sas-4-TT211 seems to be phosphorylated by Plk1/Polo kinase at the onset of mitosis (Figure 4A, i).

We then tested the composition of BI2536-treated mitotic centrosomes using antibodies specific for S-CAP components such as Cnn, Asl, *Drosophila* pericentrin-like protein (D-PLP),

and γ-tubulin. Analyzing a fraction of cells exhibiting bipolar spindles, we noticed that BI2536 treatment could significantly reduce the recruitment of Cnn and γ-tubulin, PCM proteins that are essential for PCM expansion in mitosis (Figure 4A, ii–iv). These data suggest that Plk1/Polo kinase activity is required to build proper mitotic centrosomes, and this could occur via the phosphorylation of Sas-4.

To investigate the importance of Sas-4-TT211 in binding PCM proteins *in vitro*, we performed glutathione S-transferase (GST) pull-down assays using recombinant Sas-4 variants (amino acids 1–350 of Sas-4) and the cytoplasmic fraction of *Drosophila* cell extracts lacking endogenous Sas-4. These cells were originally derived from *Drosophila* null embryos (Lecland et al., 2013; Zheng et al., 2014). By performing western blots for Cnn and γ-tubulin, we identified the Sas-4 variant that contains non-phosphorylatable -TT211AA, in which two threonine residues were replaced with two alanine residues, bind lesser amounts of these proteins as compared to wild-type protein. The amount of Asl binding did not vary significantly among the Sas-4 variants (Figure 4B). Thus, the finding that the recombinant Sas-4 binds S-CAP components Cnn, γ-tubulin, and Asl independently from endogenous Sas-4 reaffirms previous studies describing the ability of Sas-4 to form S-CAP complexes (Conduit et al., 2015; Gopalakrishnan et al., 2011).

Sas-4's Localization Expands Outward from Mitotic Centrosomes

Previous super-resolution microscopy studies have revealed that Sas-4 is a centriole wall protein that is closely associated with centriolar microtubules of interphase centrosomes (Dammermann et al., 2008; Gopalakrishnan et al., 2011). These studies have resolved that Sas-4 is associated with its interacting proteins D-PLP and Plk1/Polo, forming a cylinder-like zone around centrioles (Fu and Glover, 2012). To investigate the localization pattern of Sas-4 at the onset of mitosis at subdiffraction resolution, we performed STED microscopy of mitotic centrosomes of Schneider cells using our various anti-Sas-4 antibodies. Agreeing with previous findings using the anti-Sas-4 antibody, we noticed a preferential localization of Sas-4 to one of the centrioles, suggesting that they are the daughter centrioles (Figure 5A). However, imaging of mitotic centrosomes that are labeled with the mitotic anti-Sas-4 (Sas-4-TT211p) revealed an expanded localization of Sas-4 as a cloud surrounding both mother and daughter centrioles (Figure 5B). This expanded Sas-4 cloud is reminiscent of the PCM cloud labeled by Cnn and γ-tubulin, the major PCM components (Dammermann et al., 2008; Gopalakrishnan et al., 2011; Kirkham et al., 2003; Woodruff et al., 2014).

To verify this, we co-stained mitotic centrosomes with Cnn/γ-tubulin and mitotic anti-Sas-4 (Sas-4-TT211p). Cnn marked centrosomes as a cloud surrounding Sas-4 that is recognized by anti-Sas-4 (Figure 5C). However, we noticed that both the Cnn and γ-tubulin clouds co-localized with that of Sas-4, which is recognized by the mitotic anti-Sas-4 (Sas-4-TT211p) (Figures 5D and 5E). These findings indicate that phosphorylated Sas-4 at the onset of mitosis has a tendency to expand outward from mitotic centrosomes. This phenomenon is similar to that of bona fide PCM proteins such as Cnn and γ-tubulin that determine the centrosome size in mitosis.

Sas-4-TT211 Is Required for an Efficient Recruitment of Cnn and γ-Tubulin *In Vitro* and *In Vivo*

To test whether Sas-4-TT211 is essential for PCM recruitment function of Sas-4 functions *in vitro*, we expressed various Sas-4 mutations in Schneider cells and tested their ability to recruit PCM proteins to mitotic centrosomes (Figure S3). Sas-4 ΔP1-P2 expressing cells did show mild defects in Cnn recruitment, while D-PLP and Asl levels were unaffected. We reasoned that the observed mild phenotype is due to the presence of endogenous Sas-4 in Schneider cells.

We then turned to testing whether Sas-4-TT211 is essential for Sas-4 functions *in vivo*. For this, we generated transgenic *Drosophila* expressing GFP-tagged Sas-4^{WT} and Sas-4^{TT211AA}. As additional controls, we generated two different transgenic flies. GFP-tagged Sas-4$^{\Delta P1\text{-}P2}$, a larger deletion that includes both -P1 and -P2 sites, and Sas-4^{SST198AAA}, a mutation within the -P1 site harboring a threonine residue that can be phosphorylated by Cdk1 (Novak et al., 2016). All of these transgenic flies were constructed to express the Sas-4 gene under its own endogenous promoter. Except for Sas-4^{WT}, none of the Sas-4 transgenic flies harboring mutations or deletions rescued the un-coordination phenotypes of Sas-4 null flies, indicating that the perturbed regions of Sas-4 are required to form functional centrosomes.

In *Drosophila*, centrioles of matured spermatocytes elongate up to 2 μm and recruit Cnn and an enhanced level of γ-tubulin proteins only at the metaphase of male meiosis. These aspects allow fly spermatocytes to be an ideal system to analyze whether there are defects in centriole length and PCM recruitment (Gopalakrishnan et al., 2012; Zheng et al., 2016). Analyzing metaphase spermatocytes dissected from dark pupae of homozygous Sas-4 transgenic flies (Sas-4^{WT}, Sas-4^{TT211AA}, Sas-4^{SST198AAA}, and Sas-4$^{\Delta P1\text{-}P2}$ in *sas-4* null genetic background), we identified that germ cells contained the correct number of centrioles whose lengths, integrity, and configuration in a "V" shape remain unaffected (Figures S4A and S4B).

We then analyzed the ability of these centrosomes to recruit PCM proteins. We noticed that Asl or D-PLP recruitment was unaffected in all of the Sas-4 transgenic flies generated (Figures 6A, i and ii, and S4C, i). However, a proportion of cells in Sas-4^{TT211AA} and Sas-4$^{\Delta P1\text{-}P2}$ flies failed to recruit Cnn (~11% of cells in Sas-4^{TT211AA} and ~18% of cells in Sas-4$^{\Delta P1\text{-}P2}$ flies) and γ-tubulin (~9% of cells in Sas-4^{TT211AA} and ~13% of cells in Sas-4$^{\Delta P1\text{-}P2}$ flies) to at least one of the centriolar pairs.

We then analyzed a proportion of cells in which both centriolar pairs could recruit γ-tubulin and Cnn. Analyzing the intensity of Cnn and γ-tubulin recruitment revealed that compared to Sas-4^{WT} and Sas-4^{SST198AAA} flies, Sas-4^{TT211AA} and Sas-4$^{\Delta P1\text{-}P2}$ flies recruited relatively lesser amounts of Cnn and γ-tubulin (Figure 6C). We determined that, in contrast to metaphase centrosomes, interphase centrosomes could recruit normal levels of γ-tubulin (Figure S4D). Finally, we performed transmission electron microscopy of interphase and dividing spermatocytes and identified that Sas-4^{TT211AA} contained no visible structural defects in their centrioles. This finding further supports that

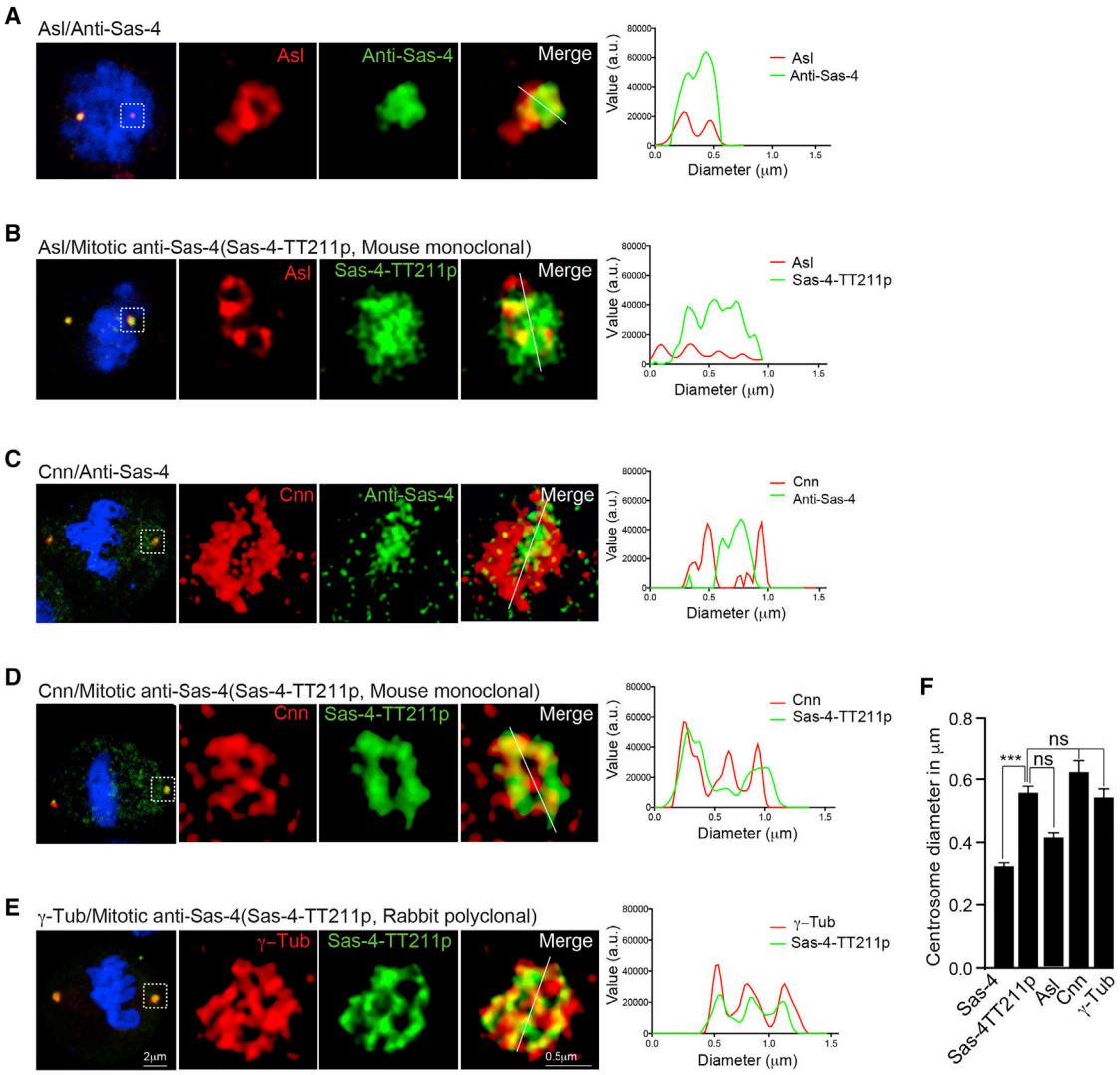

Figure 5. STED Imaging Reveals that Sas-4 Expands Outward from the Mitotic Centrosomes

(A) Localization of Sas-4 recognized by anti-Sas-4 (green) that recognizes Sas-4 throughout the cell cycle with respect to Asl (red). Note that anti-Sas-4 labels Sas-4 within a confined area.

(B) In contrast to anti-Sas-4, the mitotic-anti-Sas-4 (Sas-4-TT211p) antibody labels mitotic Sas-4 expanding outward from mitotic centrosomes (green). Asl (Red) labels both of the centrioles.

(C–E) The bona fide PCM proteins Cnn (C and D, red) and γ-tubulin (E, red) co-localize with phosphorylated Sas-4 (D and E, green). The relative diameters of centrosomal proteins are represented graphically at right.

(F) The bar graph at right represents the diameter of centrosomes distinguished by various antibodies. Note that there is no significant difference in diameter measured between phosphorylated Sas-4 and PCM proteins Cnn and γ-tubulin. At least 20 mitotic centrosomes were analyzed for each condition (n = 20). ANOVA, ***$p < 0.0001$. Error bars represent means ± SEMs.

Sas-4's TT211 is essential for PCM recruitment and does not affect the structural or numerical integrity of centrioles (Figures S5A and S5B).

Sas-4-TT211 Is Required for an Efficient Recruitment of Cnn and γ-Tubulin to Mitotic Centrosomes of Larval Brain Cells and Syncytial Embryos

Next, we tested the importance of Sas-4-TT211-mediated PCM recruitment in cell types that undergo rapid cell cycle. First, we analyzed fixed mitotic larval brain cells expressing Sas-4^{WT}, Sas-$4^{TT211AA}$, Sas-$4^{SST198AAA}$, and Sas-$4^{\Delta P1\text{-}P2}$. The mitotic cells of Sas-4^{WT} mostly contained two centrosomes, as judged by the presence of Sas-4 and Asl. In contrast, ~30% of Sas-4 mutant cells contained one centrosome (Figure S6A). Centrosomes in all cases (whether they harbor one or two centrosomes) contained nearly normal levels of Sas-4 and Asl. We then analyzed the rest of the mitotic cells that contained two centrosomes. We identified that ~30% of mitotic cells failed to efficiently recruit Cnn and γ-tubulin to at least one of the centrosomes, a phenotype that is similar to what was observed in meiotic

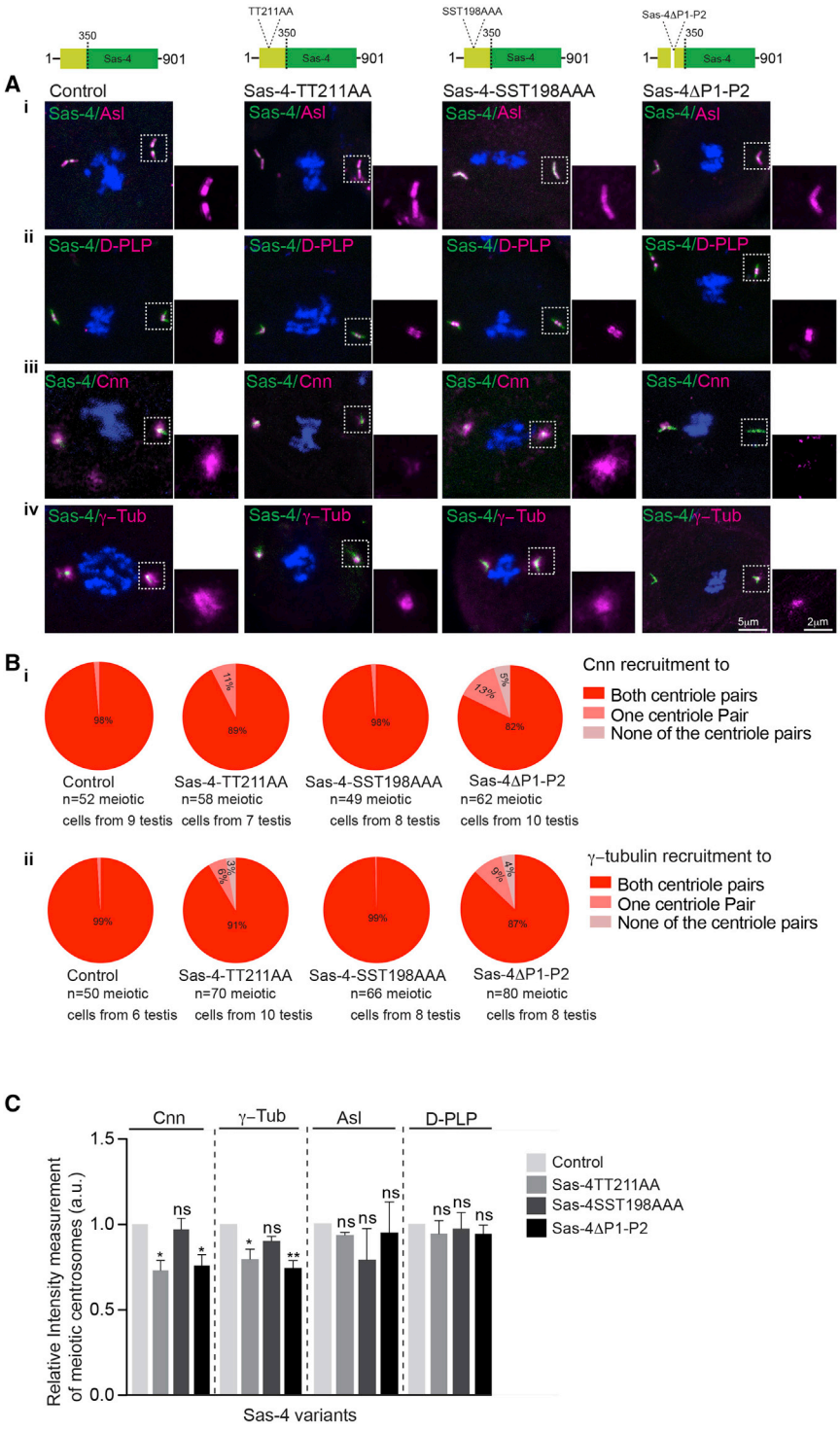

Figure 6. Sas-4-TT211 Is Required for Efficient Recruitment of PCM Proteins in Centrosomes of Meiotic Spermatocytes

(A) Asl (i, magenta) or D-PLP (ii, magenta) recruitment is unaffected in all of the transgenic flies expressing different Sas-4 variants. Cnn (iii, magenta) and γ-tubulin (iv, magenta) recruitments are reduced in Sas-4^{TT211AA} and Sas-4$^{\Delta P1\text{-}P2}$ but not in Sas-4^{SST198AAA} flies. For clarity, schematics of different Sas-4 mutations are shown at top. See also Figures S4 and S6.

(B) Pie charts represent the proportion of cells that fail to recruit Cnn (i) and γ-tubulin (ii). n represents the number of cells in each transgenic fly.

(C) Bar graph represents the relative intensities of tested proteins' recruitment to meiotic centrosomes. Note that there is a significant reduction in the recruitment of Cnn and γ-tubulin but not Asl and D-PLP in Sas-4^{TT211AA} and Sas-4$^{\Delta P1\text{-}P2}$ flies. None of these protein recruitments are affected in Sas-4^{SST198AAA} flies. At least 140 meiotic centrosomes (n = 140) from 10 testes were analyzed in each condition from 3 independent experiments. ANOVA, *$p < 0.05$, **$p < 0.001$. Error bars represent means ± SEMs.

spermatocytes (Figures S6B and S6C). Analyzing two centrosome-containing larval brain cells revealed no visible structural defects (Figure S6D).

We then continued our experiments in syncytial embryos, which are also known to undergo rapid cell division. To show the significance of phosphorylation at Sas-4-TT211, we micro-injected Sas-4-TT211p (which is the mitotic specific anti-Sas-4 antibody) to fly embryos over-expressing Cnn-red fluorescent protein (RFP). Staining centrosomes 30 min post-injection revealed a dramatic reduction in Cnn and γ-tubulin but not Asl recruitment to centrosomes that are located in the vicinity of the injection site (Figure 7). These experiments led us to conclude that an efficient recruitment of Cnn and γ-tubulin to mitotic centrosomes require Sas-4's TT211.

DISCUSSION

In this work, we identify a role for Sas-4 in building mitotic centrosomes and demonstrate how Sas-4 could be regulated at the onset of mitosis for an efficient recruitment of PCM. By using mitotic-specific anti-Sas-4 antibodies that were generated against a doubly phosphorylated threonine-containing peptide (207-YASS**TT**ASSTSPRV-220), we identify that Sas-4's -TT211 is potentially phosphorylated at the onset of mitosis (Figure 2). We then identify that Plk1/Polo is the responsible kinase that can directly interact with Sas-4 and phosphorylate at least those threonines (TT211) *in vitro*. It is known that Cnn and γ-tubulin are the bona fide PCM proteins that are required for PCM expansion during mitosis (Conduit et al.,

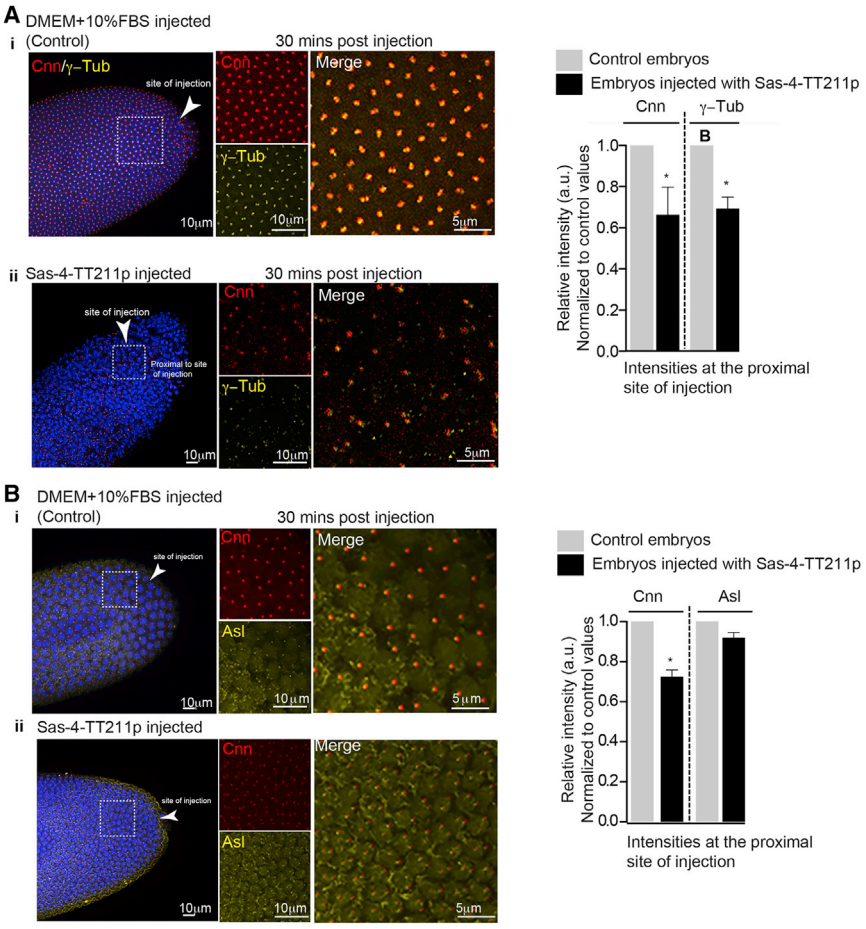

Figure 7. Phosphorylation of Sas-4-TT211 Is Required for Efficient Recruitment of Cnn and γ-Tubulin to Centrosomes of Rapidly Dividing Syncytial *Drosophila* Embryos

(A) Embryos expressing Cnn-RFP (red) under polyubiquitin promoter. Both Cnn (red) and γ-tubulin (yellow) do not seem to be affected in embryos injected with 10% fetal bovine serum (FBS) (i). Sas-4-TT211p injected embryos (ii) show dramatic reduction in both Cnn and γ-tubulin 30 min post-injection. Bar graphs represent the relative intensities of PCM proteins at mitotic centrosomes. At least 120 mitotic centrosomes (n = 120) from 4 embryos were analyzed in each condition. ANOVA, *p < 0.05. Error bars represent means ± SEMs. See also Figures S3, S4, and S6. (B) Asl (yellow) recruitment does not seem to significantly change in embryos injected with Sas-4-TT211p antibody (i and ii). Bar graphs represent the relative intensities of PCM proteins at mitotic centrosomes. At least 80 mitotic centrosomes (n = 80) from 4 embryos were analyzed in each condition. ANOVA, *p < 0.05. Error bars represent means ± SEMs.

2014; Gopalakrishnan et al., 2011; Sunkel et al., 1995). Our *in vivo* studies using *Drosophila* spermatocytes, brain cells, and syncytial embryos reveal the importance of Sas-4-TT211 in PCM expansion in dividing cells.

Plk1/Polo kinase is critical for the process of PCM recruitment (Kong et al., 2014; Wang et al., 2011). The number of Plk1/Polo substrates has been identified, which include Cnn, SPD-5, and D-PLP (Conduit and Raff, 2010; Woodruff et al., 2015; Wueseke et al., 2016). However, the significance of Plk1/Polo-mediated phosphorylation precisely at the onset of mitosis has largely been unexplored. The identification of Sas-4 as a Plk1/Polo substrate provides further insights into this process. Based on our data, it appears that phosphorylation of Sas-4-TT211 precedes the further recruitment of PCM proteins to mitotic centrosomes. This could be explained by the fact that Sas-4 is a closely associated centriolar wall protein whose phosphorylation could trigger Sas-4 to recruit subsequent PCM proteins and expand the overall size of centrosomes in mitosis. If this is true, then it is formally expected that upon phosphorylation, Sas-4 protein could remodel its own localization, spreading outward from its original location. Our STED microscopy using mitotic anti-Sas-4 antibodies (both mouse monoclonal and rabbit polyclonal Sas-4-TT211p) demonstrate an expanded localization of Sas-4 in mitotic centrosomes (Figure 5).

Our experiments further support the idea that Sas-4 is a crucial player at the early events of PCM recruitment. First, PCM recruitment begins at the onset of mitosis where Sas-4 appears to be phosphorylated by Plk1/Polo kinase (Figure 3). Second, our *in vivo* experiments using *Drosophila* that express a mildly perturbed Sas-4 (Sas-4^{TT211AA}) is sufficient to cause PCM recruitment defects in significant numbers of meiotic and mitotic centrosomes (Figures 6 and S6). Although the penetrance of the mutation seems to be minimal in slow-dividing spermatocytes, it is noteworthy that a fraction of affected centriolar pairs completely failed to recruit Cnn and γ-tubulin (Figures 6A, iii and iv, 6B, and S4C, ii and iii).

The centrosomes of Sas-4^{TT211AA} could recruit Asl but not Cnn and γ-tubulin sufficiently. This finding also suggests that PCM expansion at the onset of mitosis is to some extent dependent on the phosphorylation status of Sas-4 but not Asl. Novak et al. (2016) identified that PCM recruitment is dependent on the phosphorylation status of Sas-4. However, our findings contradict their observation that Cnn recruitment is Asl dependent. Few of our mutant flies, which encompass the Cdk1 site examined by Novak and colleagues, could normally recruit Asl (Figures 6 and S6). Although these studies provide key insights into the PCM recruitment process, the results offer a re-examination of the role of Asl in PCM recruitment. One remote possibility to explain these contrasting findings could be differences in expression levels, genetic background, and centrosome assembly mechanisms in various tissues, which are yet to be solved (Conduit and Raff, 2015).

Based on our data, it is likely that phosphorylated Sas-4 has a high affinity for PCM proteins in mitosis. The same phenomenon is observed for centrosomal P4.1-associated protein (CPAP), the

human counterpart of Sas-4, which acquires a high affinity for PCM proteins upon phosphorylation (Chou et al., 2016). Although our findings reveal that significant numbers of Sas-4^{TT211AA} and Sas-4$^{\Delta P1\text{-}P2}$ centrosomes have defects in Cnn and γ-tubulin recruitment, we notice that a certain proportion of centrosomes could still recruit a residual amount of these proteins (Figures 6 and S6). This observation suggests that Sas-4 could additionally contain Plk1/Polo kinase sites other than TT211 or involve other PCM recruitment mechanisms that are operating independently of Sas-4.

Until recently, the consequences regarding centrosomes that fail to efficiently recruit PCM proteins remain unanswered and numerous interpretations are possible. It is likely that centrosomes that are incapable of recruiting the full complement of PCM proteins fail to duplicate or to undergo centriole-to-centrosome conversion in subsequent cell divisions, as recently demonstrated by Fu et al. (2016) and Novak et al. (2016). This phenomenon is reflected in our studies that ~30% of mitotic cells in Sas-4^{TT211AA} and Sas-4$^{\Delta P1\text{-}P2}$ larval brain exhibit only one centrosome, as judged by the presence of Sas-4 or Asl proteins. This could indirectly mean that Sas-4^{TT211AA} and Sas-4$^{\Delta P1\text{-}P2}$ centrosomes that fail to recruit the full complement of PCM components are non-functional and are incapable of undergoing centriole-to-centrosome conversion in subsequent cell divisions. If this is true, then our findings here also suggest that the phenomenon of centriole-to-centrosome conversion seems to occur only in cell types that undergo rapid cell cycling, in which an efficient centrosome function is indispensable. This is substantiated by our experiments that analyze meiotic spermatocytes that have a much longer cell cycle. Despite Sas-4^{TT211AA} and Sas-4$^{\Delta P1\text{-}P2}$ expressing meiotic spermatocyte centrosomes failing to efficiently recruit PCM proteins, we never noticed single centrosome-containing cells (Figure S4A).

In summary, our experiments dissect Sas-4's function in meiotic and mitotic PCM recruitment in diverse cell types independent from its role in centriole elongation and duplication. Thus, the present data add useful insights into early events of PCM recruitment that occur at the onset of mitosis. Although great progress has been made in dissecting the order of S-CAP components' (Sas-4, Cnn, Asl, γ-tubulin, and D-PLP) recruitment to mitotic centrosomes, to what extent individual S-CAP components contribute to build functional mitotic centrosomes remains elusive. *In vitro* functional reconstitution assays of centrosomes using purified endogenous protein complexes from cell extracts depleted with individual S-CAP components may provide useful insights into the complex process of PCM recruitment in building functional centrosomes.

STAR★METHODS

Detailed methods are provided in the online version of this paper and include the following:

- KEY RESOURCES TABLE
- CONTACT FOR REAGENT AND RESOURCE SHARING
- EXPERIMENTAL MODEL AND SUBJECT DETAILS
  - Drosophila melanogaster
  - *Drosophila* Schneider cells and Sas-4 null cells (C131)
- METHOD DETAILS
  - Plasmids and cloning
  - Cell Culture and transfection
  - Antibody generation
  - Antibodies
  - Antibody injection in *Drosophila* embryos
  - Immunofluorescence and light microscopy
  - Electron microscopy
  - Peptide generation and dot blot analysis
  - *In vitro* kinase assay
  - Antibody competition experiment
  - Recombinant protein purification
  - GST Pull-down assays
  - Immunoprecipitation (IP) of Sas-4 complexes
  - Western blotting and Coomassie staining
- QUANTIFICATION AND STATISTICAL ANALYSIS

SUPPLEMENTAL INFORMATION

Supplemental Information includes six figures and can be found with this article online at https://doi.org/10.1016/j.celrep.2018.11.102.

ACKNOWLEDGMENTS

The Deutsche Forschungsgemeinschaft (DFG) grant GO 2301/2-2 and the Human Frontier Science Program (HFSP) (RGY0064/2015) supported this work. We would like to thank the members of the Laboratory for Centrosome and Cytoskeleton Biology for their technical support and advice. We also thank the light microscopy facility of the CMMC/CECAD, University of Cologne.

AUTHOR CONTRIBUTIONS

Conceptualization, J.G.; Methodology, A.R. and J.G.; Investigation, A.R.; Investigation (light microscopy, molecular biology, and biochemical analysis), A.R. and A.M.; Investigation (bioinformatics), S.M. and H.U.; Resources, A.D. and R.F.; Investigation (electron microscopy), M.G., M.R., G.C.; Writing, Editing, & Supervision, A.R., J.G., and A.M.; Funding Acquisition, J.G. All of the authors listed here have contributed to the preparation of this manuscript.

DECLARATION OF INTERESTS

The authors declare no competing interests.

Received: December 6, 2017
Revised: September 19, 2018
Accepted: November 29, 2018
Published: December 26, 2018

REFERENCES

Asteriti, I.A., De Mattia, F., and Guarguaglini, G. (2015). Cross-Talk between AURKA and Plk1 in Mitotic Entry and Spindle Assembly. Front. Oncol. *5*, 283.

Avidor-Reiss, T., and Gopalakrishnan, J. (2013). Building a centriole. Curr. Opin. Cell Biol. *25*, 72–77.

Blachon, S., Gopalakrishnan, J., Omori, Y., Polyanovsky, A., Church, A., Nicastro, D., Malicki, J., and Avidor-Reiss, T. (2008). Drosophila asterless and vertebrate Cep152 Are orthologs essential for centriole duplication. Genetics *180*, 2081–2094.

Chou, E.J., Hung, L.Y., Tang, C.J., Hsu, W.B., Wu, H.Y., Liao, P.C., and Tang, T.K. (2016). Phosphorylation of CPAP by Aurora-A Maintains Spindle Pole Integrity during Mitosis. Cell Rep. *14*, 2975–2987.

Conduit, P.T., and Raff, J.W. (2010). Cnn dynamics drive centrosome size asymmetry to ensure daughter centriole retention in Drosophila neuroblasts. Curr. Biol. *20*, 2187–2192.

Conduit, P.T., and Raff, J.W. (2015). Different Drosophila cell types exhibit differences in mitotic centrosome assembly dynamics. Curr. Biol. *25*, R650–R651.

Conduit, P.T., Brunk, K., Dobbelaere, J., Dix, C.I., Lucas, E.P., and Raff, J.W. (2010). Centrioles regulate centrosome size by controlling the rate of Cnn incorporation into the PCM. Curr. Biol. *20*, 2178–2186.

Conduit, P.T., Richens, J.H., Wainman, A., Holder, J., Vicente, C.C., Pratt, M.B., Dix, C.I., Novak, Z.A., Dobbie, I.M., Schermelleh, L., and Raff, J.W. (2014). A molecular mechanism of mitotic centrosome assembly in Drosophila. eLife *3*, e03399.

Conduit, P.T., Wainman, A., Novak, Z.A., Weil, T.T., and Raff, J.W. (2015). Re-examining the role of Drosophila Sas-4 in centrosome assembly using two-colour-3D-SIM FRAP. eLife *4*, e08483.

Dammermann, A., Maddox, P.S., Desai, A., and Oegema, K. (2008). SAS-4 is recruited to a dynamic structure in newly forming centrioles that is stabilized by the gamma-tubulin-mediated addition of centriolar microtubules. J. Cell Biol. *180*, 771–785.

Dix, C.I., and Raff, J.W. (2007). Drosophila Spd-2 recruits PCM to the sperm centriole, but is dispensable for centriole duplication. Curr. Biol. *17*, 1759–1764.

Fish, M.P., Groth, A.C., Calos, M.P., and Nusse, R. (2007). Creating transgenic Drosophila by microinjecting the site-specific phiC31 integrase mRNA and a transgene-containing donor plasmid. Nat. Protoc. *2*, 2325–2331.

Fu, J., and Glover, D.M. (2012). Structured illumination of the interface between centriole and peri-centriolar material. Open Biol. *2*, 120104.

Fu, J., Lipinszki, Z., Rangone, H., Min, M., Mykura, C., Chao-Chu, J., Schneider, S., Dzhindzhev, N.S., Gottardo, M., Riparbelli, M.G., et al. (2016). Conserved molecular interactions in centriole-to-centrosome conversion. Nat. Cell Biol. *18*, 87–99.

Giansanti, M.G., Bucciarelli, E., Bonaccorsi, S., and Gatti, M. (2008). Drosophila SPD-2 is an essential centriole component required for PCM recruitment and astral-microtubule nucleation. Curr. Biol. *18*, 303–309.

Gopalakrishnan, J., Mennella, V., Blachon, S., Zhai, B., Smith, A.H., Megraw, T.L., Nicastro, D., Gygi, S.P., Agard, D.A., and Avidor-Reiss, T. (2011). Sas-4 provides a scaffold for cytoplasmic complexes and tethers them in a centrosome. Nat. Commun. *2*, 359.

Gopalakrishnan, J., Chim, Y.C., Ha, A., Basiri, M.L., Lerit, D.A., Rusan, N.M., and Avidor-Reiss, T. (2012). Tubulin nucleotide status controls Sas-4-dependent pericentriolar material recruitment. Nat. Cell Biol. *14*, 865–873.

Haren, L., Stearns, T., and Lüders, J. (2009). Plk1-dependent recruitment of gamma-tubulin complexes to mitotic centrosomes involves multiple PCM components. PLoS One *4*, e5976.

Hung, L.Y., Chen, H.L., Chang, C.W., Li, B.R., and Tang, T.K. (2004). Identification of a novel microtubule-destabilizing motif in CPAP that binds to tubulin heterodimers and inhibits microtubule assembly. Mol. Biol. Cell *15*, 2697–2706.

Kirkham, M., Müller-Reichert, T., Oegema, K., Grill, S., and Hyman, A.A. (2003). SAS-4 is a C. elegans centriolar protein that controls centrosome size. Cell *112*, 575–587.

Kong, D., Farmer, V., Shukla, A., James, J., Gruskin, R., Kiriyama, S., and Loncarek, J. (2014). Centriole maturation requires regulated Plk1 activity during two consecutive cell cycles. J. Cell Biol. *206*, 855–865.

Lawo, S., Hasegan, M., Gupta, G.D., and Pelletier, L. (2012). Subdiffraction imaging of centrosomes reveals higher-order organizational features of pericentriolar material. Nat. Cell Biol. *14*, 1148–1158.

Lecland, N., Debec, A., Delmas, A., Moutinho-Pereira, S., Malmanche, N., Bouissou, A., Dupré, C., Jourdan, A., Raynaud-Messina, B., Maiato, H., and Guichet, A. (2013). Establishment and mitotic characterization of new Drosophila acentriolar cell lines from DSas-4 mutant. Biol. Open *2*, 314–323.

Mennella, V., Agard, D.A., Huang, B., and Pelletier, L. (2014). Amorphous no more: subdiffraction view of the pericentriolar material architecture. Trends Cell Biol. *24*, 188–197.

Nigg, E.A. (2004). Centrosomes in Development and Disease (Wiley-VCH).

Nigg, E.A., and Holland, A.J. (2018). Once and only once: mechanisms of centriole duplication and their deregulation in disease. Nat. Rev. Mol. Cell Biol. *19*, 297–312.

Nigg, E.A., and Raff, J.W. (2009). Centrioles, centrosomes, and cilia in health and disease. Cell *139*, 663–678.

Novak, Z.A., Conduit, P.T., Wainman, A., and Raff, J.W. (2014). Asterless licenses daughter centrioles to duplicate for the first time in Drosophila embryos. Curr. Biol. *24*, 1276–1282.

Novak, Z.A., Wainman, A., Gartenmann, L., and Raff, J.W. (2016). Cdk1 Phosphorylates Drosophila Sas-4 to Recruit Polo to Daughter Centrioles and Convert Them to Centrosomes. Dev. Cell *37*, 545–557.

Riparbelli, M.G., Gottardo, M., Glover, D.M., and Callaini, G. (2014). Inhibition of Polo kinase by BI2536 affects centriole separation during Drosophila male meiosis. Cell Cycle *13*, 2064–2072.

Sunkel, C.E., Gomes, R., Sampaio, P., Perdigão, J., and González, C. (1995). Gamma-tubulin is required for the structure and function of the microtubule organizing centre in Drosophila neuroblasts. EMBO J. *14*, 28–36.

Tang, N., and Marshall, W.F. (2012). Centrosome positioning in vertebrate development. J. Cell Sci. *125*, 4951–4961.

Wang, W.J., Soni, R.K., Uryu, K., and Tsou, M.F. (2011). The conversion of centrioles to centrosomes: essential coupling of duplication with segregation. J. Cell Biol. *193*, 727–739.

Woodruff, J.B., Wueseke, O., and Hyman, A.A. (2014). Pericentriolar material structure and dynamics. Philos. Trans. R. Soc. Lond. B Biol. Sci. *369*, 20130459.

Woodruff, J.B., Wueseke, O., Viscardi, V., Mahamid, J., Ochoa, S.D., Bunkenborg, J., Widlund, P.O., Pozniakovsky, A., Zanin, E., Bahmanyar, S., et al. (2015). Centrosomes. Regulated assembly of a supramolecular centrosome scaffold in vitro. Science *348*, 808–812.

Wueseke, O., Zwicker, D., Schwager, A., Wong, Y.L., Oegema, K., Jülicher, F., Hyman, A.A., and Woodruff, J.B. (2016). Polo-like kinase phosphorylation determines Caenorhabditis elegans centrosome size and density by biasing SPD-5 toward an assembly-competent conformation. Biol. Open *5*, 1431–1440.

Zheng, X., Gooi, L.M., Wason, A., Gabriel, E., Mehrjardi, N.Z., Yang, Q., Zhang, X., Debec, A., Basiri, M.L., Avidor-Reiss, T., et al. (2014). Conserved TCP domain of Sas-4/CPAP is essential for pericentriolar material tethering during centrosome biogenesis. Proc. Natl. Acad. Sci. USA *111*, E354–E363.

Zheng, X., Ramani, A., Soni, K., Gottardo, M., Zheng, S., Ming Gooi, L., Li, W., Feng, S., Mariappan, A., Wason, A., et al. (2016). Molecular basis for CPAP-tubulin interaction in controlling centriolar and ciliary length. Nat. Commun. *7*, 11874.

STAR★METHODS

KEY RESOURCES TABLE

REAGENT or RESOURCE	SOURCE	IDENTIFIER
Antibodies		
DAPI	Sigma Aldrich	Cat# 32670
Donkey anti rabbit IgG (H+L) secondary antibody, Alexa Fluor 594	Life Technologies	Cat# A21207
Donkey anti rabbit IgG (H+L) secondary antibody, Alexa Fluor 647	Life Technologies	Cat# A31573
Donkey anti-Rabbit IgG (H+L) Secondary Antibody, HRP	Thermoscientific	Cat# A16023
Goat anti mouse IgG (H+L) secondary antibody, Alexa Fluor 488	Life Technologies	Cat# A28175
Goat anti mouse IgG (H+L) secondary antibody, Alexa Fluor 594	Life Technologies	Cat# A-11032
Goat anti mouse IgG (H+L) secondary antibody, Alexa Fluor 647	Life Technologies	Cat# A21236
Goat anti-Mouse IgG (H+L) Secondary Antibody, HRP	Thermoscientific	Cat# 626520
Monoclonal mouse anti-α-Tubulin	Sigma Aldrich	Cat# T9026, Clone DM1A
Monoclonal mouse anti-γ-tubulin	Sigma Aldrich	Cat# GTU-88
Mouse monoclonal anti-phospho-Histone H3, Ser10	Cell Signaling technologies	Cat# 6G3
Mouse monoclonal anti-Sas-4	N/A	(Gopalakrishnan et al., 2011)
Mouse monoclonal mitotic anti-Sas-4	Generated for this paper	N/A
Mouse monoclonal non-mitotic anti Sas-4	Self generated for this paper	N/A
Rabbit polyclonal anti-Asl	N/A	(Blachon et al., 2008)
Rabbit polyclonal anti-Cnn	Kind gift from Dr. T. Kaufman	N/A
Rabbit polyclonal anti-D-PLP	Kind gift from Dr. J. Raff	N/A
Rabbit polyclonal mitotic anti-Sas-4	Generated at Genscript	N/A
Bacterial strains		
BL21 (DE3) competent *E. coli*	New England Biolabs	Cat# C2527I
NEB 5 alpha competent *E. coli*	New England Biolabs	Cat# C2987I
Chemicals		
37% Formaldehyde	Sigma Aldrich	Cat# F8775
BI2536	Selleckchem	Cat# S1109
Bovine serum albumin	Sigma Aldrich	Cat# A7906-100G
Concanavalin A	Sigma Aldrich	Cat# C0412-5MG
Coomassie Brillant blue G-250 (C. I. 42655)	Applichem	Cat# A3480,0025
Drosophila Schneider medium	Thermo Fischer Scientific	Cat# 21720024
Hi load 16/600 Superdex 200pg	GE Healthcare	Cat# 28-9893-35
Fetal Bovine serum (Sterile filtered)	VWR	Cat# S1810-500
Glacial acetic acid	ROTH	Cat# 3738.3
Glutaraldehyde EM Grade, 50% Aqueous Solution	Science services	Cat# E16300
Glutathione Sepharose 4 Fast flow (GST)	GE Healthcare	Cat# 17-5132-01
Protein G Sepharose 4 fast flow	GE Healthcare	Cat# 17-0618-01
Glycerol > 99% molecular biology grade	Sigma Aldrich	Cat# G5516-1L
Guanidine hydrochloride	ROTH	Cat# 35.1
Isopropylthiogalactoside (IPTG)	Sigma aldrich	Cat# I6758-1G
Methanol Rotipuran > 99.9% ACS ISO	ROTH	Cat# 4627.5
Mowiol 4-88 Histology grade	Applichem	Cat# A9011,0100
Heptane anhydrous 99%	Sigma Aldrich	Cat# 246654-1L
Non-fat dried milk powder	Applichem	Cat# A80830,1000
Osmium Tetroxide, Crystalline, Highest Purity 99,95%	Science services	Cat# E19120
Penicillin-Streptomycin (100x)	Thermofischer scientific	Cat# 15140-122

(*Continued on next page*)

Continued

REAGENT or RESOURCE	SOURCE	IDENTIFIER
Shields and Sang M3 insect medium	Sigma Aldrich	Cat# S3652
Sodium chloride	Applichem	Cat# A1149,5000
Pipes dipotasium salt	Sigma Aldrich	Cat# P7643-500G
Supersignal West Femto Chemiluminescent substrate	Thermofischer scientific	Cat# 34095
Supersignal West Pico Chemiluminescent substrate	Thermofischer scientific	Cat# 34080
PBS tablets	GIBCO	Cat#18912-014
Tris Ultrapure	Applichem	Cat# A1086,1000
Triton X-100	Applichem	Cat# A13880500
Tween-20	Applichem	Cat# A1389,1000
Peptides		
Sas-4 Control peptide (YASSTTASSTSPRV)	Generated at Genscript for this paper	N/A
Sas-4 double mutant peptide (YASSAAASSTSPRV)	Generated at Genscript for this paper	N/A
Sas-4 double phospho peptide (YASSpTpTASSTSPRV)	Generated at Genscript for this paper	N/A
Sas-4 single mutant peptide #1 YAASTTASSTSPRV)	Generated at Genscript for this paper	N/A
Sas-4 single mutant peptide #2 YASATTASSTSPRV)	Generated at Genscript for this paper	N/A
Sas-4 single mutant peptide #3 YASSATASSTSPRV)	Generated at Genscript for this paper	N/A
Sas-4 single mutant peptide #4 YASSTAASSTSPRV)	Generated at Genscript for this paper	N/A
Recombinant Proteins		
Recombinant human PLK1	Proqinase	Cat# 0183-0000-1
Recombinant Aurora A kinase	Proqinase	Cat# 0166-0000-1
Recombinant CDK1/CycA2	Proqinase	Cat# 0134-0054-1
Recombinant Sas-4(1-350)ΔP1-P2	This Paper	N/A
Recombinant Sas-4(1-350) SST198DDD	This Paper	N/A
Recombinant Sas-4(1-350) SST198AAA	This Paper	N/A
Recombinant Sas-4(1-350) SSTT209DDDD	This Paper	N/A
Recombinant Sas-4(1-350) SSTT209AAAA	This Paper	N/A
Recombinant Sas-4(1-350) TT211AA	This Paper	N/A
Critical Commercial Assays		
Effectene Transfection reagent	QIAGEN	Cat# 301425
Phusion High- Fedality DNA polymerase	New England Biolabs	Cat# M0530L
Experimental Models: Cell Lines		
Drosophila Schneider cells	Kind gift from Prof. Linda Partridge	N/A
Drosophila Sas-4 null cells (C131)	(Zheng et al., 2014)	N/A
Experimental Models: Organisms/Strains		
*D.*melanogaster P[lacW]l(3)s2214 (Sas-4^{s2214})	Bloomington	(Zheng et al., 2014)
D.melanogaster p-Ubq RFP-Cnn (II chromosome)	Kind Gift from Prof. Jorden Raff	N/A
W^{+}; Sas-4/Cyo; Sas-4 s^{2214}/ Sas-4^{s2214}	BestGene(USA)	N/A
W^{+}; Sas-4 $^{\Delta P1\text{-}P2}$ /Cyo; Sas-4 s^{2214}/ Sas-4^{s2214}	BestGene(USA)	N/A
W^{+}; Sas-4^{SST198AAA}/Cyo; Sas-4^{s2214}/ Sas-4^{s2214}	BestGene(USA)	N/A
W^{+}; Sas-4^{TT211AA} /Cyo; Sas-4 s^{2214}/ Sas-4^{s2214}	BestGene(USA)	N/A
W^{+}; Sas-4^{TT211DD} /Cyo; Sas-4 s^{2214}/ Sas-4^{s2214}	BestGene(USA)	N/A

(*Continued on next page*)

Continued

REAGENT or RESOURCE	SOURCE	IDENTIFIER
Oligonucleotides		
Sas-4 Genomic forward primer GGCGCGCCTATTTTTTGAATCA TAAATGATTAA	Sigma Aldrich	N/A
Sas-4 Genomic Reverse primer GCGGCCGCCTAATACTTGGC ATAGTCTGTGTC	Sigma Aldrich	N/A
Sas-4 1-350 CDS Forward primer GGAATTCCATATGCAGGAG GCTGGCGAAAGTCCTGTTGGA	Sigma Aldrich	N/A
Sas-4 1-350 CDS Reverse primer TTCCGCGGCCGCTATGGCC GACGTCGACCTCGTCCCCCTCCTGCAGTTCCTGC	Sigma Aldrich	N/A
Recombinant DNA		
PattB-UAST vector	(Zheng et al., 2014)	N/A
pGEX-6P-1	Kind Gift from Prof. Haitao Li.	N/A
Software and Algorithms		
Fiji Win64 (ImageJ d 1.47)	Wayne Rasband, NIH, USA	N/A
Adobe Illustrator CC 2017	Adobe	N/A
Adobe Photoshop CC 2015	Adobe	N/A
Huygens for image deconvolution	Scientific Volume Imaging	N/A

CONTACT FOR REAGENT AND RESOURCE SHARING

Jay Gopalakrishnan (Institute of Human Genetics, Heinrich-Heine-Universität Düsseldorf) is the lead contact for this paper and is responsible for any reagent and resource request. Enquiries should be sent to Jay Gopalakrishnan (jay.gopalakrishnan@hhu.de).

EXPERIMENTAL MODEL AND SUBJECT DETAILS

Drosophila melanogaster

P[lacW]l(3)s2214 (Sas-4s2214) was obtained from the Bloomington Stock Center. Sas-4^{WT}, Sas-4^{TT211AA}, Sas-4^{TT211DD} Sas-4^{SST198AAA} and Sas-4 $^{\Delta P1\text{-}P2}$ were cloned into pUAST-attb-GFP vector and sent to BestGene(USA) for generating transgenic flies. All the genes were expressed under Sas-4 endogenous promoter and were inserted at the identical sites in the second chromosome. The flies obtained were balanced to generate stable stocks. Each of the Sas-4 transgenic flies were expressed in the background of Sas-4 null homozygous mutation. The generated flies have been listed in the key resource table.

Drosophila Schneider cells and Sas-4 null cells (C131)

Drosophila Schneider cells were cultured in Schneider's *Drosophila* medium (Thermo Fischer Scientific) containing 10% fetal bovine serum (Bio-west) and the *Drosophila* cells lacking Sas-4 (Zheng et al., 2014) were cultured in Shields and Sang M3 insect medium (Sigma Aldrich) containing 10% fetal bovine serum (Bio-west). The cells were grown at 25°C and split 1/3 once every 4 days.

METHOD DETAILS

Plasmids and cloning

Full length Sas-4-WT (control), Sas-4-TT211AA, Sas-4-TT211DD, Sas-4-SST198AAA, and Sas-4 ΔP1-P2 genes were amplified from *Drosophila* genomic DNA and cloned into PattB-UAST-GFP (C-terminal GFP) vector between AscI and NotI cloning sites under endogenous Sas-4 promoter for generating transgenic *Drosophila*. The Sas-4 variants (as stated above) spanning 1-350aa residues were amplified using Phusion polymerase (NEB) and cloned into pGEX-6p1 vector between NdeI and SalI for protein expression and purification. The genes consisted of fused N-terminal GST tag for purification purposes.

Cell Culture and transfection

Drosophila Schneider cells were cultured in Schneider's *Drosophila* medium (Thermo Fischer Scientific) containing 10% fetal bovine serum (Bio-west) and the *Drosophila* cells lacking Sas-4 were cultured in Shields and Sang M3 insect medium. The cells were split 1/3 once every 4 days. Transfection in *Drosophila* S2 cells was carried out using the Effectene transfection reagent (QIAGEN) as per the manufacturer's protocol.

Antibody generation

Non-mitotic anti-Sas-4 was generated by injecting mice with Sas-4 peptide (150-300aa). Later the epitope for the antibody was narrowed down to the peptide sequence spanning 190-220aa (refer to Figure 1A). Mouse monoclonal mitotic anti-Sas-4 (Sas-4-TT211p) was raised against a phosphorylated peptide (207-YASSpTpTASSTSPRV-220, generated by GenScript, NJ, USA) (refer to Figures 2B and S1F).

Antibodies

For immunofluorescence, monoclonal mouse anti-Sas-4 (1:50)(Gopalakrishnan et al., 2011) mouse non-mitotic anti-Sas-4 (1:50, generated in our lab), mouse mitotic anti-Sas-4 (Sas-4-TT211p, 1:2, generated in our lab), rabbit mitotic anti-Sas-4 (Sas-4-TT211p, 1:100, GenScript), rabbit anti-Asl (1:500)(Blachon et al., 2008), rabbit anti-Cnn (1:500, courtesy of Dr. T. Kaufman), rabbit anti-D-PLP (1:500, Courtesy of Dr. J. Raff), mouse anti-γ-tubulin (1:400, Sigma aldrich) and mouse anti-phospho-Histone H3, Ser10 (1:250, Cell Signaling Technology) were used. DAPI (1 μg/ml. Sigma) was used to stain DNA. Secondary antibodies, Alexa fluor dyes (goat or donkey anti-mouse/ anti-rabbit) were used at 1:1000 dilution (Life technologies). For STED imaging, Abberior STAR dyes (anti-mouse 647 and anti-rabbit 594) were used.

For western blotting and dot blot analysis, monoclonal mouse anti-Sas-4 (1:100)(Gopalakrishnan et al., 2011) mouse non-mitotic anti-Sas-4 (1:100, generated in out lab), mouse monoclonal mitotic anti-Sas-4 (Sas-4-TT211p, 1:10), rabbit polyclonal mitotic anti-Sas-4 (Sas-4-TT211p, 1:1000, GenScript), rabbit anti-Asl (1:3000)(Blachon et al., 2008) rabbit anti-Cnn (1:3000, courtesy of Dr. T. Kaufman), mouse anti-γ-tubulin (1:3000, Sigma aldrich) mouse anti-α-tubulin (1:3000, Sigma Aldrich), rabbit anti-α-tubulin (1:3000, courtesy of Prof. Dr. Angelika A. Noegel) and rabbit anti-Human Plk1 (1:1000, NEB) were used. Secondary antibodies (anti-mouse and anti-rabbit) (1:5000, Thermo Fischer Scientific) were used.

Antibody injection in *Drosophila* embryos

Drosophila flies expressing Cnn-RFP under poly-ubiquitin promoter were allowed to lay eggs on grape juice agar medium for 1-week prior to injection at 25°C. The flies were flipped to new plate once every 24 hr. 1hr old syncytial embryos were collected and de-chorionated using 50% commercial bleach for 3 mins. Following dechorionation, the embryos were washed with water on a nylon mesh, arranged on a piece of cut agar with the help of a fly stereomicroscope. The embryos were then desiccated using Silica gel in a desiccator for 10 minutes. The desiccated embryos were injected with either mitotic-anti-Sas-4 antibody (Sas-4-TT211p) or DMEM +10% FBS using an inverted microscope as described (Fish et al., 2007). The injected embryos were allowed to stand at RT for 30 mins. The embryos were then fixed and stained as described in the immunofluorescence and light microscopy section.

Immunofluorescence and light microscopy

For light microscopy, as well as for STED, the required amount of Schneider cells were seeded on concanavalin treated coverslips and allowed to adhere for 10 mins. The cells were then washed with PBS and fixed with 3.7% formaldehyde for 10 mins. Further, the cells were washed 2x times with PBS and permeabilized with 0.1% Triton X-100 in PBS (PBT) for 15 minutes, followed by blocking in PBT containing 2% Bovine serum albumin (BSA) for 30 mins.

Primary antibody staining was carried out at room temperature (RT) for 1 hr or overnight at 4°C. After labeling, the antibody was removed and the samples were washed 3x times with PBS. Further, the respective secondary antibodies along with DAPI were used against the primary antibody and incubated at RT for 1 hr. Confocal images were obtained using Olympus Fluoview FV1000 and Leica SP8 Laser scanning confocal microscope. For confocal microscopy, chromatic aberrations were checked using tetraspeck beads (Invitrogen).

STED imaging was performed using TCS SP8 gSTED, Leica. Far-red depletion laser (STED-Laser 775nm) was used for STED imaging. The alignment between channels was monitored using the Gatta STED Nanoruler (Gatta quant, Germany) to monitor STED performance. The PL Apo 100x/1.40 Oil STED Orange (Leica) objective was used, resulting in 100 × overall magnification with ~50nm lateral and 120nm axial resolution. Signals were detected using, gateable hybrid detectors (HyD). Nyquist sampling criteria was maintained during imaging to achieve *X-Y* resolution of 120nm. Images obtained were deconvoluted using Huygens essential deconvolution software. Line profiles were plotted based on fluorescent intensity values. The images were further processed using ImageJ and Adobe Photoshop.

For light microscopy of fly testes expressing the different Sas-4 variants, the dark pupae testes were dissected in PBS and transferred to a fixative solution containing 3.7% formaldehyde for 10 mins. The samples were then placed on pre-labeled slides and squished with the help of a coverslip and further immersed into liquid nitrogen for 30 s. The slides were removed and the coverslips were flicked off before placing them in a beaker, containing methanol for 10 mins. The samples were permeabilized with 0.1% Triton X-100 in PBS for 10 mins and blocked with 2% BSA, 0.1% Triton X-100 in PBS for 1 hr at RT. The samples were labeled with primary antibodies at RT for 1-2 hr or overnight at 4°C and further washed and labeled with secondary antibodies for 1 hr at RT along with DAPI. Analyses of the samples were carried out as described above. For the *Drosophila* neuroblast staining, the third instar larvae were dissected and stained similar to the testis staining.

Injected *Drosophila* embryos were transferred to a 1.5ml eppendorf containing the fixative (4% formaldehyde and 50% n-heptane in PBS) and incubated with constant rotation for 1 hr at RT. After fixation, 80% of the lower phase of the fixative was removed and the tube was filled with 1ml cold methanol and vortexed for 1 min. After most of the embryos settled to the bottom, the liquid was

removed, and the embryos were further washed thrice with methanol. PBT (PBS+0.3% Tritonx100) was used to re-hydrate the embryos followed by blocking using 2% BSA, 0.1% Triton X-100 in PBS for 1 hr at RT. Primary antibody staining was carried out overnight at 4°C. After labeling, the antibody was removed, and the samples were washed 3x times with PBT. The respective secondary antibodies along with DAPI were used against the primary antibody and incubated at RT for 4-5 hr. The embryos were washed 3x times with PBT and mounted on a slide containing two coverslips placed next to each other with a gap of 4 mm. The embryos were carefully placed in the gap and excess PBT was drained off. A third coverslip was then placed over the embryos with the help of Mowiol and allowed to dry. The embryos were imaged as described above.

Electron microscopy

Testes from *Drosophila* mid-aged pupae expressing different Sas-4 transgenes (Sas-4^{WT}, Sas-4^{TT211AA}, Sas-4^{SST198AAA} and Sas-4 $^{\Delta P1\text{-}P2}$) were dissected and transferred to a solution containing 2.5% glutaraldehyde buffered in PBS overnight at 4°C. The samples were washed with PBS and post-fixed in 1% osmium tetroxide in PBS for 2hrs at 4°C. Furthermore, the samples were carefully rinsed in PBS. The washed material was then dehydrated with graded series of ethanol; embedded in a mixture of Epon-Araldite resin and further polymerized for 48hrs at 60°C. Reichert Ultracut E ultramicrotome was used to obtain 60-70nm thick sections. The microtome consisted of copper grids with a mounted diamond knife, which was then stained with samarium triacetate and lead citrate. Morada CCD camera (Olympus) equipped Tecnai Spirit Transmission Electron Microscope (FEI) functioning at 100 kV was used to observe the samples. The images obtained were processed using Adobe Photoshop.(Fu et al., 2016)

Peptide generation and dot blot analysis

The peptides mentioned in Figure S1 were generated commercially (GenScript, NJ, USA). Peptides were thawed on ice prior to use. 5 micro-liters of each peptide (50 μM final conc.) were added to the nitrocellulose membrane and the membrane was allowed to dry for 15 minutes. The membrane was blocked using 5% milk in 1xTBST for 1 hr and then incubated with the primary antibodies overnight at 4°C. Next day the blots were washed with 1x TBST and then incubated with the respective secondary antibodies for 1 hr at RT. The membrane was further washed 3x times with 1x TBST and developed using the Super signal west pico/ femto chemilluminescent substrates that were used to detect the peroxidase activity in the samples.

In vitro kinase assay

The invitro kinase assay was as previously described (Novak et al., 2016). In brief, synthetic Sas-4 peptides (with a final concentration of 50 μM) were incubated with 200ng of Plk1/Polo, Cdk1 or AuroraA in 1x NEB buffer for protein kinases along with cold ATP (100 μM) for 30 mins at RT. For the inhibitor experiments, 1 μM BI2535 (Plk1/Polo inhibitor) was added to the reaction mixture containing Sas-4 peptide and Plk1/Polo kinase. The reaction was then stopped by adding 7.5M guanidine-hydrochloride. 2 μL from each of the mixtures were spotted onto nitrocellulose membranes for dot blot analysis as described above. The mitotic anti Sas-4 (Sas-4-TT211p) was used to analyze the phosphorylation status of peptides.

Antibody competition experiment

Mitotic anti-Sas-4 antibody (Sas-4-TT211p) and anti-Sas-4 antibody are treated with increasing concentrations of either non-phosphorylated Sas-4 peptide (207-YASSTTASSTSPRV-220, 0.9 μM and 3.5 μM) or Sas-4 phosphorylated peptide (207-YASS**TT**AS STSPRV-220, 0.9 μM and 3.5 μM). The antibodies are then used to label Sas-4 in Schneider cells as described in the immunofluorescence and light microscopy section.

Recombinant protein purification

Sas-4 1-350, Sas-4-TT211AA, Sas-4-SST198AAA and Sas-4 ΔP1-P2 were cloned in PGEX-6p and expressed in E-coli strain BL-21 (DE3) and the protein was induced using isopropylthiogalactoside. The cells were sonicated to release the proteins and spun at 25000 rpm to obtain lysate containing soluble fraction of the proteins. The proteins were purified using GST-agarose beads and then washed with buffer containing 50mM Tris-Hcl, 200mM Nacl (pH 8.0) and high salt buffer containing 50mM Tris-Hcl, 500mM Nacl (pH 8.0). The proteins are then cleaved overnight at 4°C using P3C precision enzyme. The supernatant was then concentrated and subjected to FPLC analysis. The fractions obtained were then tested by Coomassie staining as well as western blot for confirmation.

GST Pull-down assays

GST tagged recombinant proteins Sas-4 1-350, Sas-4-TT211AA, and Sas-4 ΔP1-P2 were expressed and purified as described above. The purified proteins bound to GST were incubated with *Drosophila* cell extracts lacking Sas-4 for 3 hours at 4°C. The beads were then washed with buffer containing 50mM Tris-Hcl, 200mM Nacl (pH 8.0) and high salt buffer containing 50mM Tris-Hcl, 500mM Nacl (pH 8.0) 3x times. The buffer was removed and the beads were boiled for 10 mins after adding 2x Laemmli buffer. The samples were then analyzed using western blotting.

For direct interaction analysis with Plk1/Polo, the GST tagged Sas-4 proteins bound to the beads were used as a bait to capture pure Plk1/Polo-GST protein from the supernatant. To clarify that the GST tag alone does not mediate the interaction between Sas-4 proteins and Plk1/Polo, recombinant GST protein was used as a negative control.

Immunoprecipitation (IP) of Sas-4 complexes

Protein G Sepharose beads (Sigma Aldrich) were coated with anti-Sas-4 antibody overnight at 4°C. The coated beads were then incubated with *Drosophila* embryonic high speed lysate (HSL) for 3hrs at 4°C. The lysates were prepared by lysing the embryonic extracts with 1x BRB80 buffer (extract buffer) as described by (Gopalakrishnan et al., 2011). After incubation, the beads were washed 1x times with extract buffer containing 1% triton x100 and 2x times with the extract buffer alone. The washed beads were then eluted by boiling them in 2x Laemmli buffer at 98°C. The beads were analyzed by western blotting for the Sas-4 complexes.

Western blotting and Coomassie staining

Protein samples in 4x Laemmli buffer were heated at 98°C for 10 mins before use. Samples were resolved using 10% polyacrylamide gels. The proteins were then transferred to nitrocellulose membrane for 1 hour at 135V. The membrane was blocked using 5% milk in 1xTBST for 1 hr and then incubated with the primary antibodies overnight at 4°C. Next day, the blots were washed with 1x TBST and then incubated with the respective secondary antibodies for 1 hr at RT. The membrane was further washed 3x times with 1x TBST and developed using the Super signal west pico/ femto chemilluminescent substrates that were used to detect the peroxidase activity in the samples.

For Coomassie staining, the samples were resolved in 12% polyacrylamide gel as described above. The gel was stained with Coomassie blue staining dye (10% methanol, 20% acetic acid, 70% water and 0.025% Coomassie dye) for 10 mins. De-staining was carried out using buffer containing 10% methanol, 20% acetic acid and 70% water.

QUANTIFICATION AND STATISTICAL ANALYSIS

Statistical analysis was carried out using Graph Pad Prism software (version 6.0). Student's T- test (Unpaired, one tailed) or ordinary one-way ANOVA followed by Tukey's multiple comparison tests were used to analyze the results. The error bars are expressed as mean ± s.e.m. Significance depicts p value (*$p < 0.05$, **0 < 0.001, ***$p < 0.0001$). The ''n'' represents number of centrosomes analyzed in interphase/ mitotic cells. The intensity of mitotic and interphase centrosomes were measured using ImageJ and were further calculated relative to controls.

Cell Reports, Volume *25*

Supplemental Information

Plk1/Polo Phosphorylates Sas-4 at the Onset of Mitosis for an Efficient Recruitment of Pericentriolar Material to Centrosomes

Anand Ramani, Aruljothi Mariappan, Marco Gottardo, Sunit Mandad, Henning Urlaub, Tomer Avidor-Reiss, Maria Riparbelli, Giuliano Callaini, Alain Debec, Regina Feederle, and Jay Gopalakrishnan

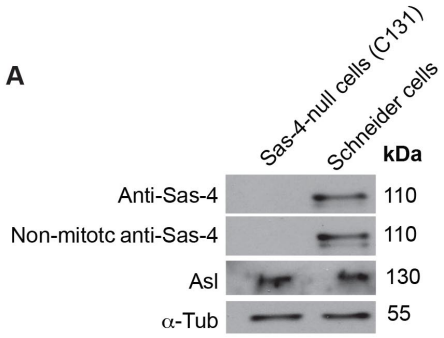
A
Sas-4-null cells (C131)
Schneider cells
kDa
Anti-Sas-4
110
Non-mitotc anti-Sas-4
110
Asl
130
α-Tub
55

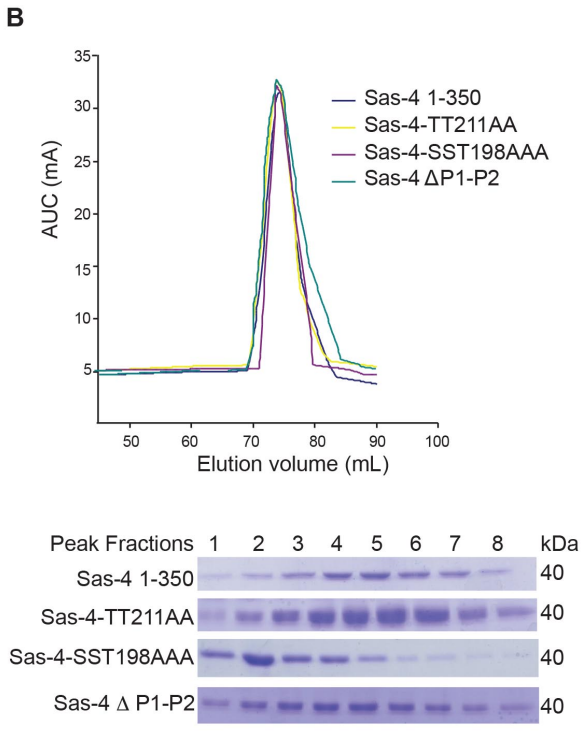
B
AUC (mA)
Elution volume (mL)
Sas-4 1-350
Sas-4-TT211AA
Sas-4-SST198AAA
Sas-4 ΔP1-P2
Peak Fractions 1 2 3 4 5 6 7 8
kDa
Sas-4 1-350
40
Sas-4-TT211AA
40
Sas-4-SST198AAA
40
Sas-4 Δ P1-P2
40

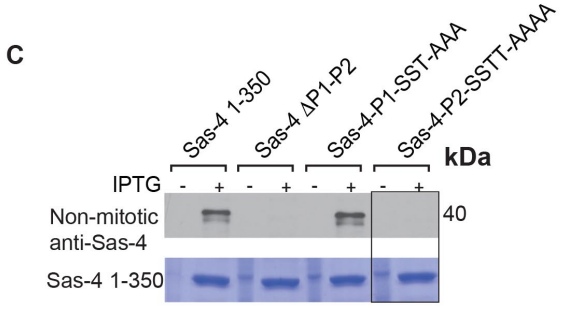
C
Sas-4 1-350
Sas-4 ΔP1-P2
Sas-4-P1-SST-AAA
Sas-4-P2-SSTT-AAAA
kDa
IPTG
Non-mitotic anti-Sas-4
40
Sas-4 1-350

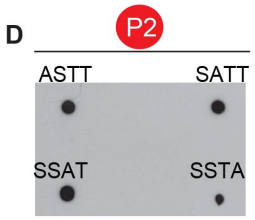
D
P2
ASTT
SATT
SSAT
SSTA

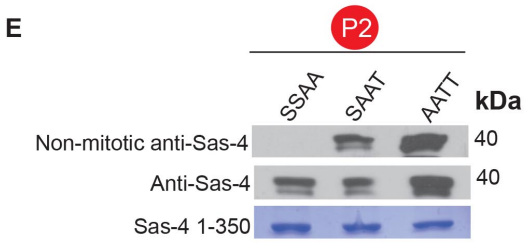
E
P2
SSAA
SAAT
AATT
kDa
Non-mitotic anti-Sas-4
40
Anti-Sas-4
40
Sas-4 1-350

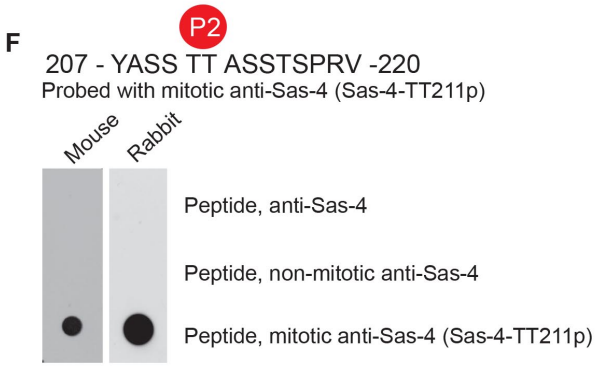
F
P2
207 - YASS TT ASSTSPRV -220
Probed with mitotic anti-Sas-4 (Sas-4-TT211p)
Mouse
Rabbit
Peptide, anti-Sas-4
Peptide, non-mitotic anti-Sas-4
Peptide, mitotic anti-Sas-4 (Sas-4-TT211p)

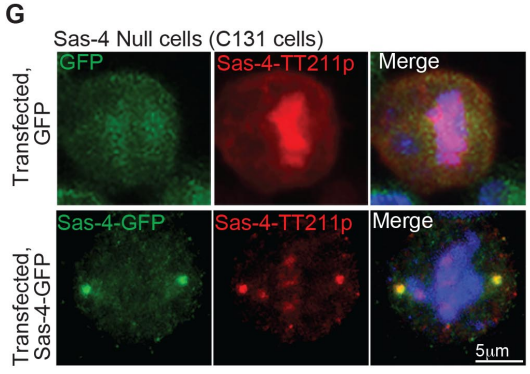
G
Sas-4 Null cells (C131 cells)
GFP
Sas-4-TT211p
Merge
Transfected, GFP
Sas-4-GFP
Sas-4-TT211p
Merge
Transfected, Sas-4-GFP
5μm

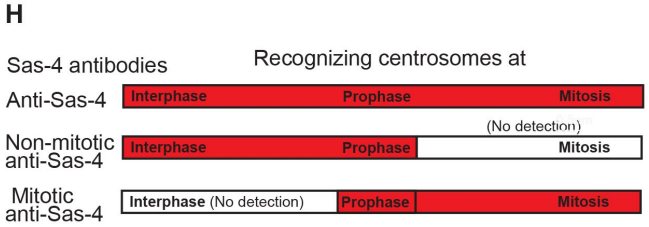
H
Sas-4 antibodies
Recognizing centrosomes at
Anti-Sas-4
Interphase
Prophase
Mitosis
Non-mitotic anti-Sas-4
(No detection)
Interphase
Prophase
Mitosis
Mitotic anti-Sas-4
Interphase (No detection)
Prophase
Mitosis

Figure S1. *In vitro* validation of anti-Sas-4, non-mitotic anti-Sas-4 and Sas-4-TT211p (mitotic specific Sas-4) antibody. Related to figures 1, 2 and 5.

(**A**) Western bot analysis to validate the Sas-4 antibodies using Schneider cells and Schneider cells lacking Sas-4 protein (C131 cells). The anti-Sas-4 antibody and the non-mitotic anti-Sas-4 antibody recognize Sas-4 only in the Schneider cells and not in the C131 cells. Tubulin and Asterless (Asl) are used as loading controls.
(**B**) Fast protein liquid chromatography (FPLC) analysis of purified Sas-4 1-350 variants. All of the variants elute at similar elution volume and have a similar area under the curve (AUC). Coomassie staining of peak fractions (fractions 1 to 8) is shown below.
(C) The non-mitotic anti-Sas-4 is specific for -P2 site. Coomassie blue staining of recombinant Sas-4 1-350 is given at the bottom panel. Plus sign (+) denotes IPTG induction of recombinant protein expression. Minus sign (-) denotes un-induced loading control.(**D**) Dot-blot shows that the non-mitotic anti-Sas-4 is able to recognize Sas-4 peptides (207-220aa) with single amino acid replacements at the -P2 site.
(**E**) The non-mitotic anti-Sas-4 is specific for Sas-4-TT211 as it fails to recognize double amino acid replacements at the -P2 site. Note in contrast to the non-mitotic anti-Sas-4, anti-Sas-4 recognizes all forms of the protein. Coomassie blue staining of recombinant Sas-4 1-350 is given at the bottom panel.
(**F**) Generation of mouse monoclonal and rabbit polyclonal anti-Sas-4 antibodies (Sas-4-TT211p) raised against phosphorylated peptide. This phosphorylated peptide (207-YASSpTpTASSTSPRV-220) is a specific substrate only for the mitotic anti-Sas-4 (Sas-4-TT211p).
(**G**) Schneider C131 cells (lacking Sas-4 protein) expressing –GFP (green, control) or Sas-4-GFP (green). The Sas-4-TT211p antibody (red) labels Sas-4 at mitotic centrosomes only in cells expressing Sas-4-GFP, showing that it is specific for Sas-4. Sas-4-TT211p seems to non-specifically label the DNA. Data not shown for Sas-4-TT211p raised in mouse.
(**H**) Schematic representation of the three different Sas-4 antibodies to compare the localization of Sas-4 at interphase and mitosis. The anti-Sas-4 antibody that recognizes centrosomal Sas-4 at interphase, prophase and metaphase (First bar). The non-mitotic anti-Sas-4 antibody recognizes Sas-4 only at the interphase and prophase (Middle bar); however, the mitotic anti-Sas-4 (Sas-4-TT211p) antibody recognizes Sas-4 only at pro-metaphase and metaphase of the cell cycle (Bottom bar).

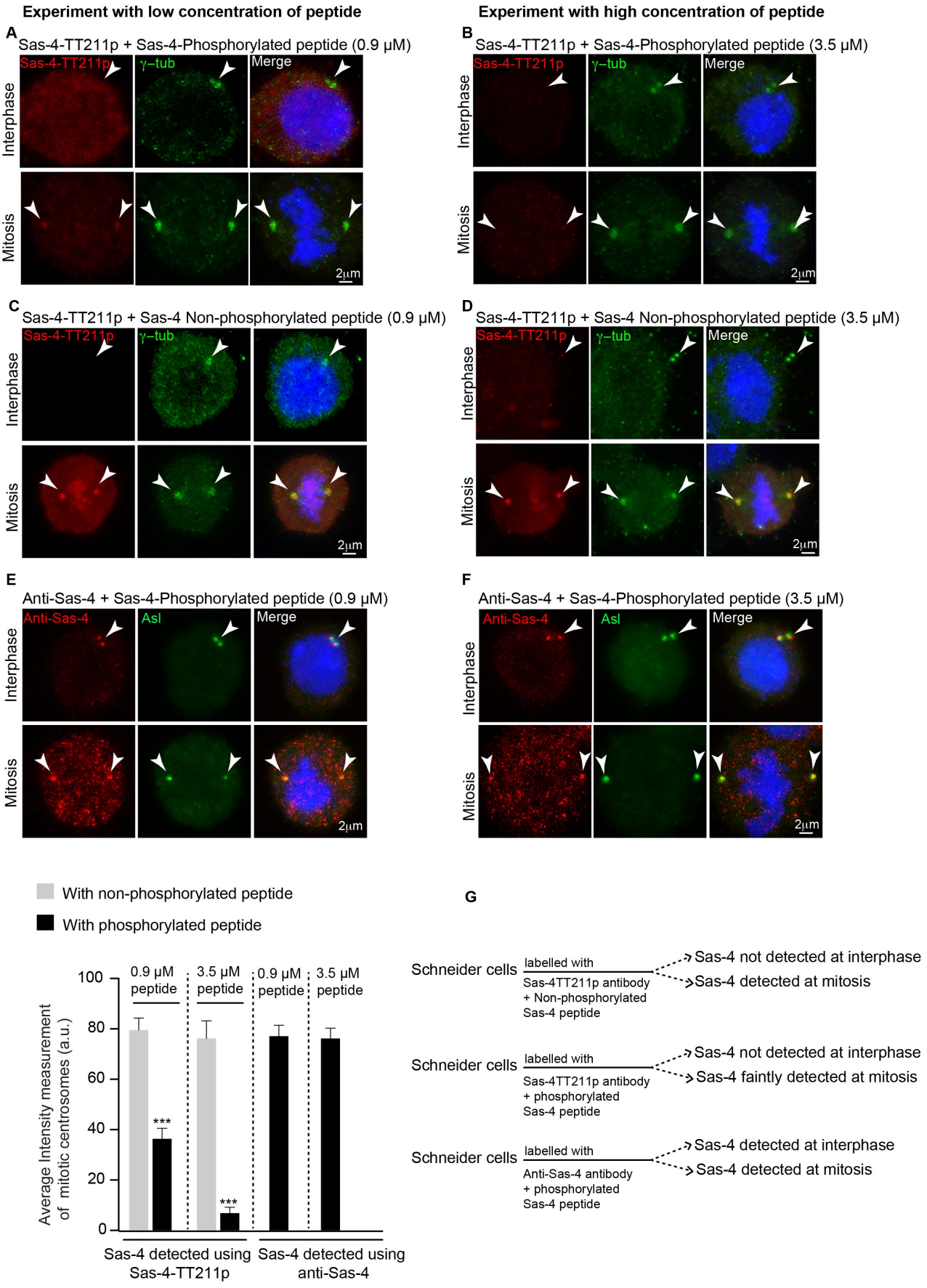

Figure S2. Sas-4 peptide-based competition experiment in Schneider cells. Related to Figures 2 and 5.

(**A-D**) Characterization of Sas-4-TT211p (red, mitotic-specific Sas-4 antibody) in the presence of increasing concentrations of Sas-4 phosphorylated peptide (207-YASS**TT**ASSTSPRV-220, 0.9 µM and 3.5 µM) or Sas-4 non-

phosphorylated peptide (207-YASSTTASSTSPRV-220, 0.9 μM and 3.5 μM). In the presence of higher concentration of Sas-4 phosphorylated peptide, Sas-4-TT211p failed to recognize mitotic Sas-4 (**A-B**). γ-tubulin (green) labels centrosomes. In contrast, Sas-4-TT211p normally labels Sas-4 at mitotic centrosomes in the presence of Sas-4 non-phosphorylated peptide (**C-D**). In either case, Sas-4-TT211p did not recognize Sas-4 at centrosomes of interphase cells. (**E-F**) Anti-Sas-4 antibody (red, whose epitope differs from Sas-4-TT211p) used as a control, recognizes Sas-4 at both interphase and mitosis in the presence of increasing concentrations of Sas-4 phosphorylated peptide. Asl (green) labels centrosomes. The arrowheads mark the centrosomes. The bar graph below represents the average intensity measurements of Sas-4 at mitotic centrosomes. At least 60 mitotic centrosomes *(n=60)* were analyzed from three independent experiments. ANOVA, ***$P<0.0001$. Error bars represent mean ± s.e.m.
(**G**) Experimental scheme of peptide-based competition experiment.

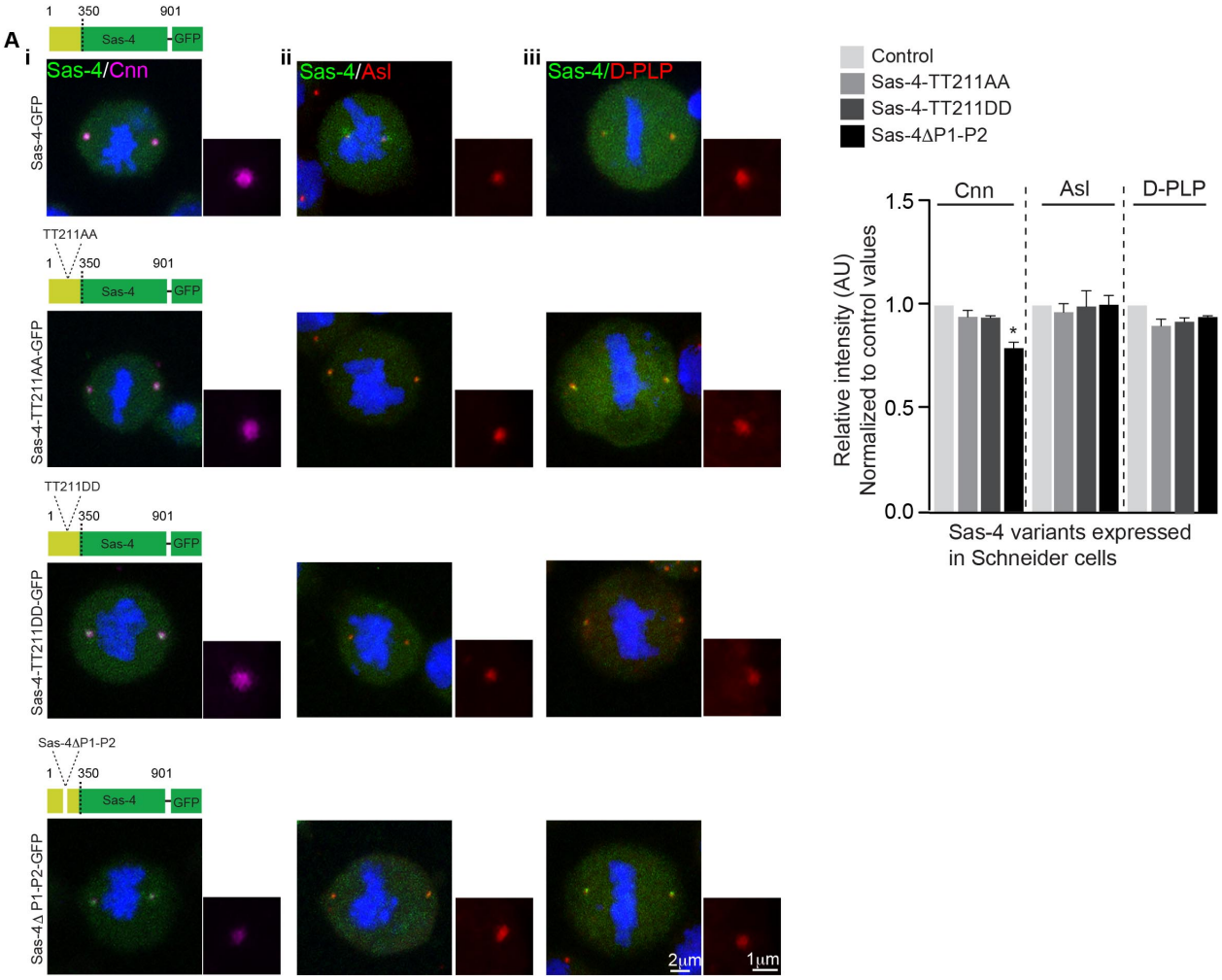

Figure S3. The Sas-4ΔP1-P2 mutation seems to mildly perturb the recruitment of Cnn to mitotic centrosomes in *Drosophila* Schneider cells. Related to figures 3 and 6.

(**A**) Schneider cells expressing different Sas-4 variants as -GFP (green). Sas-4ΔP1-P2 expressing cells showed mild defects in Cnn (**i**, magenta) recruitment at mitotic centrosomes. The bar graph on the right represents the relative intensity of PCM proteins at mitotic centrosomes. At least 40 mitotic centrosomes *(n=40)* were analyzed from three independent experiments. ANOVA, **P*<0.01. Error bars represent mean ± s.e.m.

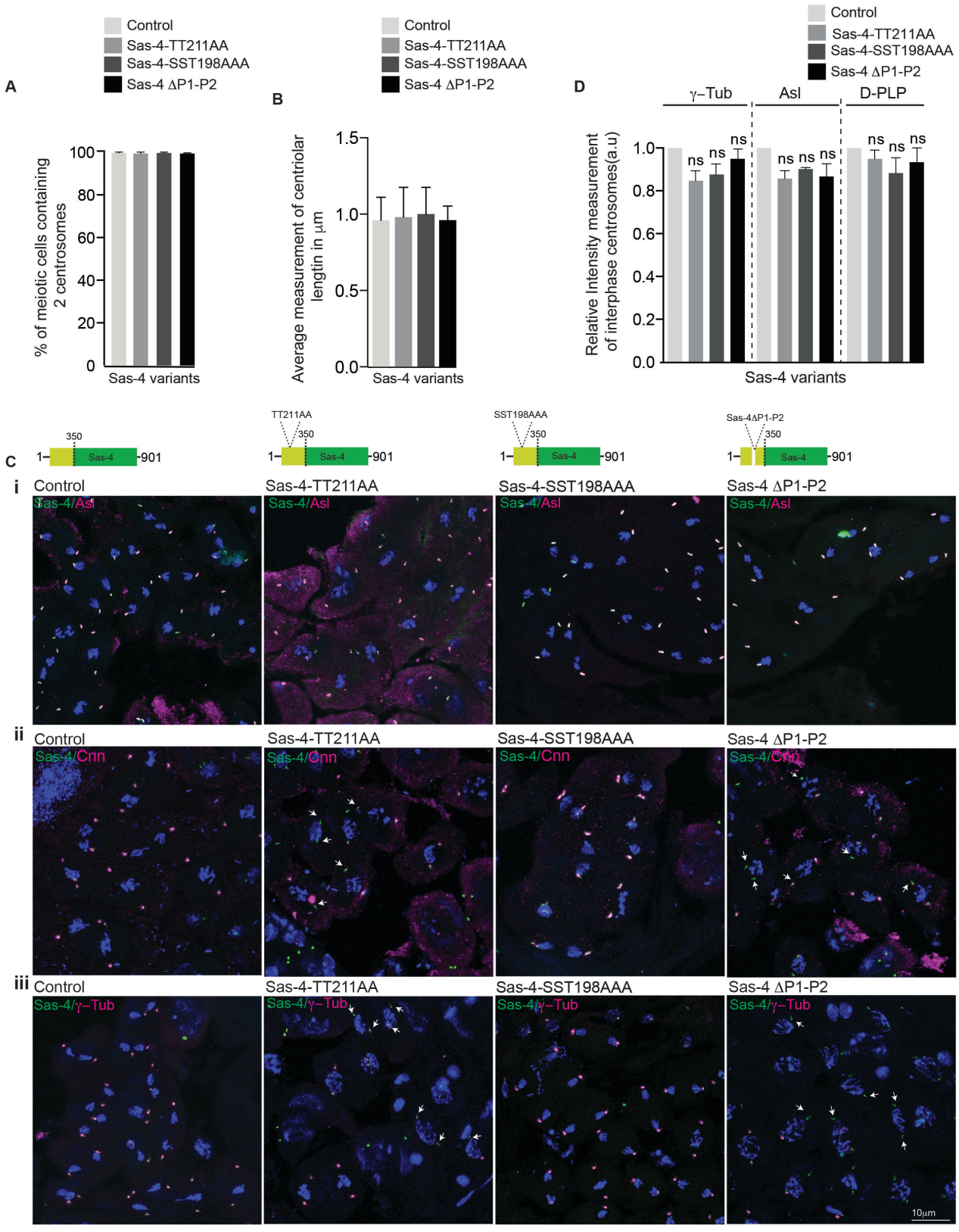

Figure S4. Sas-4 mutants used in this study do not alter centriolar numbers, lengths but perturb an efficient PCM recruitment. Related to figures 4 and 6.

(**A**) None of the Sas-4 variants display aberrant numbers of centrioles. At least 120 meiotic centrosomes (*n*=120) from testes were analyzed for each condition from three independent experiments. ANOVA. Error bars represent mean ± s.e.m.

(**B**) Flies expressing different Sas-4 variants show similar centriolar lengths. At least 80 meiotic centrosomes (*n*=80) from testes were analyzed for each condition from three independent experiments. ANOVA. Error bars represent mean ± s.e.m.

(**C**) Low magnification immunofluorescence images of meiotic cells of testes dissected from various Sas-4 variants. Note normal recruitment of Asl (magenta) in all of the Sas-4 variants **(i).** Defective recruitment of Cnn **(ii,** magenta**)** and γ-Tub **(iii,** magenta**)** is observed only in Sas-4^{TT211AA} and Sas-4$^{\Delta P1\text{-}P2}$ transgenic flies.

(**D**) Bar graph representing the relative intensities of γ-tubulin, Asl and D-PLP at interphase centrosomes of mature spermatocytes expressing various Sas-4 variants. Note that these protein recruitments are not affected in any of the Sas-4 mutants. At least 60 meiotic centrosomes (*n*=60) from testes were analyzed for each condition from three independent experiments. ANOVA. Error bars represent mean ± s.e.m.

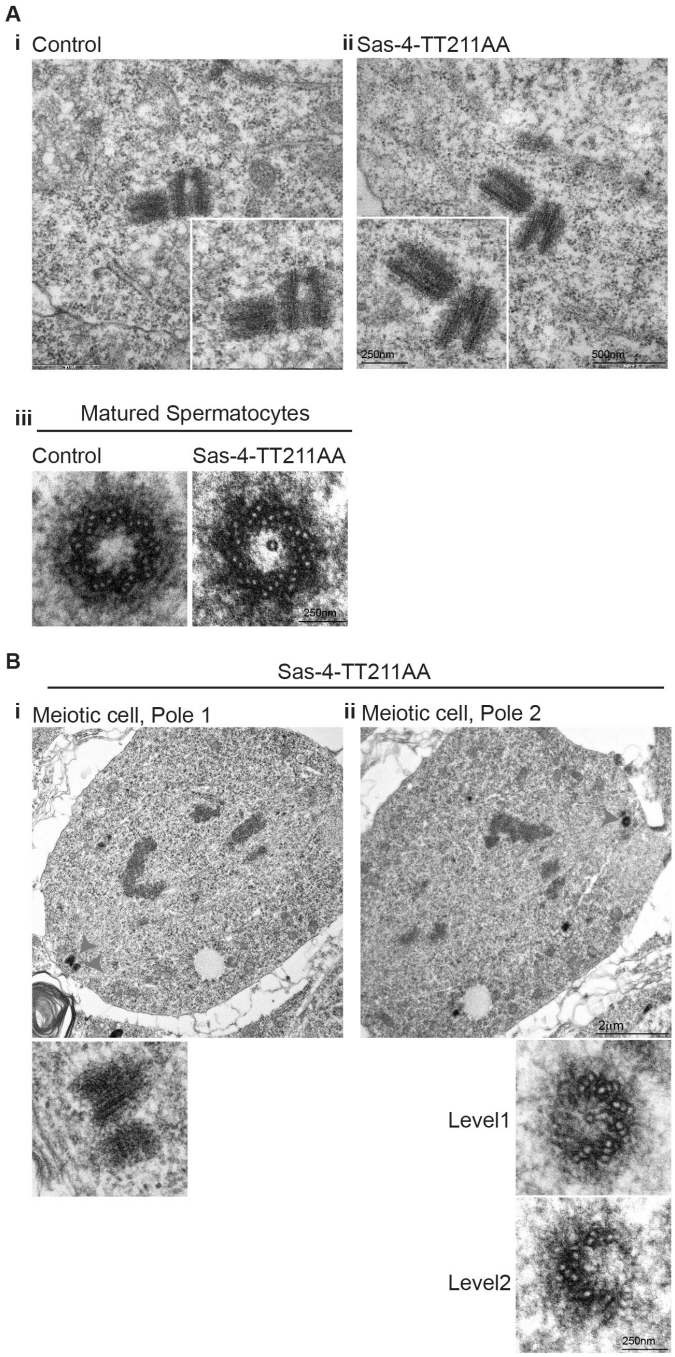

Figure S5. Sas-4^{TT211AA} expressing transgenic flies display structurally normal centrioles. Related to figures 4 and 6.

(**A**) EM micrographs showing normally looking centriole pairs in spermatocytes of control (Sas-4 wild type) **(i)** and Sas-4^{TT211AA} transgenic flies **(ii)**. Cross-sectioned centriolar structures of control (Sas-4 wild type) and Sas-4^{TT211AA} transgenic flies show no structural abnormalities **(iii).**

(B) Similarly, no defects are found in centrosomes of dividing spermatocytes of control (Sas-4 wild type) and Sas-4^{TT211AA} transgenic flies. Serial sectioning EM shows spindle poles (Arrowheads, **i** and **ii**) at two different slices. Cross sections show no defects in the over all structure of centrioles. Level 1 and level 2 are two adjacent sections. Note that the missing part of centriolar structure containing region of the level 1 is imaged at the level 2.

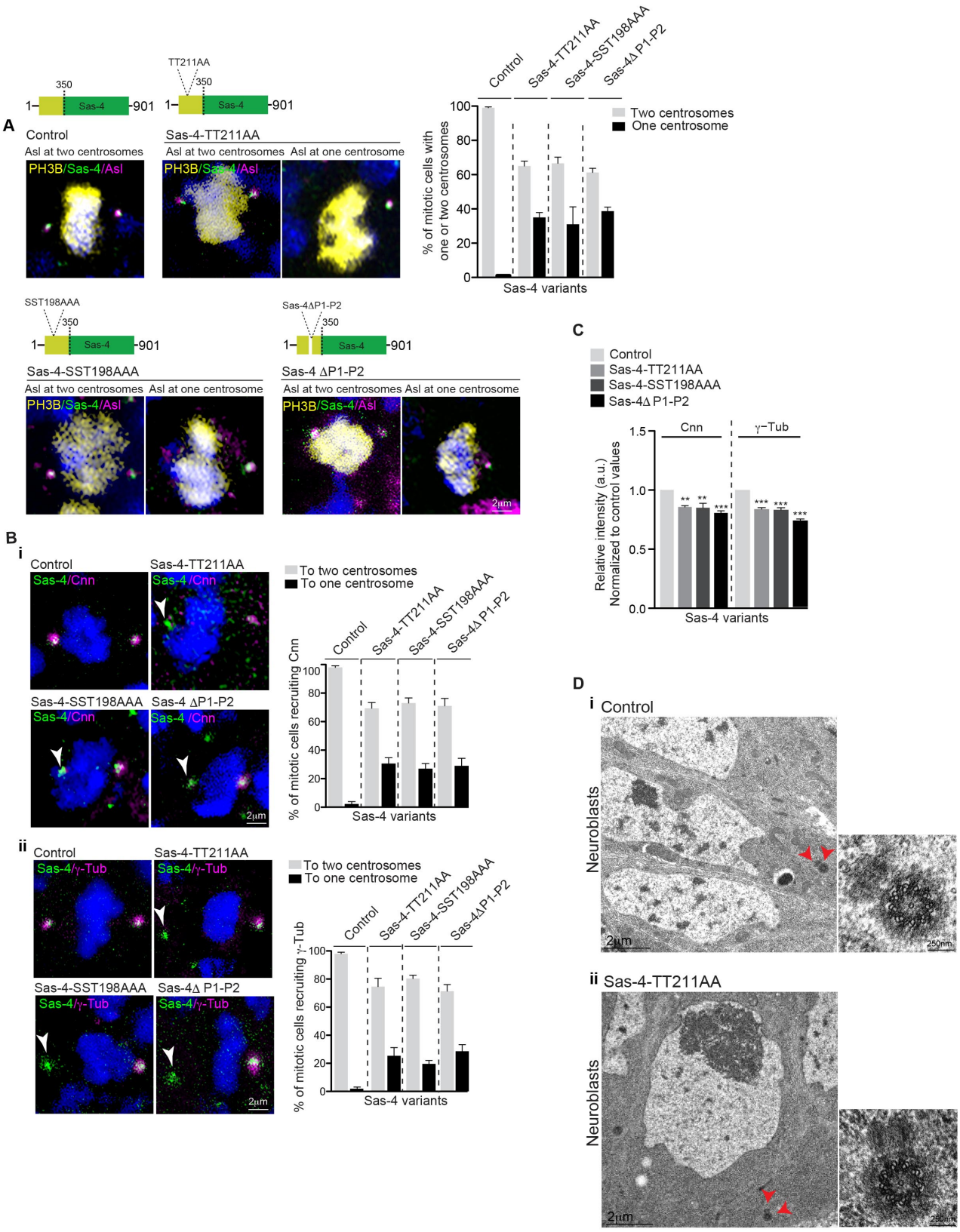

Figure S6. Sas-4-TT211 is required for an efficient recruitment of Cnn and γ-tubulin to the mitotic centrosomes of larval brain cells. Related to figures 6 and 7.

(**A**) Distribution of one and two-centrosome containing cells in various Sas-4 mutants as judged by the presence of Asl and Sas-4. Note Asl (magenta) recruitment appears to be unaffected. Anti-phospho-Histone H3 antibody (PH3B,

yellow) was used to identify mitotic cells. The bar graphs at right represent the percentage of mitotic cells recruiting Asl to either one or two centrosomes. At least 100 mitotic centrosomes (*n*=100) were analyzed for each condition from three independent experiments. ANOVA. Error bars represent mean ± s.e.m. Schematics representing the different Sas-4 mutations have been shown at the top for clarity.

(B) Reduced recruitment of Cnn (**i,** magenta) and γ-tubulin (**ii**, magenta) in two-centrosome containing mitotic cells expressing Sas-4^{TT211AA}, Sas-4^{SST198AAA} and Sas-4$^{\Delta P1\text{-}P2}$. The bar diagrams represent the percentage of mitotic cells recruiting Cnn and γ-tubulin to either one centrosome or both of the centrosomes. At least 80 mitotic centrosomes *(n=80)* were analyzed in each condition from three independent experiments. ANOVA. Error bars represent mean ± s.e.m.

(C) Bar graph representing the relative intensities of Cnn and γ-tubulin at mitotic centrosomes of larval neuroblasts expressing different Sas-4 mutations. Both Cnn and γ-tubulin recruitment is perturbed in flies expressing the different Sas-4 mutations. At least 80 mitotic centrosomes (*n*=80) from neuroblasts were analyzed for each condition from three independent experiments. ANOVA. ****P*<0.0001, ***P*<0.001. Error bars represent mean ± s.e.m.

(D) EM micrographs showing normally looking centriole pairs in interphase cells of larval neuroblasts of control (Sas-4 wild type) **(i)** and Sas-4^{TT211AA} transgenic flies, red arrow heads **(ii)**. Cross-sectioned centriolar structures of control (Sas-4 wild type) and Sas-4^{TT211AA} transgenic flies shows no structural abnormalities**.**

Summary

The conserved centrosomal-P4.1-associated protein (CPAP) and its fly ortholog Sas-4 have long been known as mere centriole duplication factors. Despite its role in assembling PCM complexes, its specific function in building functional centrosomes remained controversial. Here, in this study, I demonstrate that both CPAP and Sas-4 have a prominent role in building functional centrosomes. The crystal structure of CPAP PN2-3-tubulin complex achieved in this study has unraveled the mysteries that precluded the incorporation of tubulin dimers into growing centriolar microtubules. The work in this thesis sheds light on how CPAP binds and releases its bound tubulin at the site of centrioles in a controlled manner via a clutch like mechanism. The C-terminal PN2-3 region of CPAP is found to bind to an acidic microtubule outer surface of β-Tubulin; whereas, the N-terminal loop helix forms a necklace that binds to the α-β interphase of β-Tubulin, thereby blocking the binding of the next α-β Tubulin dimer.

CPAP binds to tubulin dimers with high affinity via its F375 residue located at C-terminal of the PN2-3 domain. This high affinity inhibits the spontaneous polymerization of tubulin dimers. How the bound tubulin is exactly released at the centriolar microtubules is not well understood; however, it is possible that the bound tubulin is taken to the centrioles, where CPAP binds to the centriolar microtubules via its microtubule binding domain (MBD). The tubulin dimers are then released by a reduction in the affinity at the EE343 site located at the N-terminal of the PN2-3 region. This reduced affinity could be a result of post-translational modification occurring in CPAP during centriole elongation. This is because, $CPAP^{EE343RR}$ or $Sas\text{-}4^{EE78RR}$, which uncap the binding site for more tubulin dimers, indeed show elongated centrioles and cilium.

After deciphering the role of CPAP/Sas-4 in centriolar elongation, I aimed to decipher the role of Sas-4 in pericentriolar material (PCM) recruitment. In the previous study by Gopalakrishnan et al., Sas-4 was found to be a scaffold for several PCM proteins, including the bona-fide components that expand the PCM at mitosis. This was re-affirmed by a study in *C. elegans*, wherein the PCM size was regulated by the amount of Sas-4. Therefore, I speculated Sas-4's role in PCM expansion and centrosome maturation. This study identified two different monoclonal anti-Sas-4 antibodies. One of the antibodies recognizes Sas-4 at all stages of the cell cycle; whereas the second recognizes Sas-4 only at interphase and not at mitosis. Therefore, I proposed that Sas-4 might be modified at this

epitope at the onset of mitosis. Biochemical studies of mutant Sas-4 proteins and peptides coupled with immunofluorescence analysis show that the TT211 site of Sas-4 is phosphorylated at the onset of mitosis. *In vitro* kinase assay identifies Plk1/Polo to be the responsible kinase phosphorylating Sas-4 at the TT211 site, at the onset of mitosis. This is confirmed using BI2536, an inhibitor for Plk1/Polo, which did inhibit the phosphorylation. The functional significance of this phosphorylation is studied *in vivo* using *Drosophila* expressing different Sas-4 mutants. Flies expressing the Sas-4^{TT211AA} mutation show reduced recruitment of bona-fide PCM proteins such as Cnn and γ-Tubulin. This indeed confirms that Sas-4 is required for expanding PCM at mitosis.

In summary, my experiments have revisited the role of Sas-4, which was only known to be a centriole duplication factor and uncovered the mechanism by which CPAP/Sas-4 regulates centriole/ cilium length and PCM recruitment in mitotic centrosomes. These two aspects are the fundamental process of building functional centrosomes in animal cells.

Summary in German (Zusammenfassung)

Das konservierte Centrosomal-P4.1-assoziierte Protein (CPAP) und sein Fliegenortholog Sas-4 sind seit langem als bloße Zentriol-Duplikationsfaktoren bekannt. Trotz seiner Rolle beim Aufbau von PCM-Komplexen blieb seine spezifische Funktion beim Aufbau funktionaler Zentrosomen umstritten. Hier in dieser Studie zeige ich, dass sowohl CPAP als auch Sas-4 eine herausragende Rolle beim Aufbau funktionaler Zentrosomen spielen. Die in dieser Studie erreichte Kristallstruktur des CPAP PN2-3-Tubulinkomplexes hat die Rätsel gelöst, die den Einbau von Tubulindimeren in wachsende zentriolare Mikrotubuli ausschließen.
Die Ergebnisse in dieser Arbeit veranschaulichen, wie CPAP sein an der Zentriolenstelle gebundenes Tubulin in kontrollierter Weise über einen kupplungsartigen Mechanismus bindet und frei gibt. Es wurde gezeigt, dass die C-terminale PN2-3-Region von CPAP an eine saure Mikrotubuli-Außenfläche von β-Tubulin bindet; wohingegen die N-terminale Schleifenhelix eine Kette bildet, die an die α-β-Interphase von β-Tubulin bindet, wodurch die Bindung des nächsten α-β-Tubulindimers blockiert wird.

CPAP bindet an Tubulindimere mit hoher Affinität über seinen F375-Rest am C-Terminus der PN2-3-Domäne. Diese hohe Affinität hemmt die spontane Polymerisation von Tubulindimeren. Wie genau das gebundene Tubulin an den zentriolaren Mikrotubuli freigesetzt wird, ist nicht eindeutig geklärt. Es ist jedoch möglich, dass das gebundene Tubulin zu den Zentriolen gebracht wird, wo CPAP über seine Mikrotubuli-bindende Domäne (MBD) an die Zentriolar-Mikrotubuli bindet. Die Tubulindimere werden dann durch eine Verringerung der Affinität an der EE343-Stelle am N-Terminus der PN2-3-Region freigesetzt. Diese verminderte Affinität könnte ein Ergebnis einer posttranslationalen Modifikation sein, die in CPAP während der Zentriol-Elongation auftritt. Dies liegt daran, dass CPAP^{EE343RR} oder Sas-4^{EE78RR}, welche die Bindungsstelle für mehr Tubulindimere freisetzen, tatsächlich verlängerte Zentriolen und ein verlängertes Cilium zeigen.

Nach der Entschlüsselung der Rolle von CPAP/Sas-4 bei der Zentriol-Elongation versuchte ich, die Rolle von Sas-4 bei der Rekrutierung von Pericentriolarmaterial (PCM) zu entschlüsseln. In der vorherigen Studie von Gopalakrishnan et al. wurde gefunden, dass Sas-4 ein Gerüst für mehrere PCM-Proteine ist, einschließlich der Komponenten, welche das PCM bei Mitose ausdehnen. Dies wurde durch eine Studie in *C. elegans* bestätigt, in der die PCM-Größe durch die Menge an Sas-4 reguliert wurde. Daher vermutete ich, dass

Sas-4 eine Rolle bei der PCM-Expandierung und der Reifung von Zentrosomen spielt. Diese Studie identifizierte zwei verschiedene monoklonale Anti-Sas-4-Antikörper. Einer der Antikörper erkennt Sas-4 in allen Stadien des Zellzyklus; während der zweite Antikörper Sas-4 nur in der Interphase und nicht in der Mitose erkennt. Daher untersuchte ich, ob Sas-4 zu Beginn der Mitose an diesem Epitop modifiziert wurde. Biochemische Untersuchungen sowie Immunfluoreszenzanalysen von mutierten Sas-4-Proteinen und -Peptiden zeigen, dass die TT211-Stelle von Sas-4 zu Beginn der Mitose phosphoryliert wird. Ein *in vitro* Kinase-Assay identifiziert Plk1/Polo als verantwortliche Kinase, die Sas-4 an der TT211-Stelle zu Beginn der Mitose phosphoryliert. Die Verwendung von BI2536, einem Inhibitor für Plk1/Polo, bestätigt dies, da die Phosphorylierung inhibiert wurde. Die funktionelle Bedeutung dieser Phosphorylierung wird *in vivo* untersucht, indem Drosophila verschiedene Sas-4-Mutanten exprimiert. Fliegen, welche die Sas-4^{TT211AA}-Mutation exprimierten, zeigten eine verringerte Rekrutierung von PCM-Proteinen wie Cnn und γ-Tubulin. Dies bestätigte tatsächlich, dass Sas-4 für die Expandierung von PCM während der Mitose erforderlich ist. Zusammenfassend haben meine Experimente die Rolle von Sas-4, das bisher nur als Zentriolen-Duplikationsfaktor bekannt war, überarbeitet und den Mechanismus aufgedeckt, durch den CPAP/Sas-4 die Zentriolen- und Cilium-Länge und die Rekrutierung von PCM in mitotischen Zentrosomen reguliert. Diese beiden Aspekte sind der grundlegende Prozess zum Aufbau funktionaler Zentrosomen in tierischen Zellen.

Acknowledgement

I would first like to thank Prof. Jay Gopalakrishnan for giving me an opportunity to be a part of his research group. He provided me with immense support to procure the DAAD fellowship that funded three years of my studies in Germany. I was highly encouraged to discuss my ideas and hypothesis, which has improved my scientific and reasoning abilities. This has in turn motivated me to independently make scientific decisions and execute some of the exciting self-planned experiments. Living and doing science in Germany has transformed my career and attitude in a positively optimistic way. My gratitudes are always there for German culture and academic system.

I would like to especially thank the Center for molecular medicine (CMMC) microscopic facility, that was extremely crucial for my doctoral research. I am also thankful to the Interdisciplinary Program Molecular Medicine at University of Cologne, (IPMM) which has shaped my doctoral research enhancing my presentation and scientific writing skills.

During my doctoral studies, we were successful in receiving a DFG funding, which funded me after my DAAD scholarship. This funding has supported me to complete a good doctoral thesis and acquire relevant publications.

I am very grateful to my colleagues who spent a significant proportion of their time to train me at the beginning of my doctoral research. Prof. Jay and Arpit Wason trained me as a biochemist. I received training in cell culture from Dr. Elke Gabriel and became experienced in light microscopy due to efforts from Dr. Arul Jothi Mariappan. Also, I gained experience in molecular biology by training with both Arpit Wason and Xiangdong Zheng, who joined our lab as a guest scientist from China. Prof. Jay trained me in basic *Drosophila* genetics, which helped me in addressing very exciting questions in flies. In addition, I am thankful to Dr. Marco Gottardo, who has performed electron microscopy and Dr. Sunit Mandad from Prof. Henning Urlaub's Lab who has performed Mass spectrometric analysis for my Ph.D. project. Also, I would like to thank Gladiola goranci, Robin Gutsche and Kaustubh Kalamkar, who have been very supportive throughout my Ph.D. and have given me feedbacks during informal discussions and also Lara and Beate for translating the summary of my thesis.

My advisor from Manipal University, Dr. Smita Shenoy and Dr.V.V. Ranade from Mumbai University have been very supportive and have always encouraged me to pursue further research to become independent in the future.

After enrolling at the University of Duesseldorf, Prof. Thomas Klein agreed to be my mentor for the Doctoral procedure. I am very thankful for his support and advice on my

project. I would also like to extend my gratitude to Frau Athina Stefanidou, who has assisted me in quickly enrolling into the doctoral program without any delay.

My friends, Khannaphaphone Phakhounthong, Subhankar Dutta, Kallol Roy, Dr. Saravanan, and Sridevi Raysam have been my major stress busters. They were there during some of my tough days of research, making them much pleasant.

Special thanks to my parents and my sister, who have motivated me, no matter how many failures I have encountered. They had a vision of me developing into a young scientist in the family even before I began as a Ph. D student in Germany. This indeed motivated me to push forward through some of the bad times in my career. With all of these opportunities, motivation and support, I believe that I will be able to do tangible science as my career.

Biographical sketch

Anand Ramani was born in 1987 in Mumbai, India. He completed his Bachelor of Science in Microbiology (2003-2008) from Mumbai University and Master of Science in Medical pharmacology from Manipal university (2008-2011), securing First Class. Anand Ramani received the Deutscher Akademischer Austausch Dienst (DAAD) fellowship in 2011, to pursue his Ph.D in Prof. Dr. Jay Gopalakrishnan's Laboratory at University of Cologne and University of Dusseldorf. During his Ph.D research, Anand Ramani has gained expertise in *Drosophila* genetics, molecular biology techniques and human cell culture, which helped him to address the role of CPAP/Sas-4 in building functional centrosomes. Anand Ramani has attended several workshops and presented his work at conferences, which has not only improved his scientific knowledge, but has also given him exposure to the scientific community. The following publications arose during the period of his doctoral study.

.

1. **Ramani A***, Mariappan A, Gottardo M, Mandad S, Urlaub H, Avidor-Reiss T, Riparbelli M, Callaini G, Debec A, Feederle R, Gopalakrishnan J*. Plk1/Polo Phosphorylates Sas-4 at the Onset of Mitosis for an Efficient Recruitment of Pericentriolar Material to Centrosomes. Cell Rep, 25(13):3618-3630 (2018)

2. Zheng X*, **Ramani A***, Soni K, Gottardo M, Zheng S, Ming Gooi L, Li W, Feng S, Mariappan A, Wason A, Widlund P, Pozniakovsky A, Poser I, Deng H, Ou G, Riparbelli M, Giuliano C, Hyman AA, Sattler M, Gopalakrishnan J*, Li H*. Molecular basis for CPAP-tubulin interaction in controlling centriolar and ciliary length. Nat Commun 7, 11874 (2016)

3. Mariappan A, Soni K, Schorpp K, Zhao F, Minakar A, Zheng X, Mandad S, Macheleidt I, **Ramani A**, Kubelka T, Dawidowski M, Golfmann K, Wason A, Yang C, Simons J, Schmalz HG, Hyman AA, Aneja R, Ullrich R, Urlaub H, Odenthal M, Büttner R, Li H, Sattler M, Hadian K, Gopalakrishnan J*. Inhibition of CPAP-tubulin interaction prevents proliferation of centrosome-amplified cancer cells. EMBO J., 25(13):3618-3630 (2018)

4. Gabriel E, **Ramani A**, Karow U, Gottardo M, Natarajan K, Gooi LM, Goranci-Buzhala G, Krut O, Peters F, Nikolic M, Kuivanen S, Korhonen E, Smura T, Vapalahti O, Papantonis A, Schmidt-Chanasit J, Riparbelli M, Callaini G, Krönke M, Utermöhlen O, Gopalakrishnan J*. Recent Zika virus isolates induce premature differentiation of neural progenitors in human brain organoids. Cell Stem Cell, 20:1-10 (2017).

5. Gabriel E, Wason A, **Ramani A**, Gooi LM, Keller P, Pozniakovsky A, Poser I, Noack F, Telugu NS, Calegari F, Šarić T, Hescheler J, Hyman AA, Gottardo M, Callaini G, Alkuraya FS, Gopalakrishnan J*. CPAP promotes timely cilium disassembly to maintain neural progenitor pool. EMBO Journal., 35(8):803-19 (2016).

* Authors have contributed equally.

Declaration

I hereby confirm that this thesis is an original work conducted at the Laboratory of Prof. Dr. Jay Gopalakrishnan. The data has been written and published following the principles of good scientific practice and does not contain unreferenced data and information from other researchers to the best of my knowledge. Data that is taken from other publications has been adequately cited in the text and also, credits have been given to colleagues who have distantly participated in this study.

In addition, I declare that the sole purpose of this study was to improve our understanding in the field of centrosome biology and does not intend to use the data for any commercial purposes.

Düsseldorf
Date:

Anand Ramani